SHEAR CONNECTIONS FOR THE DEVELOPMENT OF A FULL-DEPTH PRECAST CONCRETE DECK SYSTEM

A Thesis

by

MATTHEW DALE HENLEY

Submitted to the Office of Graduate Studies of
Texas A&M University
in partial fulfillment of the requirements for the degree of

MASTER OF SCIENCE

May 2009

Major Subject: Civil Engineering

SHEAR CONNECTIONS FOR THE DEVELOPMENT OF A FULL-DEPTH PRECAST CONCRETE DECK SYSTEM

A Thesis

by

MATTHEW DALE HENLEY

Submitted to the Office of Graduate Studies of
Texas A&M University
in partial fulfillment of the requirements for the degree of

MASTER OF SCIENCE

Approved by:

Chair of Committee,	John Mander
Committee Members,	Monique Hite Head
	Anastasia Muliana
Head of Department,	David Rosowsky

May 2009

Major Subject: Civil Engineering

ABSTRACT

Shear Connections for the Development of a Full-Depth Precast Concrete Deck System.
(May 2009)
Matthew Dale Henley, B.S., Texas A&M University
Chair of Advisory Committee: Dr. John Mander

A full-depth precast concrete deck system presents several safety, timeline, and cost benefits to the process of constructing a bridge, however the relevant professional codes do not provide dependable design models due to the limited amount of research conducted on the subject. One area lacking design direction is the development of a shear connection between the full-depth precast deck and a precast concrete girder via a pocket-haunch-connector system. Push-off tests are performed to investigate the effects of various pre- and post-installed shear connectors, haunch height, surface roughness, grouping effects, and grout composition as compared to cast-in-place specimens. The experimental results are presented along with a method for normalizing the variations of results by connection yield strength. This method is used to evaluate each connector type and connection parameter investigated. Ensuring sufficient shear reinforcement within the beam near the shear connector anchorage is found to be a vital aspect of holistic design. A simplified design procedure is outlined, the design connection force-displacement behavior is shown, and an example problem is solved. Recommendations for additions and modifications to current code and practice are prescribed.

ACKNOWLEDGEMENTS

I would like to thank Dr. John Mander, my thesis advisor, and the other professors on my committee, Dr. Monique Head from the Civil Engineering Department and Dr. Anastasia Muliana from the Mechanical Engineering Department, for their support, direction, and advice.

The experimental work described in this thesis was part of a bigger research initiative by the Texas Transportation Institute for the Texas Department of Transportation on developing a precast overhang bridge deck system (Project 0-6100). Dr. Trejo was the Research Supervisor for that project, and, along with the funding for the experimental work, his encouragement is gratefully acknowledged.

I would like to thank my research partners, Thomas Mander and Reece Scott, for their tireless teamwork throughout this project. I also appreciate the assistance of several other student research assistants who lent a hand during various stages: Jeong Joo Kim, Yong Hoon Kim, John Orsak, Luis Van Der Velde, and Jason Zidek. Additionally, I would like to thank the staff of the High Bay Materials and Testing Laboratory, Dr. Peter Keating, Matt Potter, and Steve Smith, for all of their support, guidance, and hard work.

A special thanks to the United States Air Force, the Air Force Institute of Technology's Civilian Institute program, and the Civil Engineer and Services School Faculty Sponsorship for the tremendous opportunity of returning to school to pursue this advanced degree. Disclaimer: the views expressed in this thesis are those of the author and do not reflect the official policy or position of the United States Air Force, Department of Defense, or the U.S. Government.

Finally, for their love and support during this challenging time, I would like to thank my family and friends, especially my wife, Allison.

NOMENCLATURE

AASHTO	American Association of State Highway Transportation Officials
ACI	American Concrete Institute
AISC	American Institute of Steel Construction
BC	Bolt with coupler shear connection
CCD	Concrete capacity design
CIP	Cast-in-place
KB	Kwik-bolt mechanical anchor shear connection
LRFD	Load and resistance factor design
LVDT	Linear variable differential transducer
NCHRP	National Cooperative Highway Research Program
NS	Nelson stud
R	R-bar shear connection within a pocket system
SIP	Stay-in-place
TR	Threaded rod shear connection
TRC	Threaded rod with coupler shear connection
TRE	Threaded rod post-installed in epoxy
TRS	Threaded rod post-installed in SikaGrout® 212
TRS/AG	Threaded rod post-installed in an alternative grout
TTI	Texas Transportation Institute
TxDOT	Texas Department of Transportation
VTRC	Virginia Transportation Research Council
w/p	Water-to-powder ratio
a	Width of shear test beam
A_{cv}	Concrete shear interface area
A_s	Area of one shear connector
A_{sc}	Cross-sectional area of stud shear connector
$A_{se,v}$	Effective cross-sectional area of a single anchor in shear

A_{sf}	Area of steel in one fastener
A_{sh}	Area of steel in one hoopset
A_{sv}	Combined connector area
A_{vf}	Area of interface reinforcement area crossing the shear plane
c	Cohesion factor
d	Stud diameter
e	Eccentricity
E_c	Concrete modulus of elasticity
E_s	Steel modulus of elasticity
F	Shear force
f'_c	Concrete compressive strength
f_{cu}	Concrete cube compressive strength
f_u	Ultimate strength of steel
f_{uf}	Tensile strength of shear connector
f_{uta}	Specified tensile strength of anchor steel
f_y	Reinforcement, connector yield stress
f_{ya}	Specified yield strength of anchor steel
f_{yf}	Yield stress of shear connector
f_{yh}	Yield stress of hoop steel
H	Stud height
h_{ef}	Anchor effective embedment depth
jd	Distance between resultant internal compressive and tensile forces
l_p	Length of precast deck panels
n	Number of hoopsets, pockets, or anchors required
n_f	Number of fasteners in a pocket
P	Prestressing anchoring force
P_c	Permanent net compressive force normal to the shear plane
P_n	Additional normal force
P_u	Maximum shear load

q	Shear per unit length
Q	Design shear
Q_n	Nominal strength of one stud shear connector
Q_p	Design shear per panel
Q_u	Ultimate shear strength
s	Center-to-center spacing of hoopsets, pockets
V	Lateral force
V_{in}	Interface shear per unit length
V_{sa}	Nominal strength of an anchorage
v_{ui}	Shear stress at initial breakaway
$v_{ui}/\sqrt{f'_c}$	Normalized shear stress
y	Height above laboratory floor
μ	Friction factor
μ_c	Inferred friction coefficient
μ_f	Effective coefficient of friction for a fastener system
μ_g	Coefficient of friction of the grout-to-panel interface
σ	Maximum floor stress
φ	Compression strut angle from vertical

TABLE OF CONTENTS

CHAPTER Page

LIST OF FIGURES

FIGURE Page

FIGURE Page

LIST OF TABLES

CHAPTER I
INTRODUCTION

1.1 Background

In the United States and elsewhere, there is a concerted push to develop accelerated methods of construction for bridges in order to reduce the direct and indirect impacts to cost and downtime of the transportation infrastructure. Bridges are commonly constructed from steel or precast prestressed concrete girders with bridge deck that is either cast-in-place (CIP) (see Fig. 1(a)) or composed of stay-in-place (SIP) partial-depth precast deck panels with a second-stage CIP pour to complete the deck (see Fig. 1(b)). The on-site placement of the reinforcing steel and the casting of the deck for either of these methods slow the construction progress significantly. This research is about speeding up that particular construction activity by using full-depth precast prestressed deck panels in conjunction with steel or precast prestressed concrete girders.

If full-depth precast deck panels are also used in the construction of the bridge, a method is required to connect the panels to the girders. In this thesis, methods that utilize shear fasteners to provide this connection are investigated. Pockets that are 7 x 10 in. (178 x 254 mm) are formed through the entire depth of the precast deck panels at the time of casting and then used as a means of access to attach the fasteners to the girders (see Fig. 1(c)). Therefore no field placement of concrete needs to be undertaken, and site work is limited to installing the fasteners and placing grout in the pockets to complete the connection and provide cover. Thus this construction method has the potential to provide significant time and cost savings for the project, provided that the connection can be designed to reliably transfer the shear load.

Prior to the development of the precast bridge deck overhang system investigated within this thesis, composite action between a CIP deck or SIP precast panel deck and

---

This thesis follows the style of *Journal of Structural Engineering*.

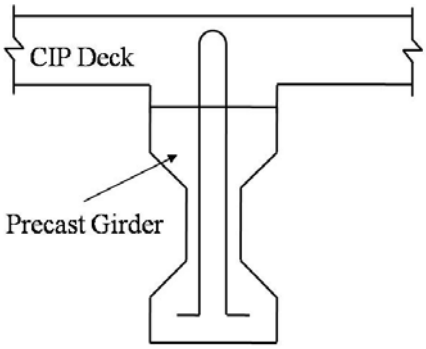

(a)

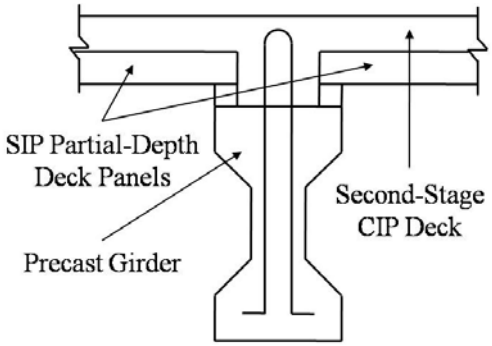

(b)

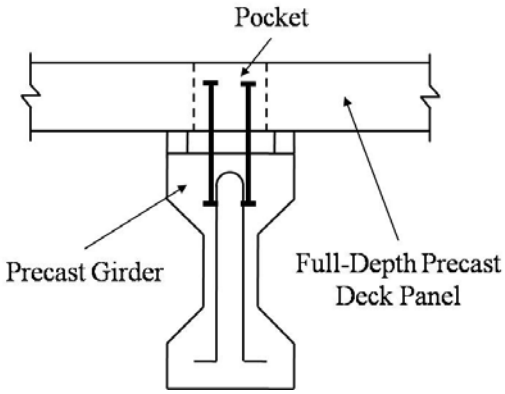

(c)

Fig. 1–Bridge deck construction methods. (a) CIP construction (b) conventional construction utilizing SIP partial-depth panels (c) proposed precast deck panel system investigated in this research.

the precast concrete girders was achieved through reinforcement extended beyond the top surface of the girder. This reinforcement commonly consisted of inverted U-shaped bars, referred to in Texas Department of Transportation (TxDOT) drawings as R-bars. Continuity was established by a CIP pour, thereby linking a second layer of continuous reinforcement to the existing reinforcement located between the panels at the deck-girder interface.

Despite eliminating the need for formwork where the panels are placed, the SIP system still requires formwork for the CIP overhang system. The construction of this formwork is a safety concern, as it is entirely elevated and extended outside the fascia girders. Additionally the construction of this formwork slows the progress of construction, adding to direct and indirect costs of the structure. Therefore if a full-depth precast deck system, including the overhang, were developed, there is a potential to save time, money, and minimize a hazardous working environment.

Due to the inherent nature of having a precast overhang, options are needed to achieve precast deck panel to concrete girder composite action through the use of shear pockets within the panels. However, the code generally governs bridge construction, the American Association of State Highway Transportation Officials (AASHTO) Load and Resistance Factor Design (LRFD) Bridge Design Specification (AASHTO, 2007), does not address this design consideration for interface shear transfer (shear friction) in full-depth panels. More specifically, AASHTO LRFD C5.8.4.1 states

> Composite section design utilizing full-depth precast deck panels is not addressed by these provisions. Design specifications for such systems should be established by, or coordinated with, the Owner.

Therefore, the connection detail of these shear pockets needs to be examined in terms of force-deformation performance and constructability and then compared to conventional construction to ensure the new precast system is not inferior.

In this thesis, the design methodology is based on the state-of-the-art and state-of-the-practice to determine the number and spacing of shear studs needed in a pocket as well as the spacing of pockets over the length of the beam. This is based on a dual approach that includes both experimental and rational mechanics theories. Several

combinations of grout and shear stud spacing not currently covered in the literature were evaluated and tested. Experiments were conducted that realistically represent the boundary conditions in a prestressed concrete girder bridge, as the aspects of the connection's interaction with the structure of the girder and deck are vital to developing a dependable design envelope for the composite system. Specifically, there are four objectives of this thesis:

1. To capture the force-displacement behavior of various connectors and configurations due to increasing applied lateral load
2. To compare the performance of these connectors within the deck-haunch-beam system to validate the proposed standard construction practice of shear connections for full-depth precast bridge decks
3. To evaluate different alternatives to optimize the performance of the system while considering constructability, cost, and accessibility of materials.
4. To prepare a simple design model and illustrate its application through an example shear connector/pocket design for a prototype prestressed concrete girder bridge with a full-depth concrete deck

1.2 What then is particularly new in this thesis?

As with any experimental research, the actual experiments performed for this thesis and presented herein are unique. Somewhat similar testing has been accomplished previously, but the experimental test setup is particularly different in order to more precisely simulate the connection of a prestressed concrete girder and a full-depth concrete deck via a pocket system. The set of shear connectors tested is also unique and provides data both for construction of a prototype bridge and for exploration of different types of connections to be applied in the practice of designing future structures.

Another valuable, though unintended, aspect of this thesis is the discovery of the importance of the hoop reinforcing in the experiment's shear test beams due to the concentration of shear demand. This also reminds researchers and practicing engineers of the importance of holistic look at a system, particularly those that are not well

understood, and the importance of ensuring proper detailing in the application of such a system to structural design.

This thesis also presents a design method for application of this full-depth panel system. An example of the design method is shown for a 36.5-m (120-ft.) span bridge to demonstrate its efficacy.

1.3 Organization of thesis

This thesis is organized into chapters of related information. Following on from this introductory chapter, Chapter II outlines the state-of-the-practice by reviewing the current professional codes and the state-of-the-art by reviewing the relevant technical literature on the subject. Chapter III explains the experimental test setup and the specimens to be tested. Chapter IV presents the results of the experiments while Chapter V contains a detailed analysis of those results. Chapter VI presents a simple design procedure along with an example that can be followed for designing the shear connections for a bridge span of this type. Chapter VII contains the summary, findings, conclusions, and recommendations for future research and engineering practice.

CHAPTER II
STATE-OF-THE-PRACTICE AND -ART

2.1 Introduction

This chapter first reviews the state-of-the-practice currently used in the design of concrete shear connections as per the pertinent sections of professional codes currently in use in engineering practice, including AASHTO LRFD (AASHTO, 2007), American Concrete Institute (ACI) Building Code Requirements for Structural Concrete, ACI 318-08 (ACI Committee 318, 2008), and American Institute of Steel Construction (AISC) 13th Steel Construction Manual, AISC-13, (AISC, 2005). Also included in the review of the state-of-the-practice is an overview of the research that led to the formulae used in the professional codes.

The latter portion of this chapter covers the state-of-the-art of concrete shear connections by providing a review of recent research on the subject. Contributions to the understanding of structural behavior are noted, as are shortfalls in application to the specific situation covered in this thesis.

2.2 State-of-the-practice: current professional codes

2.2.1 AASHTO LRFD bridge design specification

The AASHTO LRFD Bridge Design Specification Section 5.8.4 covers interface shear transfer by shear friction, though the commentary specifically states "*Composite section design utilizing full-depth precast deck panels is not addressed by these provisions. Design specifications for such systems should be established by, or coordinated with, the Owner.*" Nevertheless, the principles for calculating the shear resistance of the interface plane can serve as an effective starting point for this thesis. Equation 5.8.4.1-3 provides the nominal shear resistance of the interface plane, V_{ni}, as

$$V_{ni} = cA_{cv} + \mu\left(A_{vf}f_y + P_c\right) \quad (1)$$

where c is the cohesion factor, A_{cv} is the concrete shear interface area, μ is coefficient of friction, A_{vf} is the area of interface shear reinforcement crossing the shear plane within

the area A_{cv}, f_y is the yield stress of reinforcement, and P_c is the permanent net compressive force normal to the shear plane. This equation reflects two mechanisms that resist interface shear forces: the bond between the separate castings and the clamping-friction provided by the shear connection. The average bond breakage shear stress between the separate castings is generally approximated as $0.5\sqrt{f'_c}$ for f'_c in MPa ($4\sqrt{f'_c}$ for f'_c in psi), a value which corresponds closely to the c values provided in AASHTO LRFD 5.8.4.3 for use in Equation (1), which range from 0.17 to 2.75 MPa.

It is notable that AASHTO LRFD discriminates the values of the constants for Equation (1) based on whether or not the concrete surface has been intentionally roughened. Specifically, a roughened surface provides a better bond with the concrete cast upon it and a higher coefficient of friction. For example, for concrete placed against a clean concrete surface, free of laitance, but not intentionally roughened, AASHTO LRFD 5.8.4.3 gives c=0.075 ksi and μ=0.6. For an otherwise identical case with a surface intentionally roughened to an amplitude of 0.25 in., the code gives c=0.24 ksi and μ=1.0. Therefore, the c value is drastically increased and the μ value is also increased due to intentional surface roughening.

2.2.2 ACI 318-08: Building Code Requirements for Structural Concrete

ACI 318-08 Appendix D contains the code and commentary pertinent to anchoring in concrete, including tension, shear, and combined loading of CIP and post-installed anchors. Anchorage of full-depth precast connections is not discussed directly.

For both conventional tension and shear of anchors, the concrete failure cone is assumed to be $\pm 1.5h_{ef}$ on either side of the anchor, where h_{ef} is the effective embedment depth of the anchor. Factors are outlined for dealing with single anchors, groups of anchors, eccentric loading, edge effects, and cracking. The steel strength of the anchor in shear is outlined in D.6.1.2, which gives the nominal strength of an anchorage, V_{sa}, for a cast-in headed stud anchor and for a cast-in headed bolt or post-installed anchor as Equations (2) and (3), respectively

$$V_{sa} = nA_{se,v}f_{uta} \tag{2}$$

$$V_{sa} = n0.6A_{se,v}f_{uta} \tag{3}$$

where n is the number of anchor(s) in the group, $A_{se,v}$ is the effective cross-sectional area of a single anchor in shear, and f_{uta} is the specified tensile strength of the anchor steel ($\leq 1.9f_{ya}\ and\ 125\ ksi$, where f_{ya} is the specified yield strength of the anchor steel). The commentary specifies that the tensile strength is in the calculations for nominal shear strength rather than the yield strength because most anchor materials lack a well-defined yield point. The commentary also specifies that welded stud anchors develop a larger shear strength due to the fixity of the weld.

When comparing Equations (2) and (3) with (1), it follows that ACI 318-08, perhaps rightly, neglects the cohesive anchorage in the expectation that it will inevitably fail, but this is overtaken by the frictional resistance arising from the tie-down force. Equations (2) and (3) infer that the coefficient of friction is μ=1.0.

2.2.3 AISC-13

Chapter I of AISC-13 prescribes the provisions for design of composite members within a structure, that is, "steel beams supporting a reinforced concrete slab so interconnected that the beams and the slab act together to resist bending." The shear connection between the steel member and the reinforced concrete slab is generally provided by a channel or headed stud, though current practice tends heavily toward the latter due to ease of installation. AISC-13 calculates Q_n, the nominal strength of one stud shear connector:

$$Q_n = 0.5A_{sc}\sqrt{f'_c E_c} \leq A_{sc}F_u \tag{4}$$

where A_{sc} is the cross-sectional area of stud shear connector, f'_c is the specified compressive strength of the concrete, E_c is the modulus of elasticity of the concrete, and F_u is the specified minimum tensile strength of a stud shear connector.

Though this thesis focuses almost exclusively on the connection of concrete to concrete, the behavior of a steel-concrete composite connection is somewhat similar. A concrete-concrete connection could be modeled as both halves acting as a CIP concrete component with the weaker controlling. In the case of this thesis, the precast panels introduce an additional difference in that the concrete is not cast on the studs, rather a pocket-grout connection is made.

It is not possible to infer a friction coefficient from the first part of Equation (4); presumably this is based on other serviceability performance criteria. However, the second part of Equation (4) infers the friction coefficient is μ=1.0. For strong concretes this normally governs.

2.2.4 Research that developed the state-of-the-practice

Among the earlier key works on the subject of shear connections is a study of the shear connection between steel girders and concrete specimens as provided by headed, welded studs (Olgaard et al., 1971). Though there are differences between a steel and cast-in-place concrete shear connection and a precast concrete to cast-in-place concrete shear connection, this study provides much of the basis for standards of shear connection design. Through a regression analysis of the results of a series of push-off experiments, Olgaard et al. find the following formula to closely correlate to the behavior of the specimens:

$$Q_u = 1.106 A_s {f'_c}^{0.3} {E_c}^{0.44} \quad (5)$$

However, in order to more easily utilize the empirically derived relationship in design, the authors satisfactorily simplify Equation (5) to give Equation (6).

$$Q_u = 0.5 A_s \sqrt{f'_c E_c} \quad (6)$$

where Q_u is the ultimate shear strength (kips), f'_c is the concrete compressive strength in ksi, E_c is the concrete modulus of elasticity in ksi, and A_s is the cross-sectional area of the stud shear connector (in^2). Equation (6) is the same equation currently used in AISC-13 as shown in Equation (4).

Additional guidance for current codes was taken from an earlier study on the flexural strength of composite beams (Slutter and Driscoll, 1965). In this work, steel-concrete composite beam flexure tests are performed with varying headed stud and channel shear connection arrangements. The authors conclude that there is a definite relationship between the ultimate strength of the shear connectors and the ultimate flexural capacity of the beam, that fulfilling equilibrium at ultimate load provides a suitable criterion for determining the minimum number of shear connectors, and that if enough shear connectors are used to develop the ultimate flexural capacity of the

composite section the load-deflection curve is not affected significantly by the magnitude of slip.

A relatively simple and user-friendly method for accurate and efficient calculation of shear and tensile capacities of fasteners in uncracked concrete, called the concrete capacity design (CCD) method, was developed and published in a more recent study (Fuchs et al., 1995). In this work, the tension and shear failure mechanisms of various concrete fastenings are outlined along with the failure load calculation methods prescribed by ACI 349. The CCD method for tensile and shear capacity calculation is then presented, differentiated from the ACI 349 method by the primary assumption of a failure cone of approximately 35° instead of 45° and by the use of several factors to account for differences in connection and loading details. The ACI 349 and CCD methods are then applied to a data bank of approximately 1200 American and European tests. Results show that the CCD method can accurately predict failure for a wide range of applications, while the ACI 349 method is sometimes conservative and sometimes unconservative. Due to this important disparity of accuracy and the fact that CCD methods is more user-friendly for design, Fuchs et al. recommend the CCD method as the basis for the design of fastenings. Since the publication of that paper, the CCD method has been integrated as part of the provisions for design in ACI 318-08 Appendix D.

2.3 State-of-the-art: literature review of previous research

Oehlers and Sved (1995) presents a mechanics-based analysis and explanation of composite beams with limited-slip-capacity shear connectors. A procedure is developed that can be used to design composite steel-concrete beams with very low (< 60%) degrees of shear connection, yielding good correlation to published data.

Burnet and Oehlers (2001) presents an analysis procedure for determining the flexural capacity of a partial-composite steel-concrete beam. A design procedure presented allows for the elastic, elastic-plastic, and plastic properties of the beam section and for both strength and ductility of the shear connectors. A distinction is made

between the slip capacity of the shear connectors that is required in order to reach the ultimate flexural strength of the composite beam and that capacity that is required in order to ensure full plastic deformation of the member. This allows for the prevention of premature shear connectors fracture and, therefore, a ductile failure mechanism to occur.

Shirvani et al. (2004) is the first in a coupled set of journal papers regarding breakout capacity of anchors in concrete, this one focusing on tension. The study presents a probabilistic evaluation of the 45-degree cone method, the CCD method, and a theoretical CCD method. Each predictive method was evaluated for static and dynamic loading in cracked and uncracked concrete by comparing to observed capacities concrete and by Monte Carlo analyses. The CCD and theoretical CCD methods had a lower probability for failure under known loads than the 45-degree method, particularly for deeper embedments. The CCD method generally exhibited a lower probability of brittle failure independent of load than the 45-degree and theoretical CCD methods. The theoretical CCD method gave some results that were more accurate than the two traditional methods, but there are not enough reasons to use over this method over the CCD method. One problem with the theoretical CCD method is that the exponent for the effective embedment at deeper embedments produces higher probabilities of failure than the CCD method, and the difference is not justified by experimental data.

Muratli et al. (2004) is the second in the coupled set of journal papers regarding breakout capacity of anchors in concrete, this one focusing on shear. A database of existing experimental data on shear connectors was assembled and divided into static or dynamic loading and cracked or uncracked specimen. Calculations were completed for the concrete breakout capacity per the 45-degree method, the CCD method, and a variation on the CCD method and compared to the assembled database. The study found that the CCD method is more reliable than the 45-degree method and can be used as a design tool for both CIP and post-installed connectors. The study also notes the shear breakout capacity of CIP connections is 20% higher under dynamic loading when compared to static loading and that the breakout capacities of post-installed connections are roughly 10% less than CIP connections.

Badie et al. (2006) provides a thorough review of the state-of-the-art of accelerated bridge deck construction methods is reviewed in a recently published report by the National Cooperative Highway Research Program (NCHRP). Research and case studies are presented in this document and provide a description of several methodologies for accelerated construction. Guidance is also provided to overcome the following challenges with full-depth bridge deck construction: adjustment of panel grading to meet construction tolerances, methodologies to provide structural compatibility between the girders and bridge deck, and performance of different cementitious grouts needed for the accelerated bridge deck systems.

Scholz et al. (2007) provides an introductory review of the performance of steel shear connectors and a thorough review of the effects of cementitious grout properties within a full-depth precast deck panel connection to a concrete girder in a recent report by the Virginia Transportation Research Council (VTRC). From the results of a series of grout properties tests and coupon push-off tests, a recommended grout specification for the Virginia Department of Transportation and a shear connection design with a fatigue check per AASHTO LRFD are presented. The effectiveness of several roughening techniques are reviewed and the impacts of a full-depth precast panel on a project's cost and timeline are presented. A method is also presented for calculating a coefficient of friction for shear connections by plotting the shear stress versus the clamping stress for each test at a point just past peak loading. Scholz et al. then propose that the AASHTO LRFD equation for the nominal shear resistance of the interface plane (Equation (1) in this thesis) be uncoupled and rewritten as:

$$V_{ni} = max \left| \begin{matrix} cA_{cv} \\ \mu(A_s f_y + P_n) \end{matrix} \right. \tag{7}$$

where c is cohesion factor (75 psi), A_{cv} is the concrete shear interface area, μ is taken as 0.9 for grout on concrete interface and 0.6 for grout on steel interface, A_s is the area of shear connector crossing interface, f_y is connector yield stress, and P_n is additional normal force. While this proposed calculation method for connection shear resistance exhibits good correlation with the test data presented, an artificial clamping force introduced by the experimental test setup is not present in an actual structural

connection. Thus the shear connection has been successfully isolated for experimentation but at the expense of a more holistic model of an actual structural connection.

Kwon et al. (2007) is a study by the Center for Transportation Research (University of Texas at Austin) that reviewed 11 different options for post-installing shear connectors in existing bridges with a deck system consisting of a non-composite cast-in-place slab on steel girder. After analyzing the results from a series of full-scale static, high-cycle, and low-cycle fatigue tests, the study concluded that post-installing shear connectors in these non-composite systems can substantially and economically increase the strength and stiffness of the bridge, increasing the load capacity on the order of 40-50%. The most promising anchors from the testing were double-nut bolts, adhesive anchors, and high-tension friction bolts. The study recommends computing the static strength of post-installed anchors as:

$$Q_u = 0.5 f_u A_s \tag{8}$$

where Q_u is the ultimate shear strength, f_u is the ultimate strength of the post-installed anchor, and A_s is the cross-sectional area of the post-installed anchor.

Xue et al. (2008) presents the results of 30 pushout tests of steel-concrete composite beams with headed stud connections in an effort to examine the effects of stud diameter and height, concrete strength, stud welding technique, transverse reinforcement on shear failure load. The following conditional equation was developed to improve calculations and compared to the various current equations (including Equation (6) from the AASHTO LRFD Bridge Specification and AISC-13):

$$P_u = 3\lambda A_s f_u \left(\frac{E_c}{E_s}\right)^{0.4} \left(\frac{f_{cu}}{f_u}\right)^{0.2} \tag{9}$$

$$where\ \lambda = \begin{cases} 6 - \dfrac{H}{1.05d} \\ 1.0 \\ \dfrac{H}{d} - 6 \end{cases} \quad if \begin{cases} \dfrac{H}{d} \le 5 \\ 5 \le \dfrac{H}{d} \le 7 \\ \dfrac{H}{d} \ge 7 \end{cases}$$

where P_u is the maximum shear load, A_s is the cross-sectional area of the stud, f_u is the ultimate tensile strength of the stud, E_c is the modulus of elasticity of the concrete, E_s is the modulus of elasticity of the stud, f_{cu} is the compressive strength of concrete cubes, f_u is the ultimate tensile strength of the stud, H is the stud height, and d is the stud diameter. While the study's results show an impressive correlation with experimental results, the λ factor does not take into account stud connectors with an H/d that is significantly more than 7.0, as is the case in the experiments conducted for this thesis. Clearly there is an implied limit that should be specified to avoid inadvertent application of the equation to a connection that it does not accurately model.

A number of published works are concerned with the low- and high-cycle fatigue resistance of shear connections, primarily with steel-concrete composite beams. Though these do not directly pertain to the scope of this thesis, they were reviewed in order to explore the potential for future application and research. Works reviewed in this area include *Slutter and Fisher (1966)*, *Oehlers (1990)*, *Oehlers (1995)*, *Gattesco et al. (1997)* , and *Oehlers et al. (2000)*.

CHAPTER III
EXPERIMENTAL INVESTIGATION

3.1 Scope

This chapter details experimental tests performed, including the shear connections tested, experimental test setup, specimen reinforcing details, construction and testing procedures, and specimen material properties.

3.2 Experimental plan

A total of 24 tests, were conducted in two parts to compare the performance of various connection types, number of connectors, type of grout, haunch height, and surface roughness. Tests #1-13 were conducted first, and tests #14-24 were prompted based on the system performance from the first set of tests. This ultimately yielded 16 pre-installed (precast) and 8 post-installed specimens.

Of the 16 pre-installed (precast) shear connection specimens tested, 12 were tested for validation of the TxDOT design—two tests for each of the two threaded rod connection options and the CIP control, each having haunch heights of 51 mm (2.0 in.) and 89 mm (3.5 in.). In order to provide supplementary information, three additional specimens were tested with a bolt with a coupler connection and a single additional specimen was tested with two R-bars grouted in a precast pocket.

The eight specimens assembled with post-installed shear connectors were tested in order to investigate the effects of several variables: types of post-installation connections, surface roughness of the mating concrete faces in the connection, grouping effects, and alternative grouts. Having post-installed shear connectors that have a comparable performance to pre-installed shear connectors provide on-site construction options for misaligned pockets and connectors, or for deliberate design to reduce the complexity of precast components. In order to maximize the variety of aspects investigated with these tests, no two specimens were identical, thus providing a broad exploratory look at a myriad of options that are available to designers.

3.3 Testing matrix

A testing matrix was developed to account for the 24 shear specimens tested. The nomenclature for the test specimens was based on the number of connectors within a specimen, connector type, whether the specimen was cast with a 51-mm (2.0-in.) or 89-mm (3.5-in.) haunch, and test number reference. For brevity in discussion and figures, an alias system was developed to provide all pertinent information on the specimen's components and assembly in a shortened form. Fig. 2 presents a key to show the designation of that specimen alias. Table 1 shows the testing matrix for all 24 shear specimens tested.

3.4 Design of experiment

The experiment was designed first and foremost with a concerted effort to produce an experimental test setup that represents the full-scale structure in a holistic manner. The design of the shear test specimens was developed in conjunction with the design and casting of the full-scale testing components for a companion portion of the Texas Transportation Institute (TTI)-TxDOT research project to maximize efficiency and minimize experimental differences. To accommodate the two 2.4-m (8-ft.) full-depth precast panels, 4.9-m (16-ft.) girders were cast for use in the full-scale test; the same 4.9-m (16-ft.) design was made into 1.2 m (4-ft.) quarter-beams for the purposes of the shear testing. Full-depth deck specimens for the shear tests were cast with a thickness of 203 mm (8 in.) and 178- x 254-mm (7- x 10-in.) pockets to match the design of the full-depth precast panels. The shear test panels were cast nominally 0.6-m (2-ft.) square to allow for two specimens to be tested on each 1.2-m (4-ft.) beam.

For the experimental test setup, a 2670-kN (600-k) actuator was used to push off from a reaction column that was prestressed to the laboratory strong floor to produce the shear force. The applied force was transferred to the deck portion of the specimen via two W14x109 spreader beams connected by four high-strength tie-rods. To minimize sliding and uplift, each shear test beam was anchored down to the strong floor of the

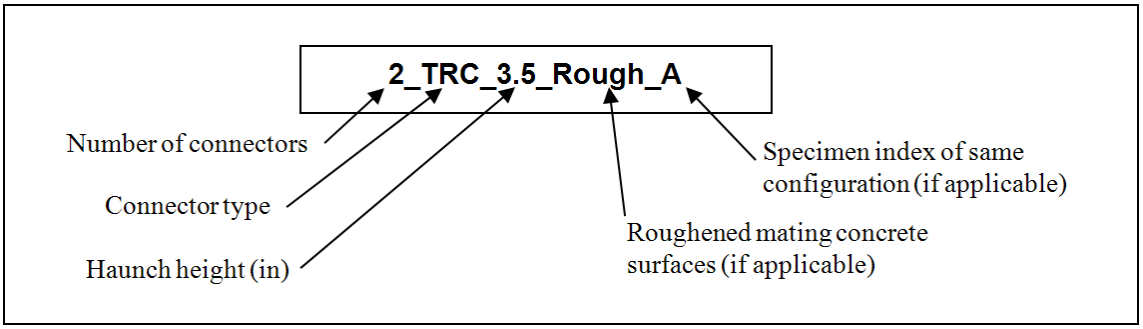

Fig. 2—Specimen alias designation key.

Table 1—Matrix of shear test specimens

Test #	Haunch height, mm (in.)	Shear test beam detail	No. of con-nectors	Connector nominal diameter, mm (in.)	Type	f'c for grout/ concrete in haunch, MPa (psi)	Specimen alias
1	51 (2.0)	CIP	4	13 (0.5)	R	62.68 (9091)	4_CIP_2.0_A
2	51 (2.0)	CIP	4	13 (0.5)	R	62.68 (9091)	4_CIP_2.0_B
3	51 (2.0)	TRC	2	25 (1.0)	TR	48.42 (7023)	2_TRC_2.0_A
4	51 (2.0)	BC	2	25 (1.0)	TR	41.78 (6059)	2_TRC_2.0_B
5	51 (2.0)	TR	2	25 (1.0)	TR	41.78 (6059)	2_TR_2.0_A
6	51 (2.0)	TR	2	25 (1.0)	TR	41.78 (6059)	2_TR_2.0_B
7	89 (3.5)	TRC	2	25 (1.0)	TR	42.28 (6132)	2_TRC_3.5_A
8	89 (3.5)	TRC	2	25 (1.0)	TR	42.28 (6132)	2_TRC_3.5_B
9	51 (2.0)	R	4	13 (0.5)	R	50.86 (7377)	4_R_2.0
10	89 (3.5)	TR	2	25 (1.0)	TR	42.75 (6200)	2_TR_3.5_A
11	89 (3.5)	TR	2	25 (1.0)	TR	42.75 (6200)	2_TR_3.5_B
12	89 (3.5)	CIP	4	13 (0.5)	R	39.34 (5706)	4_CIP_3.5_A
13	89 (3.5)	CIP	4	13 (0.5)	R	39.34 (5706)	4_CIP_3.5_B
14	51 (2.0)	BC	1	25 (1.0)	BC	45.48 (6594)	1_BC_2.0_A
15	51 (2.0)	BC	1	25 (1.0)	BC	44.94 (6517)	1_BC_2.0_B
16	51 (2.0)	BC	2	25 (1.0)	BC	44.94 (6517)	2_BC_2.0
17	51 (2.0)	Steel Plate	2	22 (0.875)	NS	44.94 (6517)	2_NS_2.0
18	51 (2.0)	Steel Plate	3	22 (0.875)	NS	44.94 (6517)	3_NS_2.0
19	51 (2.0)	Post-Installed	1	25 (1.0)	TRS	40.23 (5833)	1_TRS_2.0_Rough
20	51 (2.0)	Post-Installed	2	25 (1.0)	TRS	40.23 (5833)	2_TRS_2.0_Rough
21	51 (2.0)	Post-Installed	1	25 (1.0)	KB	40.23 (5833)	1_KB_2.0
22	51 (2.0)	Post-Installed	1	25 (1.0)	TRE	40.23 (5833)	1_TRE_2.0
23	51 (2.0)	Post-Installed	1	25 (1.0)	TRS	42.17 (6114)	1_TRS/AG_2.0_Rough
24	51 (2.0)	Post-Installed	1	25 (1.0)	TRS	40.23 (5833)	1_TRS_2.0

laboratory with high-strength prestressing threadbar. A wood reaction block between the shear test beam and the column provided additional lateral reaction to inhibit specimen sliding. Thus the entire experimental test setup was completed without introducing an artificial clamping force across the shear interface. Photographs and a drawing of the experimental test setup are shown in Fig. 3.

Fig. 4 shows a strut-and-tie model of the flow of the internal and external forces in the specimen during testing. The prestressed anchoring force, P, was constant for all tests. Thus when the shear force, F, was applied at a constant height above the laboratory floor, y, the resultant of the prestressing force developed an eccentricity, e. By solving for equilibrium of moments about point O, the relationship between the quantities is found as

$$Fy = Pe \tag{10}$$

During testing the windward side of the beam had a tendency to lift up, so the distribution of the reaction force from the floor is the triangle shown in Fig. 4 with a maximum floor stress of σ that can be calculated as

$$\sigma = \frac{3P^2}{a(bP-2Fy)} \tag{11}$$

where a is the width of the shear test beam. Thus for the expected peak loading of shear specimens, where F=355 kN, y=500 mm, P=530 kN, a=300 mm, and b=1110 mm, σ is found to be 12 MPa, a reasonable value to maintain the integrity of the experimental test setup and avoid any damage of the laboratory floor.

3.5 Fabrication of specimens

3.5.1 Shear test beam reinforcing details

During the construction process of a prototype bridge, girder curvature and deck grading are expected to vary the haunch depth some 40 mm to 100 mm. Therefore, the pre-installed connector shear tests investigated the connection strength using both 51-mm (2.0-in.) and 89-mm (3.5-in.) haunch specimens while the post- installed connector shear tests investigated the connection strength with only a 51-mm (2.0-in.) haunch but with several parametric combinations per the experimental plan.

(a)

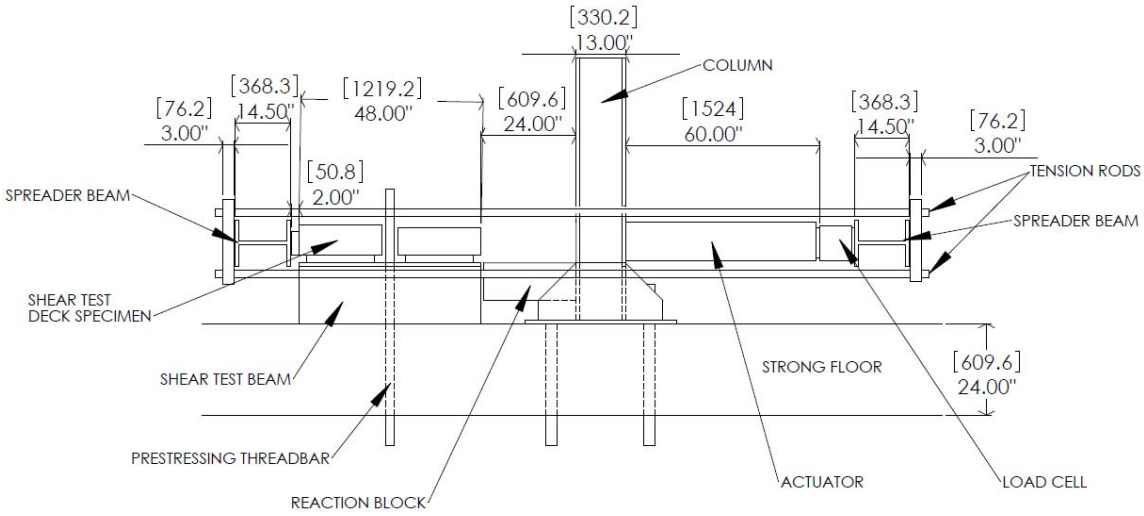

(b)

Fig. 3—Experimental test setup. (a) photograph from laboratory floor; (b) side elevation.

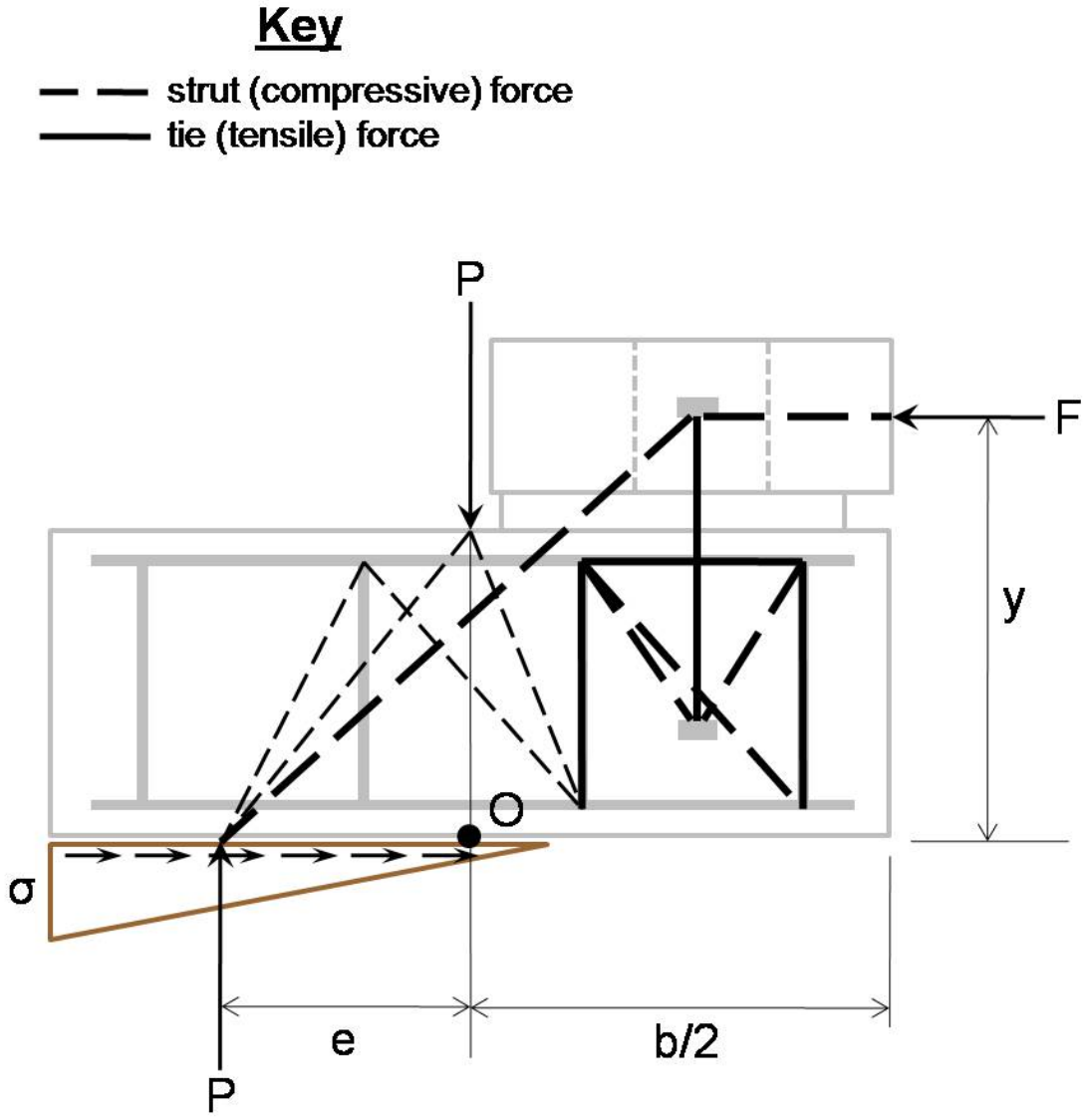

Fig. 4—Strut-and-tie model of the shear test setup.

The shear test beams for the 89-mm (3.5-in.) haunch specimens were cast 38 mm (1.5-in.) shorter those for the 51-mm (2.0-in.) haunch specimens so that the assembled specimens all placed the shear test deck at the same height, permitting use of the same test setup without modifying the height of the line of action. The same reinforcement was used in the shear test beams for both of the pre-installed (precast) options for each of the haunch heights as shown in Fig. 5. Detailing of each of the components and specimen types is explained in greater detail below.

3.5.2 Shear test specimen connection details

Four shear specimens were assembled using a CIP connection matching that of the current-practice R-bars with a second stage concrete pour. These specimens were used to verify the test setup and to serve as the control for the experiment. As required by TxDOT's standard bridge drawings, an extension of the shear stirrups was added for the CIP specimens when the haunch height was greater than or equal to 76 mm (3.0 in.). Fig. 6 shows the details of the pre-installed (precast) shear connections of the CIP specimens for the 51-mm (2.0-in.) and 89-mm (3.5 in.) haunches.

In order to provide a shear connection on the exterior beams through the full-depth precast overhang panels, the TxDOT design of the prototype bridge specified two pre-installed (precast) shear connection options, both using 25-mm (1-in.) diameter high-strength threaded rod (ASTM A193 B7) and high-strength nuts (2H). Option 1 (TRC) utilized a coupler that is precast flush with the top of the girder with a bottom anchoring rod extending into the girder, a second top rod that is inserted during the construction process, and a nut installed at the end of each rod for improved anchorage. Option 2 (TR) used a continuous rod through the top of the girder with a nut at the top and another at the bottom for improved anchorage. This option simplifies the casting process but reduces the flexibility of the construction process. Fig. 7 shows the details (beam cross-sectional view) of the TRC and TR shear connections for the 51-mm (2.0-in.) and 89-mm (3.5-in.) haunches.

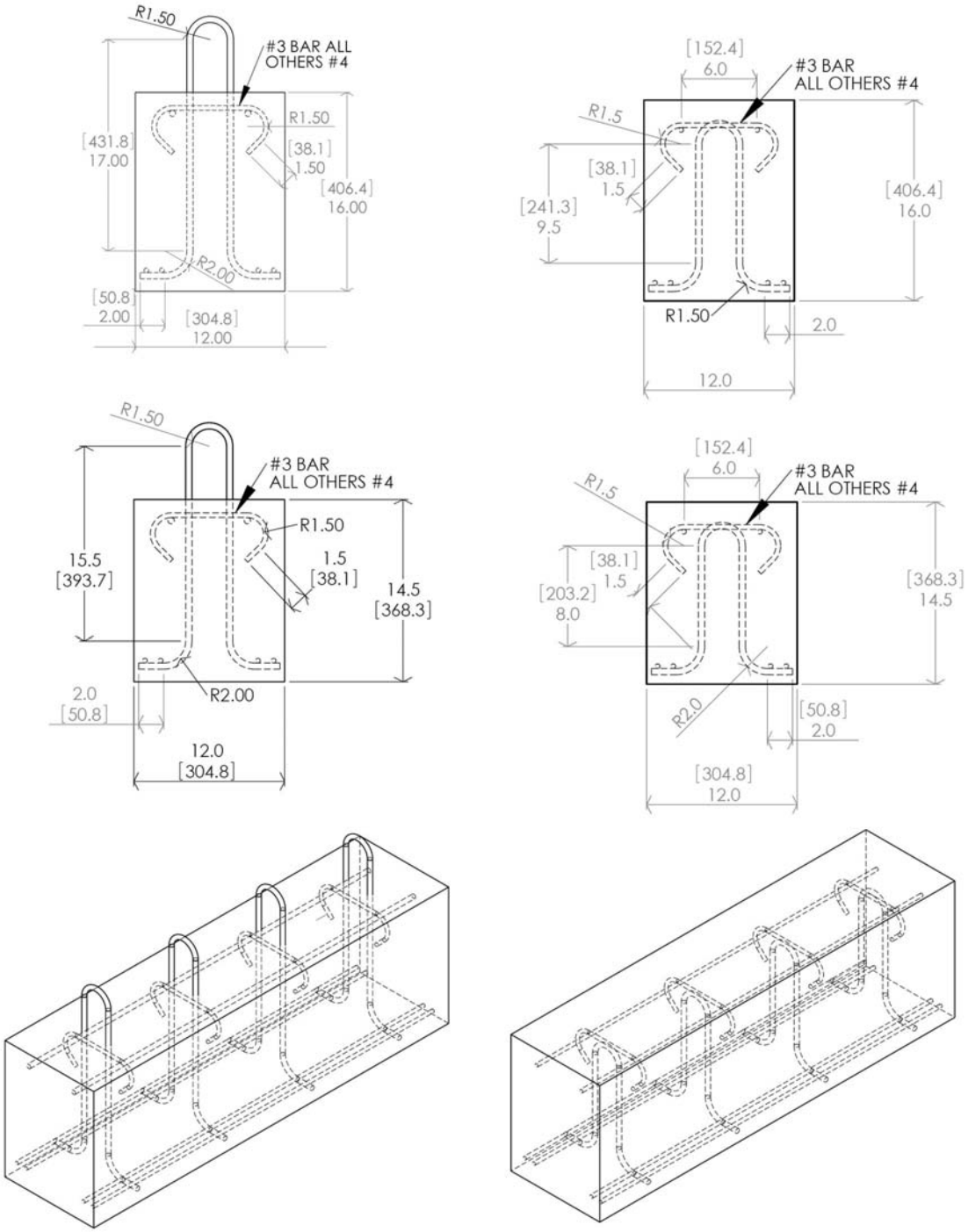

Fig. 5—Reinforcing details for shear test beams. Clockwise from top-left: cross-section of 51-mm (2.0-in.) haunch CIP, cross-section of 51-mm (2.0-in.) haunch precast, cross-section of 89-mm (3.5-in.) haunch precast, 3-D view of 51-mm (2.0-in) haunch precast, 3-D view of 51-mm (2.0-in) haunch CIP, and cross-section of 89-mm (3.5-in.) haunch CIP.

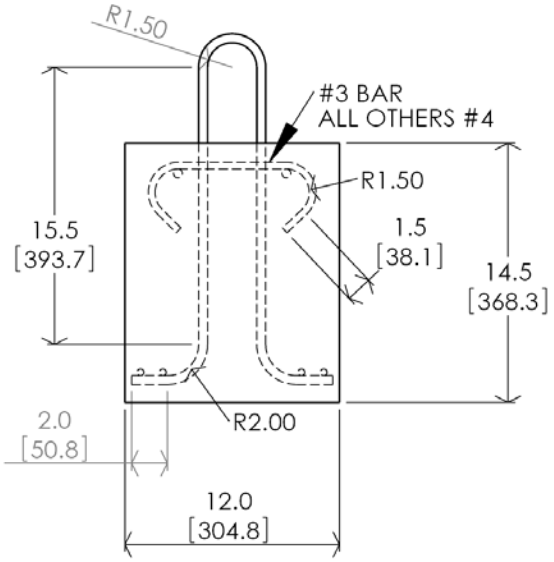

(a) 51-mm (2.0-in.) haunch

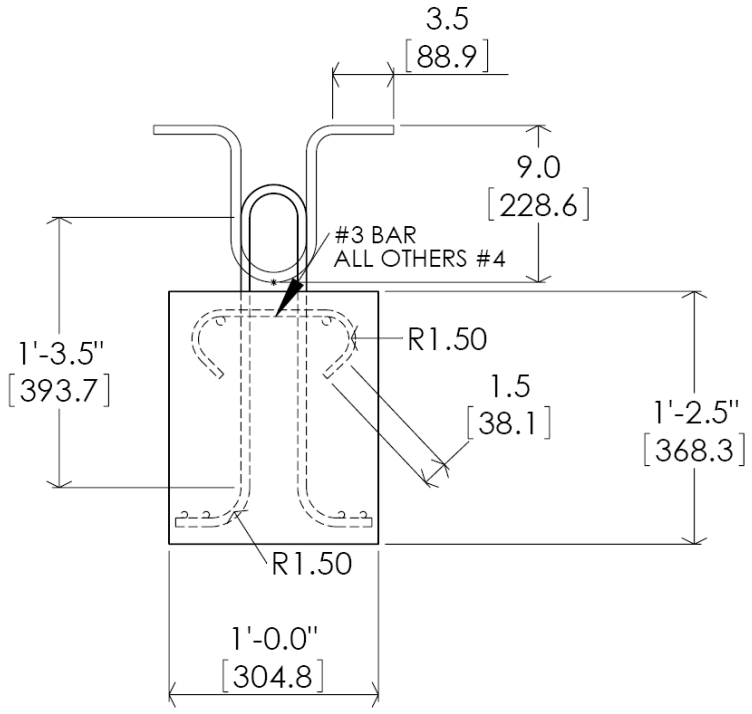

(b) 89-mm (3.5 in.) haunch

Fig. 6—CIP details of beam-to-slab shear connections.

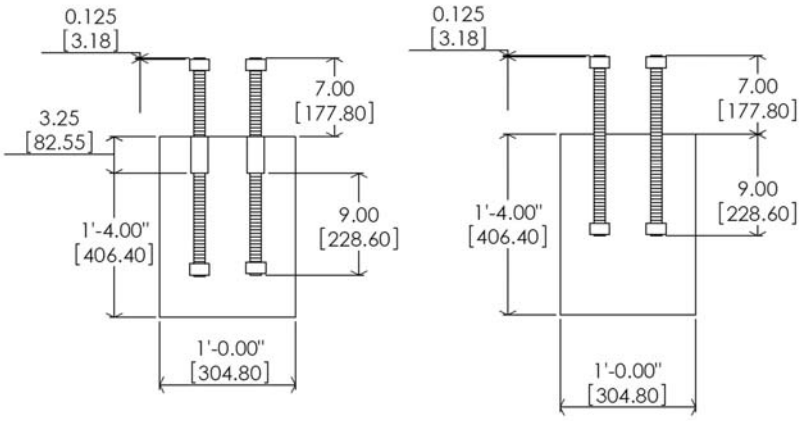

Option 1 (TRC) *Option 2 (TR)*

(a) Pre-installed (precast) shear connectors for 51-mm (2.0-in.) haunch

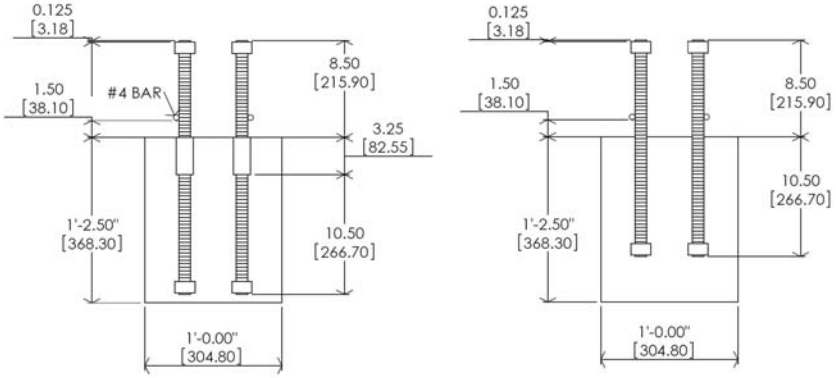

Option 1 (TRC) *Option 2 (TR)*

(b) Pre-installed (precast) shear connectors for 89-mm (3.5 in.) haunch

Fig. 7—Beam cross-sectional views and photographs of the TRC and TR shear connections tested.

As an alternative pre-installed connector, 25-mm (1-in.) diameter high strength bolt (SAE Grade 8) in a coupler was also tested for future consideration based on its performance. A photograph of a BC specimen is shown in Fig. 8.

For the eight specimens with post-installed shear connectors, the haunch height was kept constant at 51 mm (2.0 in.), but the post-installed shear connections were made in a variety of ways as shown in Fig. 9. The Nelson stud (NS) specimens were constructed using studs welded to the top and bottom of 12-mm (0.5-in.) thick steel plates that were cast in the shear test beam. Four of the post-installed connectors were TRS, assembled by coring a 51-mm (2-in.) diameter hole 229 mm (9 in.) deep in the shear test beam, filling the hole with a proprietary grout (SikaGrout® 212) with a water/powder (w/p) ratio of 0.16 and inserting a TR. The remaining two post-installed specimens utilized HILTI connection systems: the Kwik-Bolt 3 mechanical anchor (KB) and a B7 TR installed in HY150-Max epoxy (TRE), both installed as per the manufacturer's instructions.

3.5.3 Shear test deck component

Identical precast shear deck components with pockets were used in all 20 of the non-CIP specimens. For the pre-installed (precast) shear test deck components, #D12 (#4) longitudinal deformed reinforcing bars are expected to be added on the outside of the threaded rod, similar to an existing detail for casting additional concrete atop precast girders in TxDOT standard bridge drawings. The reinforcing details of these components shown in Fig. 10 match those of the full-scale precast overhang panels, utilizing #D12 (#4) bars in place of the 10 mm (#3) prestressing strands as prescribed.

The deck reinforcing details of the four CIP specimens are similar to the precast shear deck specimens described above, but there were two key differences because the CIP specimens model the shear connection of the interior girders. First, all of the bars are evenly spaced because there were no pockets to accommodate. Second, the bottom transverse steel is not continuous, simulating the edges of the two partial-depth precast panels resting on the girder. Fig. 11 is a photograph of the deck reinforcing of a typical CIP specimen.

Fig. 8—Photograph of BC pre-installed shear connection specimen.

(a) NS connectors

(b) single TRS connector

(c) single KB connector

(d) single TRE connector

Fig. 9—Photographs of post-installed shear connections specimens.

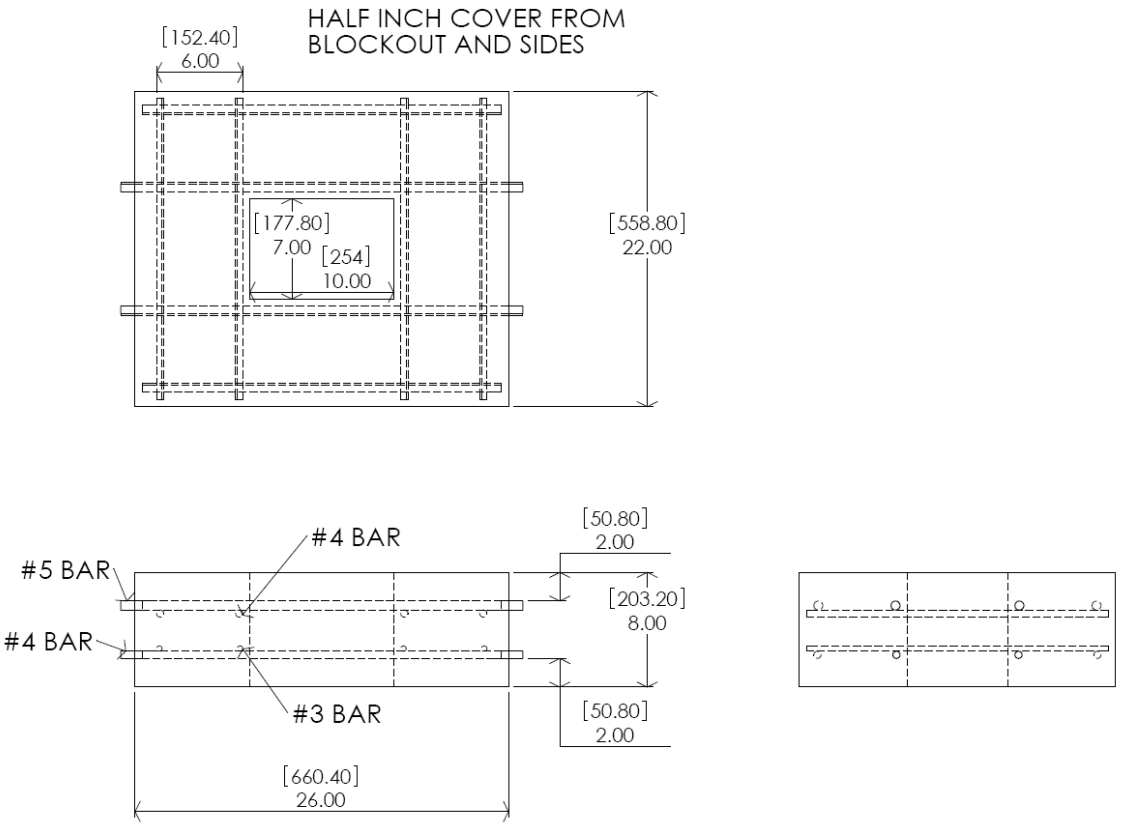

Fig. 10—Typical reinforcement layout of precast shear deck specimens.

Fig. 11—Photograph of typical reinforcing layout of a CIP shear test deck specimen.

3.6 Construction process and testing procedure

The construction and testing procedure followed for the testing of all shear test specimens is outlined as follows:

1. Cast shear test beams and decks.
2. Grout/cast completed test specimens (two per shear test beam).
3. Assemble shear test frame.
4. Insert a fully constructed test specimen into the shear test frame.
5. Load test frame to 45 kN (10 kips) to close any gaps.
6. Post-tension the tie-down high-strength prestressing threadbar. This is located at the center of each shear test beam. Apply a force of 530 kN using a center-hole jack system, and then remove the test frame load from step 5.
7. Load test frame continuously at approximately 0.67kN/s until specimen failure or the clearance limit is reached at approximately 32-mm deformation.
8. Unload test frame and shear test beam center anchor.
9. Turn shear test beam 180° for second specimen and repeat 5-8.
10. Repeat 4-9 for testing remaining shear specimens.

All non-CIP shear test specimens were assembled in the same manner. A 51-mm (2.0-in.) wide strip of stiff foam (Dow 40) was bonded to the shear test beam using a plastic adhesive (3M Scotch-Grip 4693). Another coating of the adhesive was applied to the top of the foam, and the shear test deck was placed on top. After 20 to 30 minutes of curing, the haunch grout was mixed and poured into the haunches through the pockets up to a level of approximately 25 mm above the bottom of the shear test deck to ensure the haunch was completely filled. After the haunch grout had reached initial set (approximately five hours), the pocket grout/concrete was added and the specimen's surface was finished to as smooth a surface as possible.

The CIP shear test specimens were cast using formwork constructed around a precast beam. The same 51-mm (2.0-in.) wide strips of stiff foam used in the non-CIP specimens were used in the CIP specimens to create a 51-mm (2.0-in.) or 89-mm (3.5-

in.) haunch. The concrete for the CIP decks was then placed, vibrated, and finished in the same manner as the precast deck specimens.

The key measurement acquired from the shear tests was the displacement of the shear test deck specimen relative to the shear test beam. This was accomplished with a linear variable differential transducer (LVDT) mounted on each longitudinal face of the shear test beam pushing against a reaction angle mounted to the bottom of the shear test deck specimen and aligned with its transverse centerline. By utilizing an LVDT on each side, the amount of skew that the shear test deck specimen experienced during loading could be assessed and properly accounted for. Two string potentiometers were attached to the vertical face of the shear test beam and to the soffit of the deck panel. These potentiometers indicate the degree of uplift and rotation of the deck panel unit with respect to the support beam. A photograph of the instrumentation on the specimen is shown in Fig. 12. A 9000-kN capacity load cell was attached in series to the actuator to provide accurate measure of the actual load applied to the shear test frame and shear test specimen. Half-bridge strain gauges were attached to one of the threaded rods or stirrup legs to provide information on the strain and tension the shear connector experienced during the test.

3.7 Materials

Concrete was provided by Transit Mix (Bryan, Texas) to match the specifications of TxDOT Type "S" mix, including a 100-mm slump and specified 28-day strength of 28 MPa (4000 psi). Standard grade 60 rebar was used throughout reinforced concrete components, with 10-mm (#3), 12-mm (#4), and 16-mm (#5) bars used as shown in the reinforcing details.

A proprietary grout (SikaGrout® 212) was used for the assembly of the majority of the shear test specimen components, utilizing two different mixes. A 0.19 w/p mix was used for filling the haunch for its maximum strength while providing minimum flow characteristics to fill the haunch. To fill the pockets of the shear test specimens, a 0.16 w/p was initially used, but issues with subsidence cracking and the relative expense of

Fig. 12—Exterior specimen instrumentation.

the grout led to later specimens' pockets being filled with deck concrete from another pour. An alternative grout developed by others in a companion project was used in both the haunch and pocket of one of the research specimens to provide a structural test of the design aspects of the grout.

Regardless of the material, the concrete/grout compressive strength achieved for each component of the shear test specimen (haunch, deck, deck pocket, and beam) was determined on the day of testing. A summary of these strengths is presented in Table 2. Further information regarding the concrete and grout mixes used can be found in Appendix B, Additional Material Testing Information.

Although each type of shear connector is manufactured with specified minimum yield and ultimate strengths, coupon tensile tests were conducted for each of the connector types to establish the actual yield and ultimate strengths of each of the materials (summarized in Table 3). These values and the stress-strain profiles in Fig. 13 obtained from the tensile tests allow for more accurate analysis and comparison of the behavior of the various connectors during the shear tests.

Table 2—Specimen component compressive strengths

Test #	Specimen alias	Haunch	Shear test deck		Shear test beam
		f'c, MPa	f'c - deck, MPa	f'c - pocket, MPa	f'c, MPa
1	4_CIP_2.0_A	62.7	62.7	62.7	50.6
2	4_CIP_2.0_B	62.7	62.7	62.7	50.6
3	2_TRC_2.0_A	48.4	62.7	57.3	40.9
4	2_TRC_2.0_B	41.8	55.0	36.9	43.0
5	2_TR_2.0_A	41.8	55.0	36.9	42.3
6	2_TR_2.0_B	41.8	55.0	36.9	42.3
7	2_TRC_3.5_A	42.3	55.0	36.9	42.3
8	2_TRC_3.5_B	42.3	55.0	36.9	42.3
9	4_R_2.0	50.9	62.7	57.3	43.0
10	2_TR_3.5_A	42.7	55.0	36.9	42.3
11	2_TR_3.5_B	42.7	55.0	36.9	42.3
12	4_CIP_3.5_A	39.3	39.3	39.3	42.3
13	4_CIP_3.5_B	39.3	39.3	39.3	42.3
14	1_BC_2.0_A	45.5	44.0	45.0	43.0
15	1_BC_2.0_B	44.9	62.7	57.3	43.0
16	2_BC_2.0	44.9	62.7	57.3	43.0
17	2_NS_2.0	44.9	62.7	57.3	43.0
18	3_NS_2.0	44.9	62.7	57.3	43.0
19	1_TRS_2.0_Rough	40.2	46.2	54.6	50.6
20	2_TRS_2.0_Rough	40.2	46.2	55.0	50.6
21	1_KB_2.0	40.2	65.4	55.0	50.6
22	1_TRE_2.0	40.2	65.4	55.0	50.6
23	1_TRS/AG_2.0_Rough	42.2	46.2	42.2	50.6
24	1_TRS_2.0	40.2	46.2	55.3	50.6

Table 3—Shear connector strengths

Connector Type	Specified tensile strength		Actual tensile strength	
	Yield, MPa	Ultimate, MPa	Yield, MPa	Ultimate, MPa
CIP	414	621	434	689
TR	724	862	826*	945*
BC	896	1034	982	1181
KB3	586	731	689	850
NS	352	448	362	541

* - average of four tests from different batches used

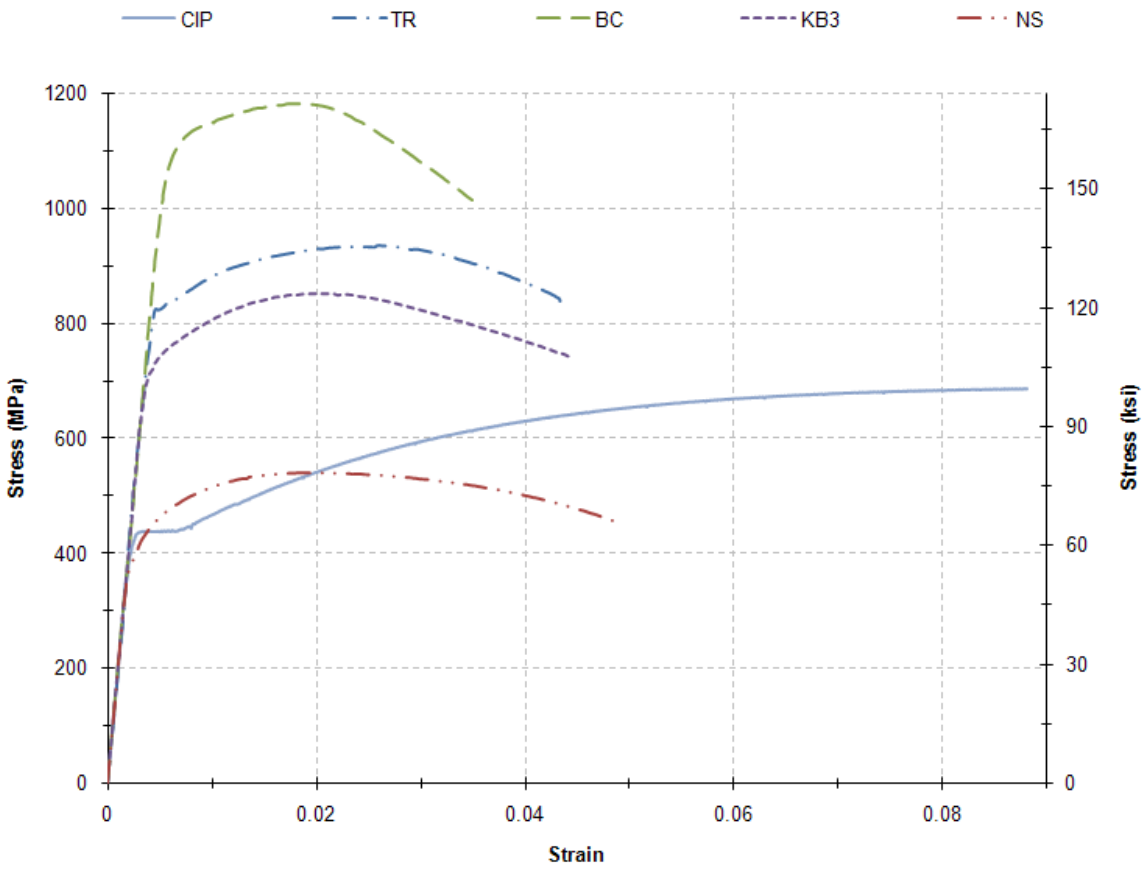

Fig. 13—Stress-strain behavior of the tested shear connectors.

CHAPTER IV
EXPERIMENTAL RESULTS

4.1 Introduction

This chapter presents the experimental data from the 24 shear tests performed, including a schematic that shows typical behavior and a table of key values. Also included is an explanation of the different failure mechanisms observed in the tests and representative photographs of specimens exhibiting each type of failure.

4.2 Raw experimental data

The experimental data from the interface shear (push-off) tests are intended to reveal the efficacy of the deck-haunch-beam system working as a composite system. The force-displacement behavior due to increasing lateral load on the system during experimentation was obtained for each of the connections and complied in Fig. 14 and Fig. 15. The ductility of the connection is also revealed in these plots. Fig. 16 shows an interpretive schematic to classify the performance of the connector based on its ductility. Connectors experiencing ultimate displacements less than 5 mm can be considered brittle with unsatisfactory ductility. Ultimate displacements in the range of 5 mm to 12 mm can be considered having satisfactory ductility, and connectors with displacements greater than 12 mm (0.5 in.) can be considered as ductile with superior ductility.

From the force-displacement plot of each specimen, the initial breakaway shear strength, post-breakaway resistance in terms of the implied coefficient of friction, and estimated displacement limits are determined. Two opposing strain gauges were attached to one connector within each test specimen to verify the tensile force in the connector. The data captured by the string potentiometers and LVDTs provided the numerical values for the relative displacements both horizontally and vertically, and enabled computations for the axial connector tension and implied coefficient of friction. Key points from the raw experimental data for all specimens corresponding to the labeled points in Fig. 16 are shown in Table 4.

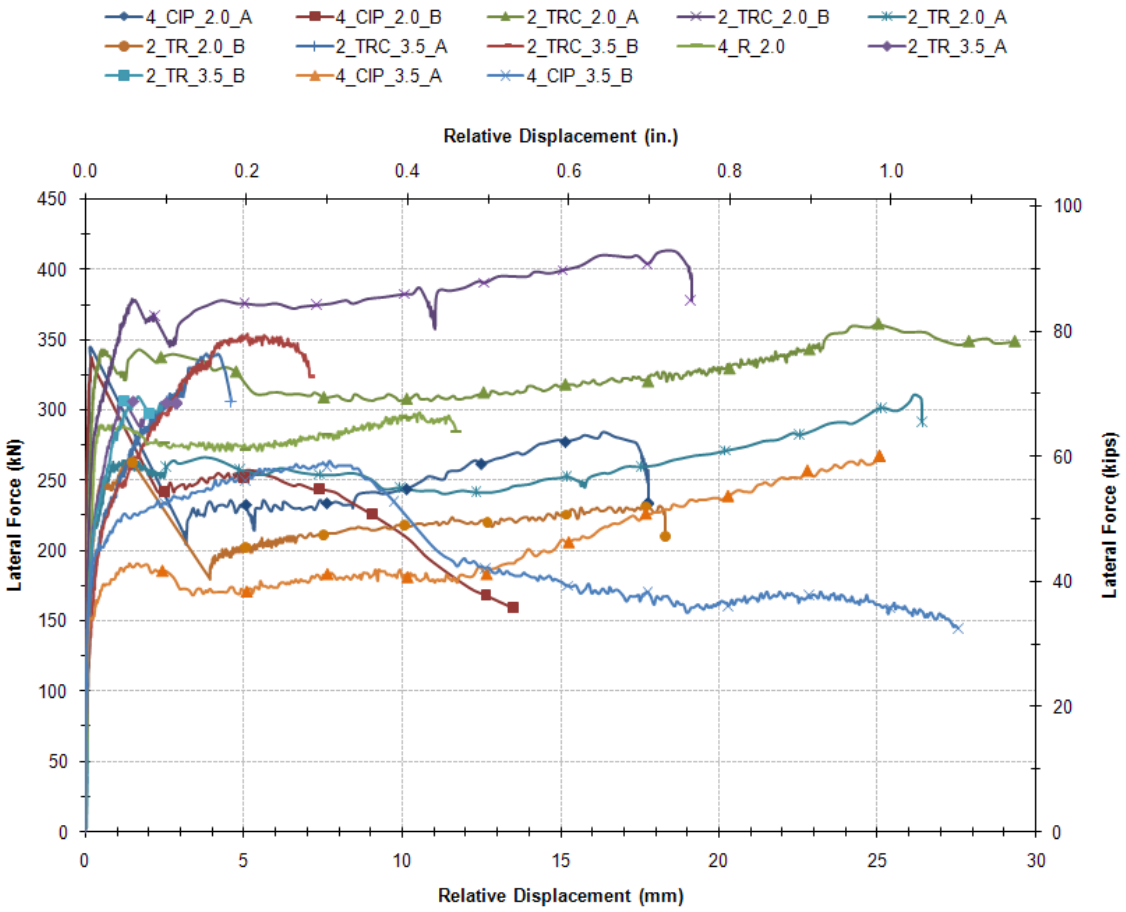

Fig. 14—Force-displacement plots for specimens #1-13.

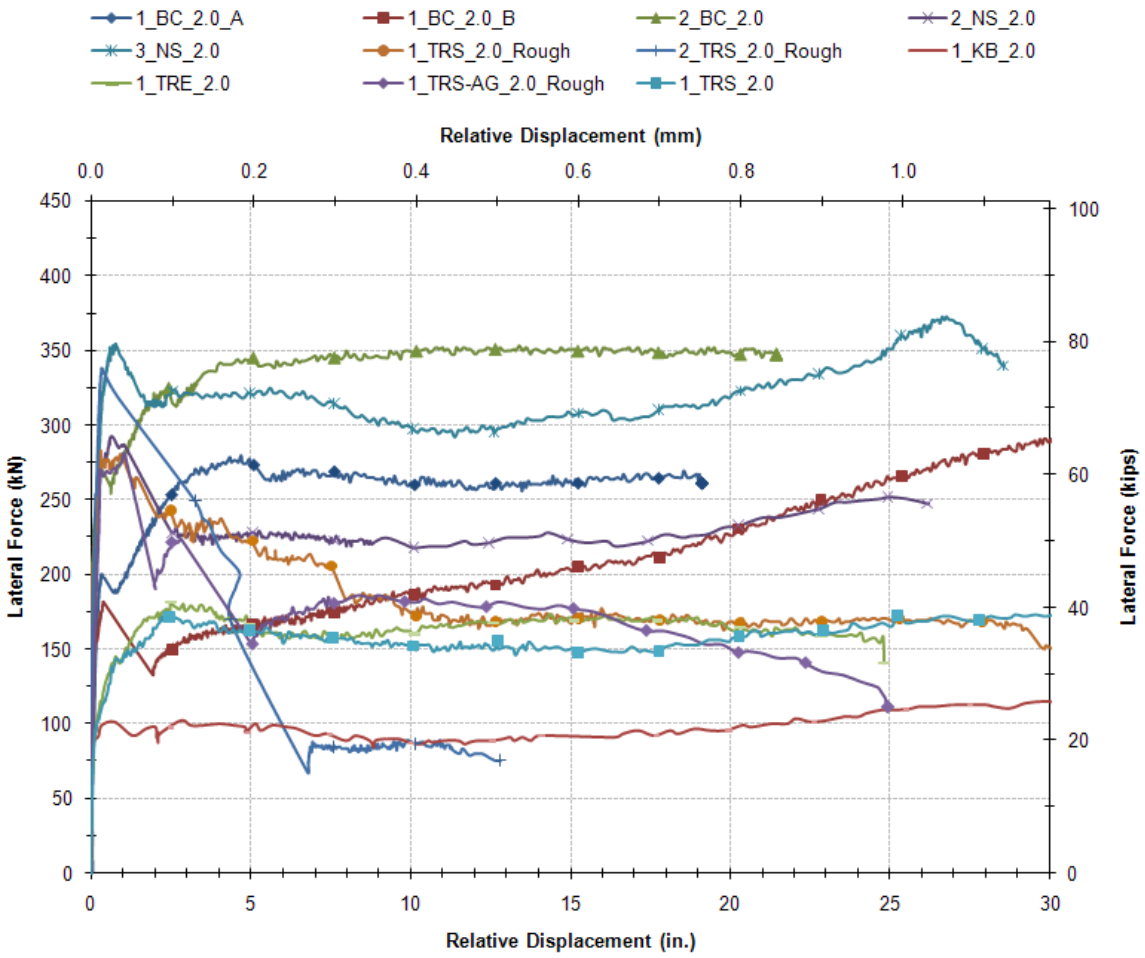

Fig. 15—Force-displacement plots for specimens #14-24.

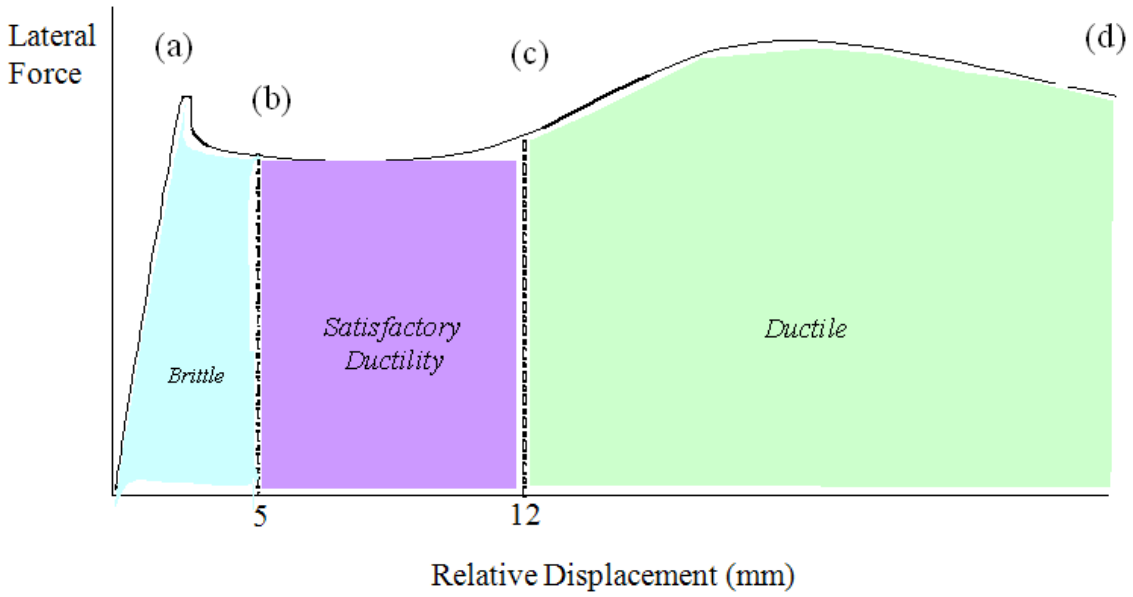

Fig. 16—Typical plot of lateral force versus relative displacement for shear specimens with critical parameters noted.

Table 4—Raw experimental data from all shear tests

Test #	Specimen alias	Initial peak displacement, mm (a)	Initial peak force, kN (a)	Force @ 5 mm, kN (b)	Peak load past initial, kN (c)	Ultimate displacement, mm (d)
1	4_CIP_2.0_A	0.203	342	227	285	18
2	4_CIP_2.0_B	0.203	338	258	258	30
3	2_TRC_2.0_A	1.676	342	311	360	40
4	2_TRC_2.0_B	1.473	378	374	414	19
5	2_TR_2.0_A	3.302	262	258	311	26
6	2_TR_2.0_B	1.422	262	200	231	18
7	2_TRC_3.5_A	4.166	338	285	338	10
8	2_TRC_3.5_B	5.105	356	351	356	9
9	4_R_2.0	0.864	289	271	298	26
10	2_TR_3.5_A	1.219	307	NA	298	2
11	2_TR_3.5_B	1.702	307	NA	307	3
12	4_CIP_3.5_A	1.397	191	173	271	35
13	4_CIP_3.5_B	0.356	200	254	258	30
14	1_BC_2.0_A	0.305	200	276	280	19
15	1_BC_2.0_B	0.406	182	156	294	36
16	2_BC_2.0	0.330	271	347	351	21
17	2_NS_2.0	0.635	294	227	294	26
18	3_NS_2.0	0.787	360	320	374	29
19	1_TRS_2.0_Rough	0.940	280	222	285	32
20	2_TRS_2.0_Rough	0.356	338	200	249	13
21	1_KB_2.0	2.108	93	98	120	32
22	1_TRE_2.0	0.787	147	165	182	25
23	1_TRS/AG_2.0_Rough	0.279	267	156	280	25
24	1_TRS_2.0	0.660	138	160	173	30

Note: NA = not achieved

4.3 Failure mechanisms

From shear testing, three classic failure mechanisms were observed: sliding shear, beam failure, and cone pullout. The first and most common was sliding shear. Typically, the rear third of the haunch separated and the yielding shear connector(s) clamped the deck down to the beam through the front two-thirds of the haunch, sliding with significant ductility. Fig. 17 contains photographs of several of the specimens that exhibited this sliding shear failure mechanism. Several of the sliding shear specimens also exhibited complete shearing of the connector(s): the photographs in Fig. 18 and Fig. 19 show two such specimens.

The second most common failure mechanism observed was brittle beam failure. This mechanism typically occurred suddenly at a low lateral load relative to the yield strength of the connectors because of insufficient hoopsets in the beam, as explained in Chapter V. Thus this failure mode gives an artificially low strength and very little ductility. Fig. 20 contains photographs of two of the specimens that exhibited this brittle beam failure mechanism.

The final failure mechanism observed was a cone pullout failure. This failure mechanism is similar to the brittle beam failure mechanism but exhibits significantly higher strength and more ductility prior to failure. Fig. 21 displays several photographs from one of the specimens that exhibited a cone pullout failure.

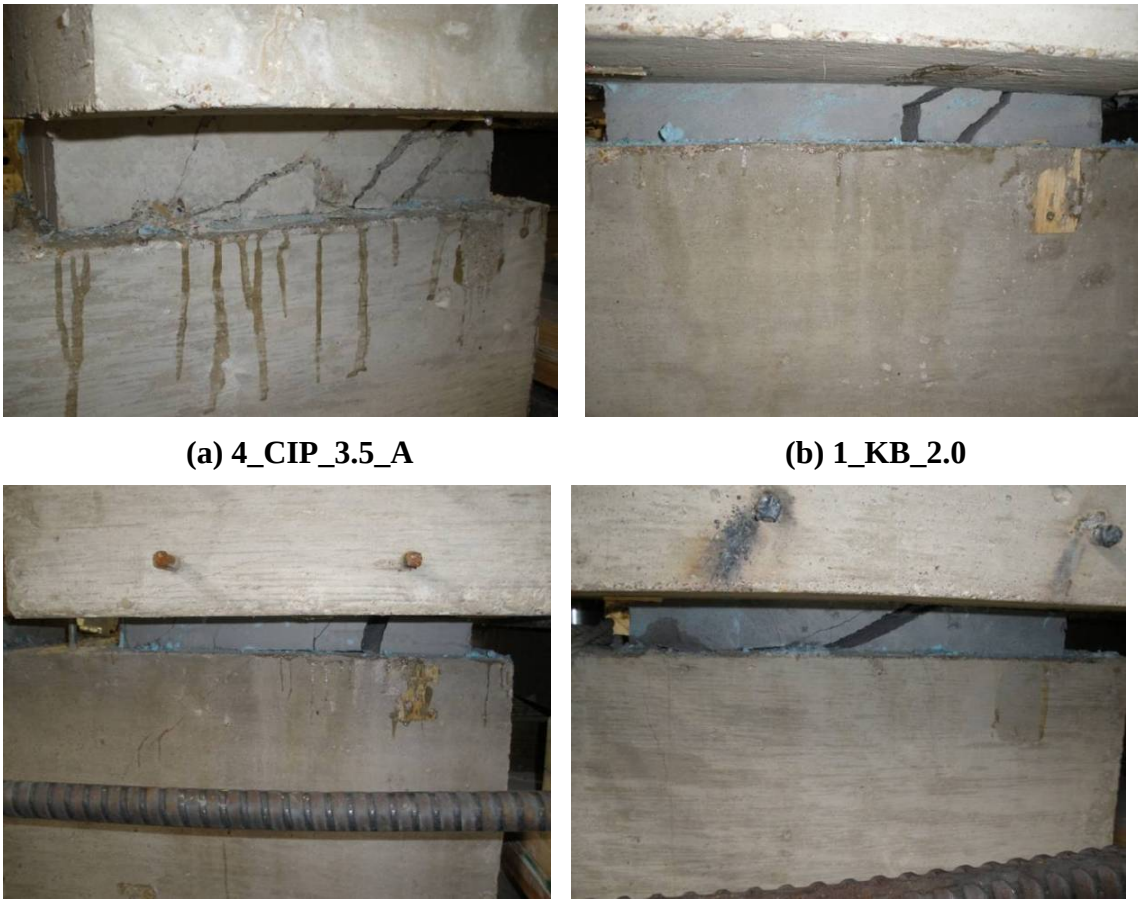

(a) 4_CIP_3.5_A **(b) 1_KB_2.0**

(c) 1_TRS_2.0 **(d) 1_BC_2.0_B**

Fig. 17—Examples of specimens that exhibited a sliding shear failure mechanism.

Fig. 18—2_NS_2.0 exhibited a sliding shear failure that resulted in both studs shearing.

Fig. 19—Photographs of 2_TRC_2.0_A after failure. After exhibiting sliding shear past 25 mm (1.0 in.) relative displacement, one of the threaded rods sheared at the top of the coupler and the beam cover concrete spalled off as the load was redistributed to the other connector.

(a) 2_TR_3.5_B

(b) 2_TRS_2.0_Rough

Fig. 20—Photographs of shear test specimens that exhibited a brittle beam failure.

Fig. 21—Photographs of the cone pullout failure exhibited by 2_BC_2.0.

CHAPTER V
ANALYSIS OF EXPERIMENTAL RESULTS

5.1 Introduction

This chapter presents an analysis of the experimental results of the 24 shear tests performed. The normalization method by which the data collected from a wide variety of specimens is compared is detailed and justified. The experimental results are then analyzed based the connection type, conventional R-bars, pre-installed, and post-installed. A series of studies on various parameters is presented to further explain the effects of those parameters on the behavior of the shear connection. Finally, an explanation of the premature failure of several specimens is presented and applied to a develop a simple, practical solution that is vital to successfully applying the full-depth precast panel construction technique.

5. 2 Normalization of data for analysis

In order to directly compare the behavior of the various shear connections tested, it was necessary to develop methods to take into account variations in specimen component properties. The primary value used to normalize the data from the shear tests was the yield force of the connector(s). This normalization assumes that after the initial breakaway due to the failure of the grout-concrete bond, the connector steel quickly yields because of the geometry of the loading and displacement. At this point, lateral resistance is provided by an effective friction coefficient between the concrete and grout and a clamping force equal to the yield force of the connector. To justify the assumption that the connection steel yields at or near this point, the data from each test was analyzed to determine the actual tensile load in the connector.

The data from the two quarter-bridge strain gauges was averaged to produce a horizontal displacement-connector strain curve at the location of the gauges up to the point of gauge-connector bond failure, generally at a strain of 0.0015-0.0030. The gauge data also exhibits a roughly linear tension region on both gauges prior to the bifurcation

that shows due to the bending of the connector, which puts the windward gauge in more tension and the leeward gauge in less tension or even compression. The data from the string potentiometers was also used to calculate the uplift at the connector by averaging the windward and leeward potentiometers and correcting for lateral displacement and skew. The uplift was then correlated to the strain from the gauges prior to the bifurcation point, providing an effective gauge length for using the potentiometer-derived vertical displacement to calculate the vertical strain in the connector as seen in Fig. 22.

The vertical strain was correlated to a stress-strain results provided by coupon tensile tests of each of the connector types (see Appendix B) and multiplied by the effective area of the connector(s) to provide the vertical tie-down force. Then by dividing the observed lateral force by the connector tie-down force, a friction coefficient can be inferred. When plotted the outcome tends to converge to the lateral force normalized by the connector yield force at approximately 2 mm (0.8 in.) as seen in Fig. 23. Because of this satisfactory agreement in the region of interest, plots of the normalized lateral force remain the primary means of comparing the results of various shear tests throughout the remainder of this chapter. A complete set of summary plots for each shear test specimen, including the strain-uplift correlation and inferred friction coefficient calculations, are provided in Appendix A of this thesis.

A secondary value used for comparison is calculated by dividing the peak lateral force by the total connection area and the square root of the compressive strength of the haunch material. This value is the normalized breakaway shear stress and represents the performance of the bond between haunch material and the top surface of the beam. Normalized breakaway shear stress values for each shear test are found in Table 5. Also presented in Table 5 for each shear test are the observed failure mechanism and the normalized lateral force values for the threshold relative displacements that define a connection as brittle, satisfactorily ductile, or ductile as discussed in Chapter IV.

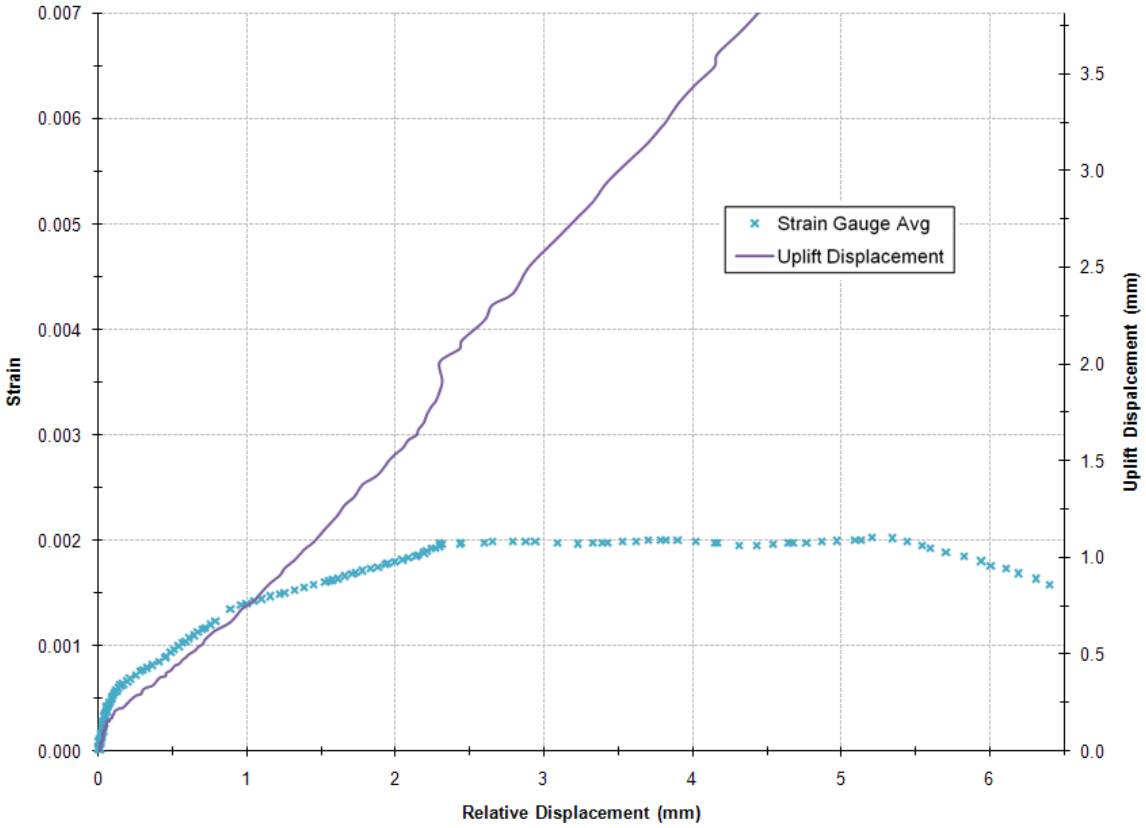

Fig. 22—Sample graphical correlation of gauged strain to measured specimen uplift (from specimen 1_TRS_2.0).

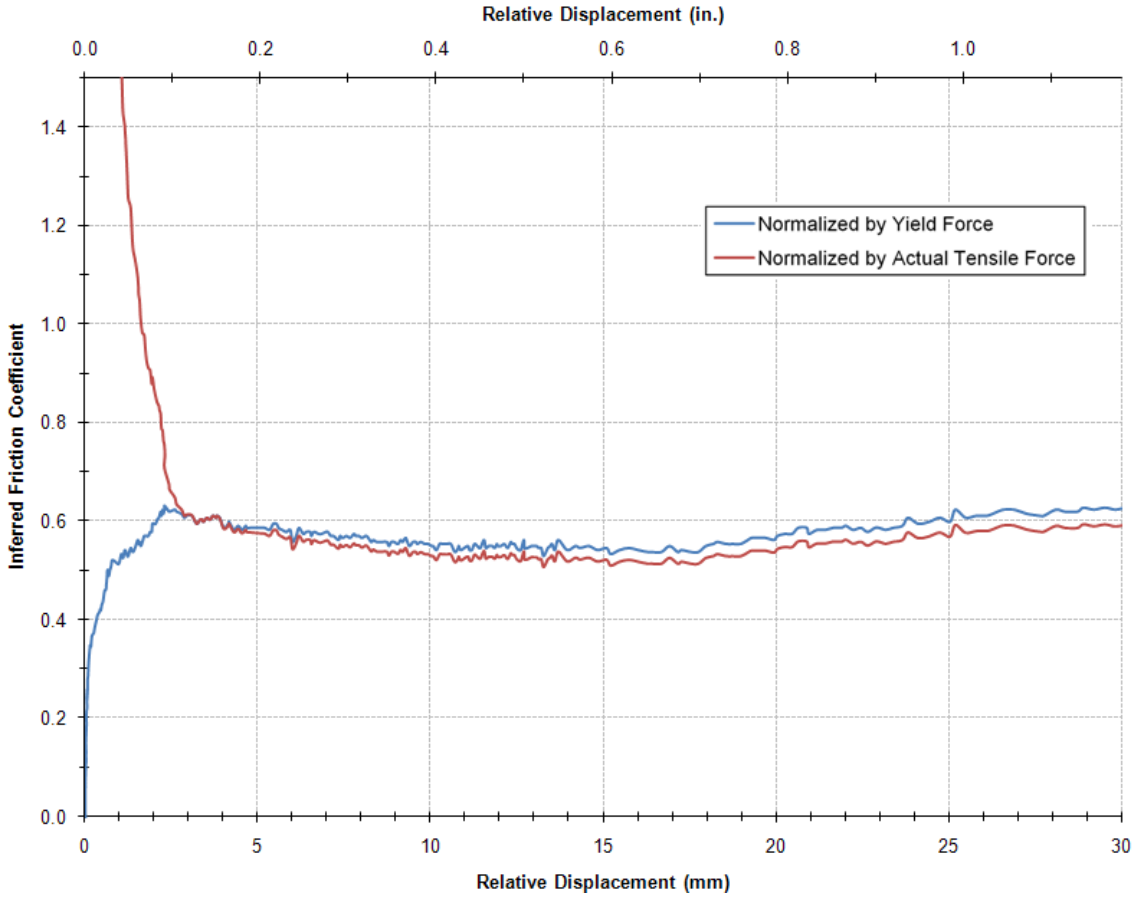

Fig. 23—Comparative plot of yield force-normalization and tensile force-normalization (from specimen 1_TRS_2.0).

Table 5—Calculated and observed values from all shear tests

Test #	Specimen alias	v_{ui}, MPa	$\frac{v_{ui}}{\sqrt{f'_c}}$, MPa	$\frac{v_{ui}}{\sqrt{f'_c}}$, psi	$\frac{V}{A_s f_y}$		Observed failure mode
					@ 5 mm	@ 12 mm	
1	4_CIP_2.0_A	3.79	0.48	5.77	1.04	1.2	Sliding shear – R-bar fracture
2	4_CIP_2.0_B	3.74	0.47	5.69	1.16	0.95	Sliding shear
3	2_TRC_2.0_A	3.79	0.54	6.56	0.56	0.56	Sliding shear
4	2_TRC_2.0_B	4.19	0.65	7.80	0.67	0.51	Sliding shear
5	2_TR_2.0_A	2.91	0.45	5.41	0.46	0.43	Sliding shear – cone failure
6	2_TR_2.0_B	2.91	0.45	5.41	0.36	0.51	Sliding shear
7	2_TRC_3.5_A	3.74	0.58	6.93	0.02	NA	Sliding shear
8	2_TRC_3.5_B	3.94	0.61	7.30	0.63	NA	Sliding shear
9	4_R_2.0	3.20	0.45	5.41	0.49	NA	Sliding shear
10	2_TR_3.5_A	3.40	0.52	6.26	NA	NA	Brittle shear beam failure
11	2_TR_3.5_B	3.40	0.52	6.26	NA	NA	Brittle shear beam failure
12	4_CIP_3.5_A	2.12	0.34	4.07	0.79	0.85	Sliding shear
13	4_CIP_3.5_B	2.22	0.35	4.26	1.16	0.85	Sliding shear
14	1_BC_2.0_A	2.22	0.33	3.96	1.00	0.94	Sliding shear
15	1_BC_2.0_B	2.02	0.30	3.63	0.56	0.71	Sliding shear
16	2_BC_2.0	3.00	0.45	5.40	0.62	0.63	Cone pullout
17	2_NS_2.0	3.25	0.48	5.84	0.85	0.83	Sliding shear
18	3_NS_2.0	3.99	0.60	7.17	0.80	0.74	Sliding shear
19	1_TRS_2.0_Rough	3.10	0.49	5.89	0.81	0.61	Sliding shear
20	2_TRS_2.0_Rough	3.74	0.59	7.11	0.36	0.14	Brittle shear beam failure
21	1_KB_2.0	1.03	0.16	1.96	0.49	0.45	Sliding shear
22	1_TRE_2.0	1.63	0.26	3.09	0.60	0.60	Sliding shear
23	1_TRS/AG_2.0_Rough	2.96	0.46	5.48	0.56	0.66	Brittle shear beam failure
24	1_TRS_2.0	1.53	0.24	2.90	0.58	0.55	Sliding shear

NA = not achieved

5.3 Analysis by connection type

The first analysis of the normalized experimental results is to compare the performance of the three basic types of connections tested: conventional, pre-installed, and post-installed. The conventional system provides a control and basis of comparison while also validating the experimental test setup and results. The pre-installed and post-installed systems each exhibit pros and cons as outlined below.

5.3.1 Conventional R-bars (control specimens)

Fig. 24 shows normalized lateral force-relative displacement plots for the control specimens of the experiment: CIP specimens with a 51-mm (2.0-in.) haunch. The R specimen is also included because it serves as a first link between the CIP specimens and most of the other specimens tested, as the connection is as close to a CIP connection as possible while still utilizing precast panels.

When the lateral relative displacements exceed 5 mm (0.2 in.), the R-bars have generally yielded. Also, in most cases the lateral force resistance increased when the displacements exceeded some 12 mm. This is attributed to the increase in the R-bar tie-down force resulting from the strain-hardening of those bars. Consequently, the lateral resistance in this range of relative displacements is indicative of the implied coefficient of friction of the cracked concrete-concrete interface that develops between the beam and the deck.

Evidently, a dependable (i.e., conservative) value for the inferred friction coefficient, μ_c, that can be assured for this class of construction is

$$\mu_c = 1.0 \tag{10}$$

Therefore, the interface shear per unit length, V_{in}, provided by the R-bars is given by

$$V_{in} = \mu_c \frac{A_{sh} f_{yh}}{s} \tag{11}$$

where A_{sh} is the steel cross-sectional area of the R-bars (hoops) and f_{yh} is the yield strength of the R-bar steel.

From the results presented in Fig. 24, it is also evident that for new or alternate shear systems a target (dependable) displacement limit should be set at least 12 mm. For

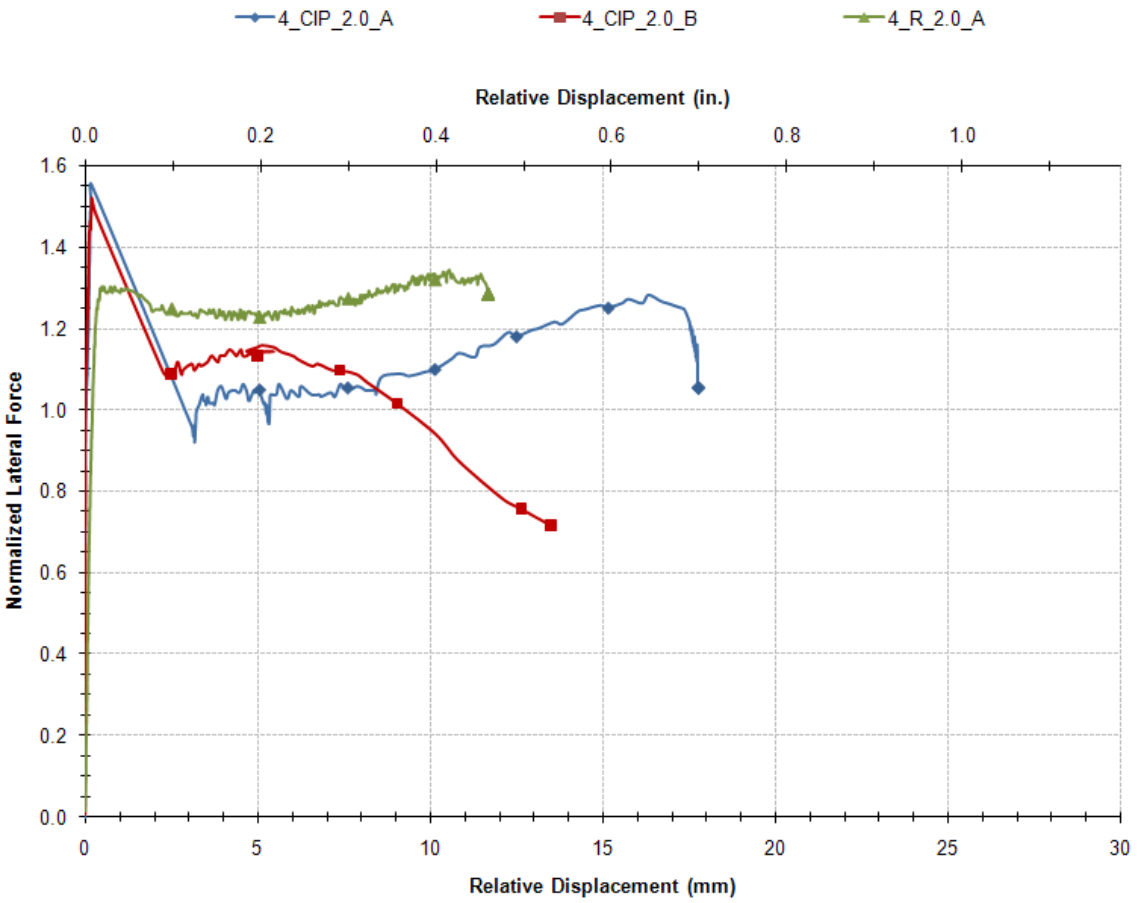

Fig. 24— Normalized lateral force vs. relative displacement for 51-mm (2.0-in.) haunch specimens with R-bar connectors.

the common class of precast concrete slab-on-concrete-girder bridge, this target deformability capability is considered sufficient, given that full composite deck-to-girder action is to be expected.

If alternative interface shear anchorage systems are to be introduced with equivalence to the standard R-bar system, then applying Equations (10) and (11), the number of shear connectors required to restrain one panel, n, is found from Equation (12), noting that a displacement capability > 12 mm should also be attained.

$$n \geq \frac{\mu_c A_{sh} f_{yh}}{\mu_f A_{sf} f_{yf}} \left(\frac{l_p}{s}\right) \tag{12}$$

where μ_f is the effective coefficient of friction for a fastener system, A_{sf} is the steel cross-sectional area of the fastener(s), f_{yf} is the yield strength of the fastener steel, l_p is the precast panel length, and s is the pocket spacing.

5.3.2 Pre-installed (precast) shear connector performance

Several specimens with pre-installed (precast) shear connectors were tested in order to show the effects of connector type and number of connectors. Although the initial breakaway behavior of the proposed system with threaded rod shear connectors was similar to those conventional specimens with R-bars, the post-breakaway behavior is somewhat different. Fig. 25 presents the normalized lateral force applied to the specimens versus the relative lateral displacement. As mentioned above, providing the fastener has yielded, which appears to be the case when the displacements exceed 5 mm, the horizontal lines on the graphs are indicative of the effective sliding friction coefficient. Continuous threaded rods exhibited the least amount of ductility for satisfactory performance given a 89-mm (3.5-in.) haunch due to large forces that were transmitted that the shear test beam could not handle, resulting in a brittle shear failure of the beam. However, the continuous threaded rod within the 51-mm (2.0-in.) haunch exhibited reasonable ductility.

In general, there are five stages of behavior that are exhibited:

1. Initially resistance is provided by the bond of the grout (or concrete in the case of conventional construction) between the precast deck panels and concrete beam.

   This stiff system is sustained until the bond between the grout and panels (or

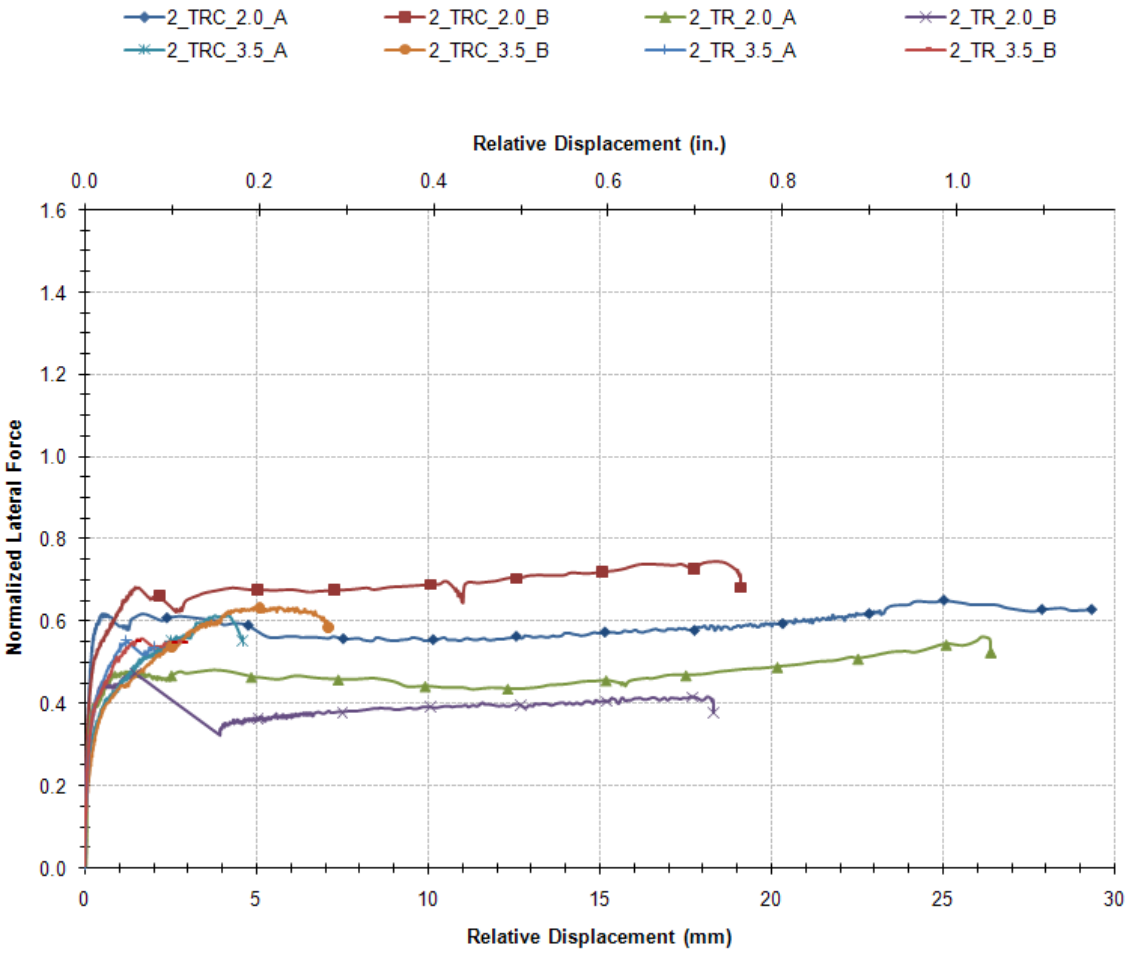

Fig. 25—Normalized lateral force vs. relative displacement for 51-mm (2.0-in.) and 89-mm (3.5-in.) haunch specimens with TR and TRC connectors.

shear test beam) suddenly breaks. Results indicate that the initial breakaway force occurs at a displacement of approximately 0.25 to 1.5 mm (0.01 to 0.06 in.) at an approximate shear stress on the haunch of $0.5\sqrt{f'_c}$ in MPa ($6\sqrt{f'_c}$ in psi).

2. Following breakaway, there is often a sudden drop off in resistance until the shear connectors (or R-bars in the case of the conventional construction) engage in tension and direct shear. This may not occur until the displacement has reached 2.5 to 4 mm.
3. As the lateral displacement increases, the deck panel uplifts in the vicinity of the fasteners, which in turn, elongate and provide a tie-down restraint force. This force is in turn resisted by a normal concrete beam-to-grout-to-panel compression nearby. The horizontal component of this compression force is a frictional force that resists the applied lateral load. Thus, a frictional sliding deck panel-to-beam mechanism results. This tends to stabilize from displacements ranging from 5 to 15 mm (0.2 to 0.6 in.). This stable force appears to result from yielded connectors.
4. As the displacements become large, the resistance increases slightly, which is attributed to strain-hardening of the connectors.
5. Failure of a well-performing system tends to take place when the displacements exceed approximately 18 mm (0.7 in.). Failure may result grout crushing, beam anchorage/shear failure, R-bar pull-out from deck panel (cone failure), and/or shear failure of the connector.

For the 89-mm (3.5-in) haunch specimens, testing ended prematurely because a brittle beam failure generally occurred. However, this revealed an important design consideration – adequate shear resistance for the concentrated shear loads must be provided in the beam using hoopsets. This consideration is discussed in greater detail later in Section 5.5. When compared to the TR system, the TRC system reveals higher initial breakaway strengths, post-breakaway resistance in terms of the implied friction coefficient, and ultimate displacement limits. At 5.1-mm (0.2-in.) displacement, the strength of the TRC systems is 311 and 374 kN versus 258 and 200 kN for the TR

system. As such, the TRC system seems to exhibit increased capacity versus the TR system, so the TRC system will be used as a baseline for comparison with the post-installed specimens and parametric studies. Clearly the response of the pre-installed (precast) shear connections is uniformly inferior to the R-bar specimens, though not necessarily because of the connectors themselves. Rather, there are other aspects of the connection that differ from the control that significantly affect the performance, notably different frictional sliding performance as a result of different infill grout material in between two smooth concrete surfaces, and different displacement limits due to the high concentration of forces anchored in the beams.

Tests #14-24 were conducted as parametric studies to address some of these issues and better understand their effects. Specifically, Section 5.4.2 addresses the very same issue identified in AASHTO LRFD C5.8.4.1, Interface Shear Transfer – Shear Friction, where roughness can be taken to affect the friction across a shear plane.

5.3.3 Post-installed shear connector performance

Eight specimens were assembled using several types of post-installed connections. Such a system would most likely be used in a situation where the pockets and cast shear connectors do not align at the construction site, but the system could also be used on a larger scale to simplify the casting procedures. Below is a summary of the four types of post-installed connections tested in a total of eight tests:

1. B7 TRs installed in 0.16 w/p grout (Sika) (TRS) – This post-installed connection was made by coring a 51-mm (2-in) diameter hole in the beam to a depth of 230 mm, cleaning the hole, filling it 2/3 full with the grout and inserting a TR with a nut. This system was used in four specimens (three singles and one double).
2. HILTI Kwik-Bolt 3 (KB) – The KB is a proprietary mechanical fastener that uses an expanding collar to set the anchor in a nominally same-sized drilled/cored hole using friction. A single 25-mm (1.0-in.) diameter KB was used as the shear connector in one of the remaining specimens.
3. B7 TR anchored in HILTI HY-150 Max epoxy (TRE) – HY-150 Max is a proprietary two-part epoxy made by HILTI that has forgiving installation

requirements, very fast setting times (30 minutes) and high strength but is costly. The connection is made by drilling a hole in the beam slightly larger than the outside diameter of the TR, 32 mm vs. 25 mm (1.25 in. vs. 1 in.). The hole is thoroughly cleaned then filled 2/3 full with the epoxy. The threaded rod is inserted with a twisting motion, displacing the epoxy to fill the remainder of the hole. One specimen was tested with a single TRE shear connector.

4. Nelson studs welded to a steel plate cast into the beam (NS) – This connection is made by welding a headed stud to a large steel plate that is cast into the beam, thereby providing significant tolerances to the construction process. Because the beam has to be modified, this connection is a somewhat hybrid (both pre- and post-installed) connection, but in this analysis it is considered a post-installed connection – motivated because of the potential to use the NS system to make the construction process easier.

Normalized lateral force is plotted vs. relative displacement in Fig. 26 for a representative sample of the post-installed specimens. The four post-installed specimens not shown in Fig. 26 tested the variation in performance due to the variety of parameters that are discussed in Section 5.4.

In comparing to the pre-installed (precast) shear connection specimens, each the post-installed shear connection specimens exhibited the same five general stages of behavior. As seen in the normalized plots in Fig. 26, both the TRS and TRE systems performed comparably to the baseline pre-installed (TRC) system in terms of both strength and ductility, while the NS system appears to provide appreciably higher strength than the baseline without sacrificing the above-satisfactory ductility. The KB also system provides superior ductility, but the strength is noticeably less than the baseline.

Aside from performance, there are constructability concerns with several of the connector types. There are doubts about the practicality of using the KB and TRE systems on a large scale due to their proprietary systems and associated costs. The feasibility of a truly post-installed NS system has not been established, as both the top

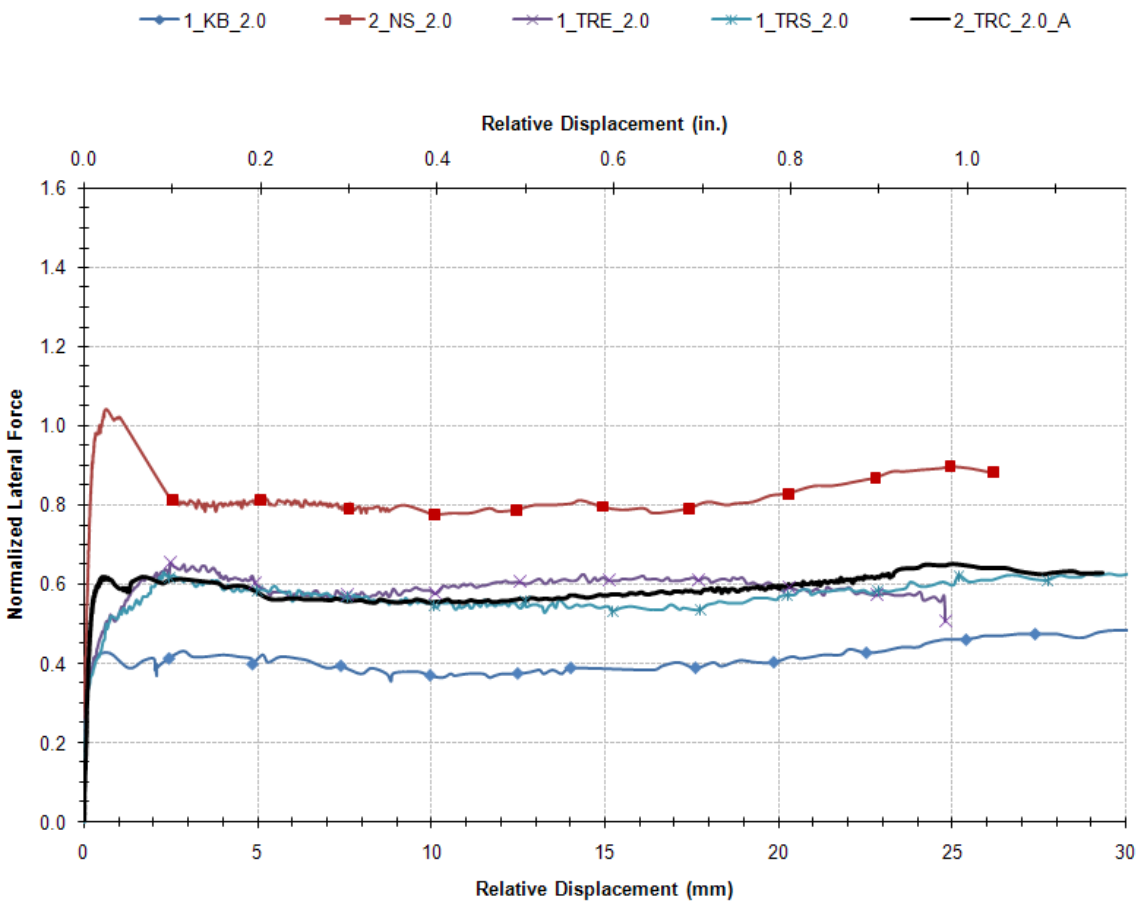

Fig. 26—Plot of normalized lateral force vs. relative displacement for each type of post-installed specimen. The 2_TRC_2.0_A plot is shown as a baseline for comparison.

and bottom studs were welded to the plates prior to casting in the shear beams for these tests. The primary logistical issue is the sizeable grounding clamp/magnet required for such a large amperage weld conflicting with stud welding gun and the studs themselves in the relatively small pocket. Until this issue is resolved, the NS system is not considered to be viable for construction with precast girders, although it may have potential for application within a steel girder bridge.

5.4 Parametric studies

The second set of analyses of the experimental test data is series of studies that examine the individual effects of key design aspects of the connection. The key aspects examined are haunch height, surface roughness, alternative grout and connectors, and grouping effects.

5.4.1 Haunch height

Tests conducted with the 51-mm (2.0-in) haunch revealed adequate ductility, where the specimens with threaded rods and couplers revealed the largest breakaway resistance, peak load, and ultimate displacement, as shown in Fig. 27. However, the results of varying the haunch height are inconclusive at the time of writing this thesis because the data from the non-CIP 89-mm (3.5-in) haunch specimens' testing was clouded by poor anchorage performance into the beam, resulting in limited displacements to less than 5 mm, as seen in Fig. 28. Brittle shear failure in the beam could not be improved since the beams used were already cast with the same hoopsets. Additional testing is necessary to verify the effect of the haunch height on the deck-haunch-beam system. However, it is known that a larger overturning moment is inherently induced given a taller haunch.

5.4.2 Surface roughness

Another aspect tested in several of the research specimens was the roughness of the mating surfaces of cast concrete. NCHRP 12-65 (Badie et al., 2006) prescribes intentionally roughening the top surface of the beam using a retardant agent and washing or another method to an amplitude of 6 mm (0.25 in.) in order to enhance the bond

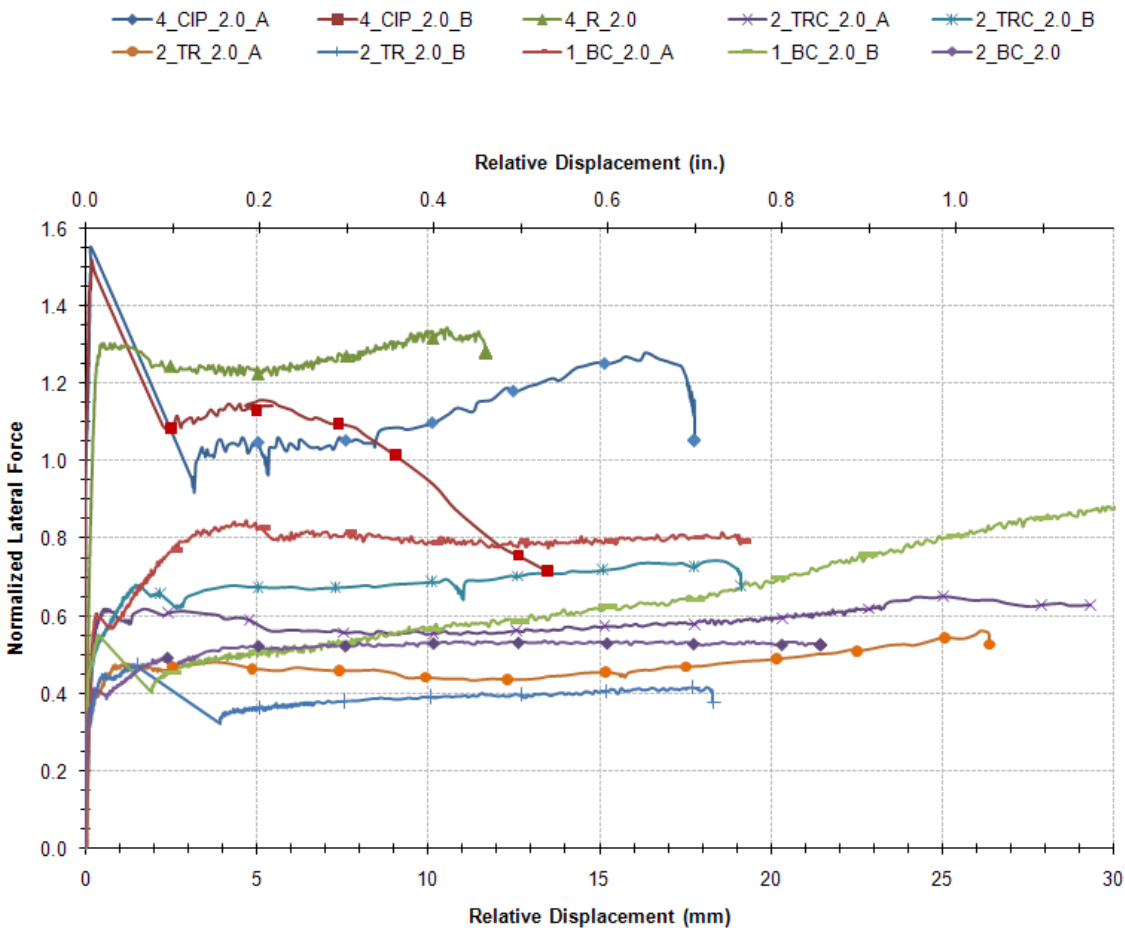

Fig. 27—Plot of normalized lateral force vs. relative displacement for all 51-mm (2.0-in) haunch pre-installed (precast) specimens.

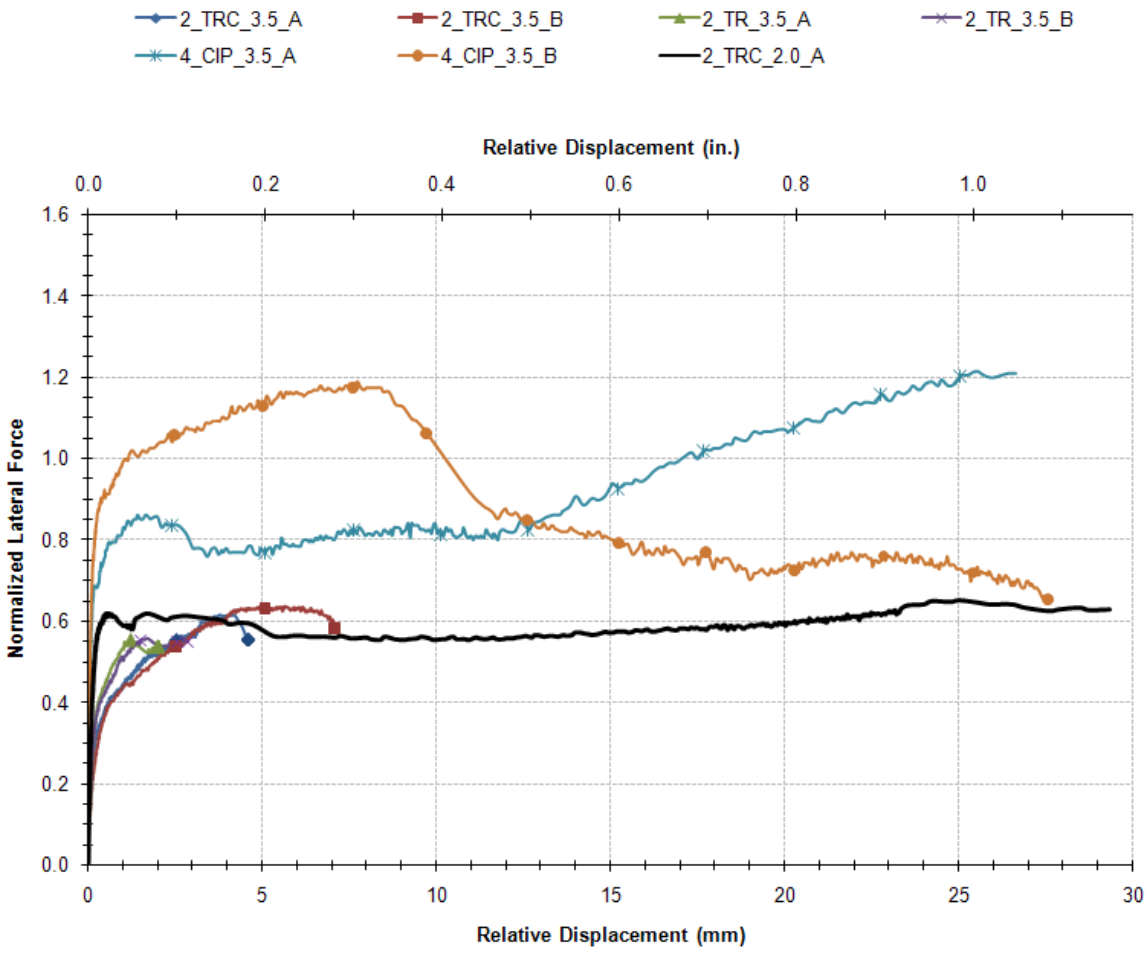

Fig. 28—Plot of normalized lateral force vs. relative displacement for all 89-mm (3.5-in) haunch pre-installed (precast) specimens. The plot of 2_TRC_2.0_A is also shown as a baseline for comparison.

capacity. In other research conducted at Virginia Tech (Scholz et al., 2007), roughness tests were performed on several surfaces, and the surfaces selected for a similar shear test setup were a raked finish for the beam top and either smooth or exposed aggregate finish for the bottom of the deck. Testing of these specimens with exposed aggregate deck bottom revealed little effect of peak shear stress and a negative effect on effective coefficient of friction when compared to the smooth deck bottom specimens, a phenomenon attributed to air voids due to casting orientation.

To explore surface roughness in this thesis, the bottom of the shear test deck and the top of the shear test beam were roughened mechanically on three post-installed specimens. Had the specimens not already been cast, the surfaces could have been cast or finished rough through a variety of methods. A mid-sized hammer drill on the chisel setting provided an appropriate degree of power and control, and the surfaces were roughed using both flat and chisel bits to an approximate amplitude of 6 mm. Fig. 29 shows photographs of the roughened surfaces that were tested.

From the normalized plots in Fig. 30, it is readily apparent both of the roughened specimens with a single connector (1_TRS_2.0_Rough and 1_TRS/AG_2.0_Rough) had a higher initial strength and a higher effective friction coefficient up through some 10 mm relative displacement when compared to their plain-finished counterpart (1_TRS_2.0). The difference between the two single-connector roughened specimens was the use of an alternate grout, a parameter discussed in Section 5.4.3. After the relative displacement exceeded 10 mm, the performance of both of the single-connector roughened specimens and the plain-finish specimen are quite similar, which is attributed to the continuing fracture of the grout bonds along another plane until the specimen is "rolling" on the crushed grout as before. The only two-connector roughened specimen (2_TRS_2.0_Rough) exhibited a rogue failure of the beam due to insufficient beam shear reinforcing as explained in Section 5.5, therefore the force-displacement behavior does not reflect a properly detailed connection of this type. Nevertheless, the normalized plot of 2_TRS_2.0_Rough is also shown in Fig. 30 for completeness.

(a) full-size view of beam surface roughened to 6-mm amplitude

(b)TRS connectors in a roughened beam

Fig. 29—Shear connections with roughened surfaces.

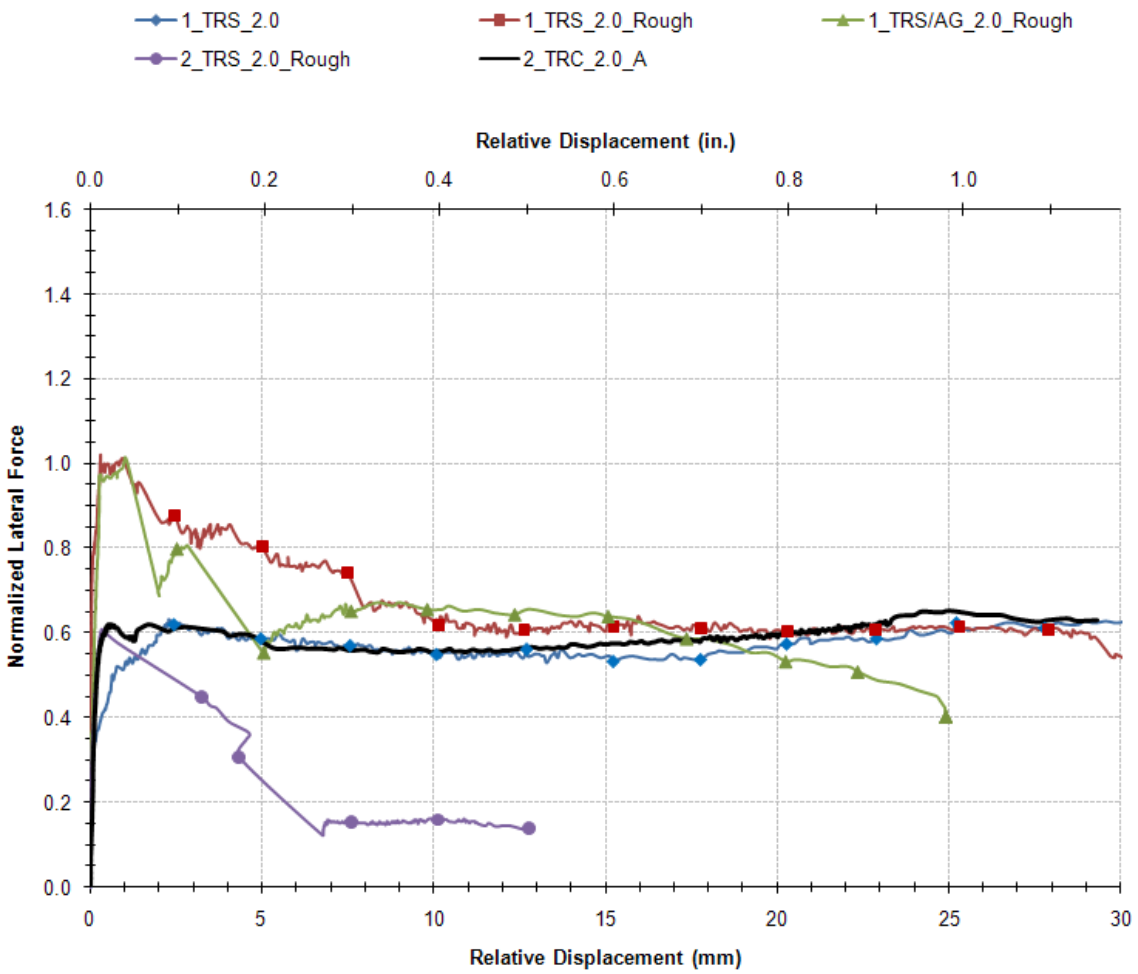

Fig. 30—Plot of normalized lateral force vs. relative displacement for all specimens with mechanically roughened mating surfaces. The plot of 2_TRC_2.0_A is also included as a baseline for comparison.

5.4.3 Performance of an alternative grout

Another solution to addressing the issue of insufficient friction is to use a different grout that still provides sufficient compressive strength and flowability but also contains larger aggregate, thereby providing a higher friction coefficient. This option was explored by assembling two identical specimens, one with proprietary grout (SikaGrout® 212) and the other with an alternate lab-mixed grout developed by others associated with this project (Trejo et al., 2008). As seen in the normalized plots of the comparative specimens in Fig. 30, the behavior of the alternate grout connection is similar to the proprietary grout in initial breakaway strength and effective friction coefficient, but it does exhibit a more variable displacement, probably due to the breaking and biting of the larger aggregate within the haunch. Thus the performance appears to be slightly inferior, but further research is warranted given the potential material cost savings of a site-mixed grout over the proprietary ready-bagged mix – estimated to be 90%.

5.4.4 Alternative connectors

While connector options 1 and 2 were prescribed by TxDOT for the prototype bridge as described in Chapter III, the experimental testing also included evaluating the performance of the BC and NS systems, both which can serve as alternative shear connectors provided their characteristics and behavior are properly understood and the appropriate situation arises for application. This section focuses on these BC and NS alternative connectors in more depth with a side-by-side comparison.

Revisiting the calculated test data in Table 5, the modulus of rupture of the alternative connectors varies from 0.30 to 0.60$\sqrt{f'c}$ (3.6 to 7.2$\sqrt{f'c}$, psi units), comparable to the pre-installed (precast) shear tests. However without sufficient testing redundancy, it is difficult to establish a lower bound for strength calculations for design or assessment calculations.

Examining the normalized plots of the test data for the alternative connectors in Fig. 31, it is notable that all specimens exhibited similar above-satisfactory ductile behavior, displacing smoothly well beyond 12 mm. Grouping effects for both the BC

and NS systems are also evident in Fig. 31. That parameter is further discussed in Section 5.4.5.

A key reason for selecting the NS connection setup was to mimic previous research done for VTRC by a research team at Virginia Tech (Scholz et al, 2007). Although this research dealt primarily with the grout material to be used in a pocketed shear connection, it also included shear tests of Nelson studs installed much the same way the NS specimens were prepared for this report. The VTRC Nelson stud specimens were assembled with 2, 3, and 4 studs per specimen. After normalizing by total connection yield, the results of the VTRC specimens and the NS specimens from this study can be ready compared.

Table 6 shows the measured and calculated values from both reports, and the normalized results are notably comparable. This correlation further emphasizes the efficacy of the experimental test setup used in this research, that is, one that does not introduce an artificial clamping force on the shear connection.

5.4.5 Grouping effects of shear connectors

Another parameter studied through the data gathered in these shear tests was the grouping effects of BC, NS, and TRS shear connections. Due to the limited number of shear specimens tested, the connection details of each specimen were selected in order to contribute to a broad scoping investigation. Consequently, as this study has a limited number of specimens tested and does not thoroughly explore different numbers of connectors or configurations of connectors within the pocket, it can only provide indicative trends for further investigation, if needed. In general, it is evident from these tests that as the number of a given connector is increased, the connectors become less efficient in resisting the lateral force.

Fig. 32 displays a normalized plot of the BC specimens. An obvious view of the grouping effect is seen when comparing the plot of 1_BC_2.0_A to 2_BC_2.0. Those two plots are very similar in shape, clearly exhibiting the five stages of behavior previously described, however the addition of a second connector drops the normalized force from approximately 0.8 to approximately 0.5. The plot of 1_BC_2.0_B does not

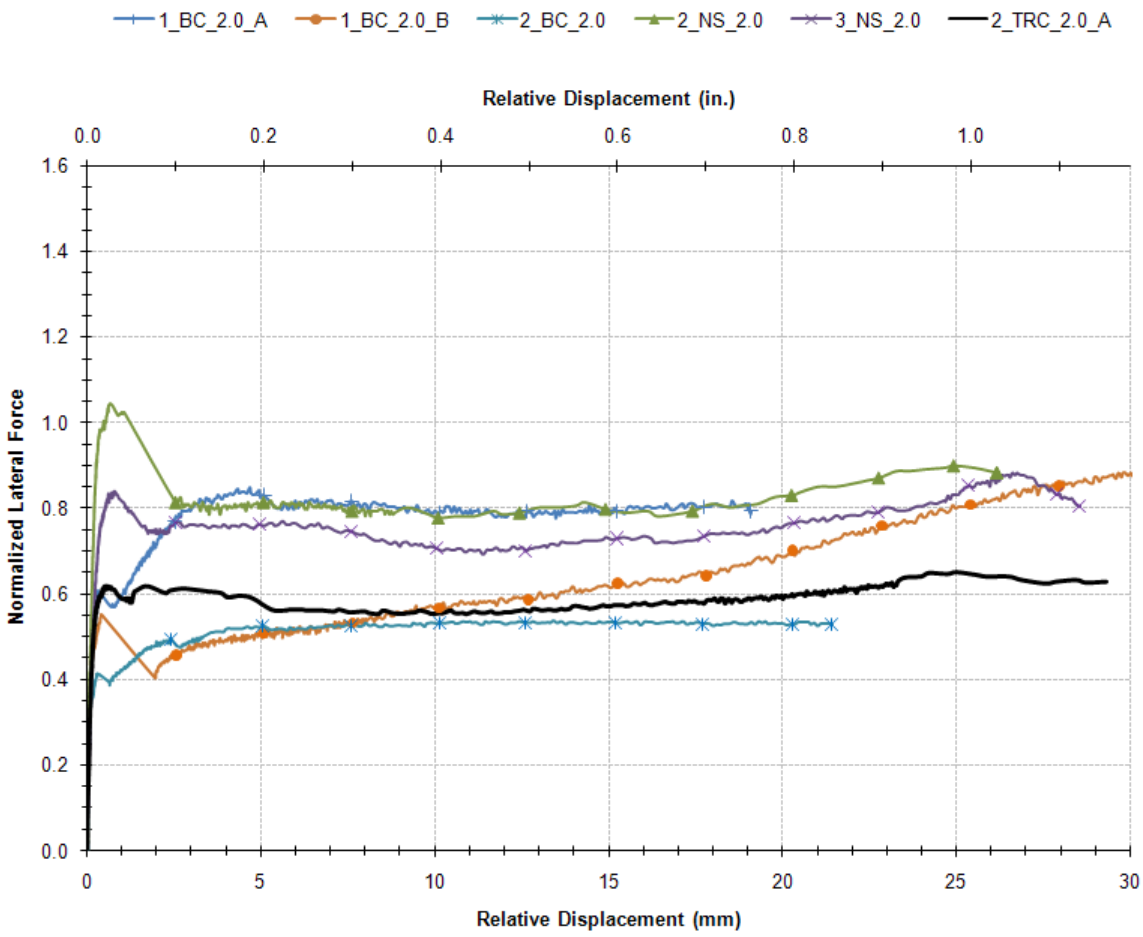

Fig. 31—Plot of normalized lateral force vs. relative displacement of the alternative connector types – BC and NS. The 2_TRC_2.0_A is also shown as a baseline for comparison.

Table 6—Comparison of NS specimen performance to VTRC research

Research organization	Specimen alias	Total shear connector area, mm^2 (in^2)	Peak load, kN (kips)	Sustained load, kN (kips)	Normalized	
					Peak load	Sustained load
VTRC	18-2NS-FSHP-SM-A	568 (0.88)	194 (44)	125 (28)	1.02	0.65
VTRC	20-2NS-FSHP-SM-B	568 (0.88)	136 (31)	102 (23)	0.72	0.53
TTI*	2_NS_2.0	776 (1.20)	294 (66)	227 (51)	**1.10**	**0.85**
VTRC	22-3NS-FSHP-SM-A	858 (1.33)	258 (58)	182 (41)	0.89	0.63
VTRC	23-3NS-FSHP-SM-B	858 (1.33)	242 (55)	212 (48)	0.84	0.74
TTI*	3_NS_2.0	1162 (1.80)	360 (81)	300 (67)	**0.90**	**0.74**
VTRC	19-4NS-FSHP-SM-A	1142 (1.77)	322 (72)	230 (52)	0.83	0.60
VTRC	21-4NS-FSHP-SM-B	1142 (1.77)	315 (71)	282 (63)	0.82	0.73

* present tests

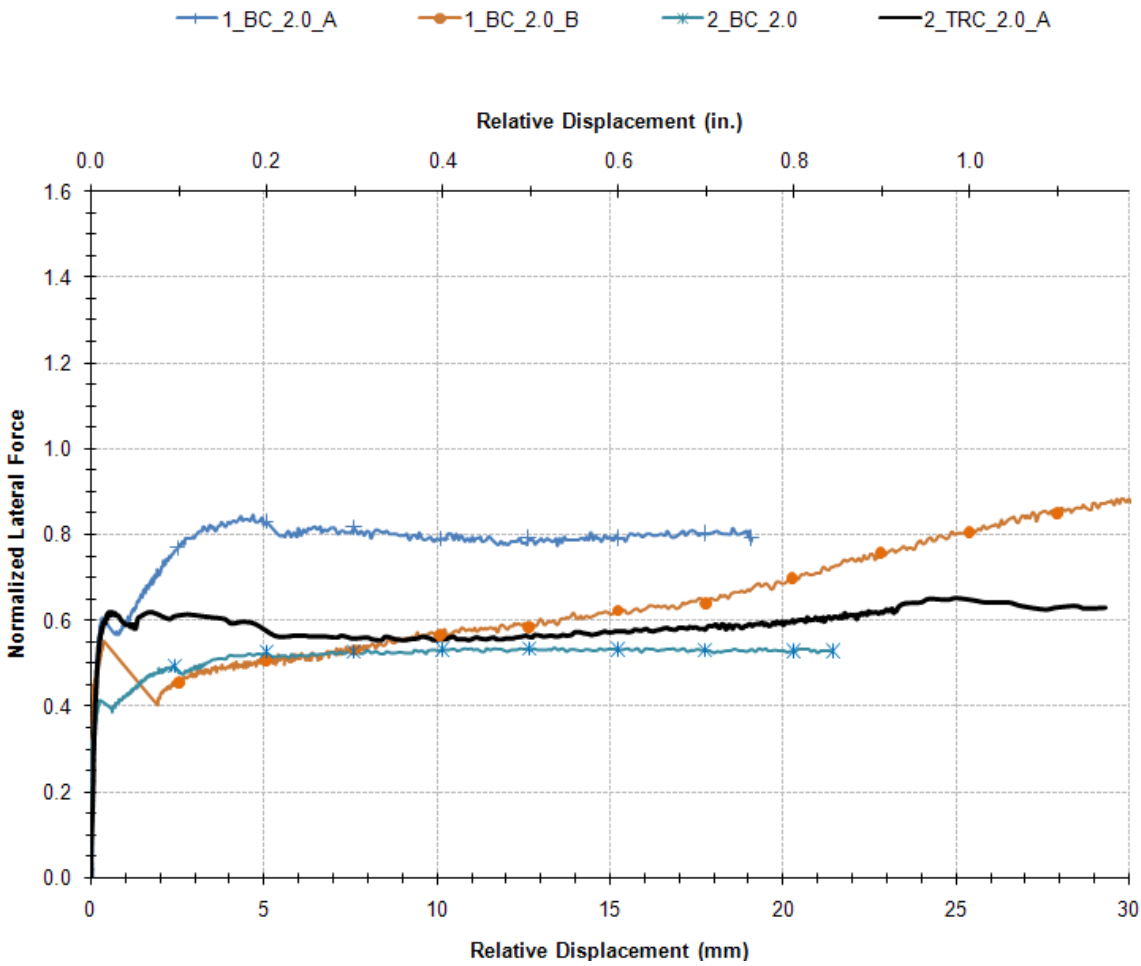

Fig. 32—Plot of normalized lateral force vs. relative displacement to show grouping effects among the BC specimens. The 2_TRC_2.0_A is also shown as a baseline for comparison.

exhibit a uniform displacement in the friction-stabilized region, instead providing a continually increasing strength that results in a final effective coefficient of friction of >1.0. The cause of this different behavior is not known and has not been replicated with any of the other tests but is shown for completeness.

Fig. 33 presents a normalized plot of the NS specimens, which exhibit a similar grouping effect as the BC specimens but to a lesser extent, with the normalized force dropping from approximately 0.85 to approximately 0.75.

No conclusive determination of grouping effects can be made from comparing the TRS-Rough specimens because the brittle beam shear failure of the 2_TRS_2.0_Rough specimen represents the failure performance of the beam rather than the connection as explained in Section 5.4.2.

5.5 Simplified force-displacement model

A simplified force-displacement model for full-depth precast panel to prestressed concrete girder connections is presented in Fig. 34, including the effects of intentionally roughening the mating surfaces of the connection.

5.6 The importance of system detailing on performance

During the course of testing it became evident that there was an inherent weakness in the detailing of the deck-haunch-beam system details. Two TR fasteners when yielded have a combined pull-out force capacity of 632 kN . This pull-out force imposes significant distress to the beam. Evidently as the threaded rods become heavily strained, much of their anchorage is provided by the headed nut, which in turn imposes a large uplift force within the concrete beam. This force is restrained by strut action from the nearby beam hoops, as previously shown in Fig. 4. However, the initial analysis did not take into account the provisions outlined in ACI 318-08 Appendix D, specifically that the concrete failure cone is estimated at approximately 35° per the CCD method (Fuchs et al., 1995) and that in order to transfer the shear load, sufficient anchor reinforcement must be placed symmetrically within $0.5h_{ef}$ of the anchorage, where h_{ef}

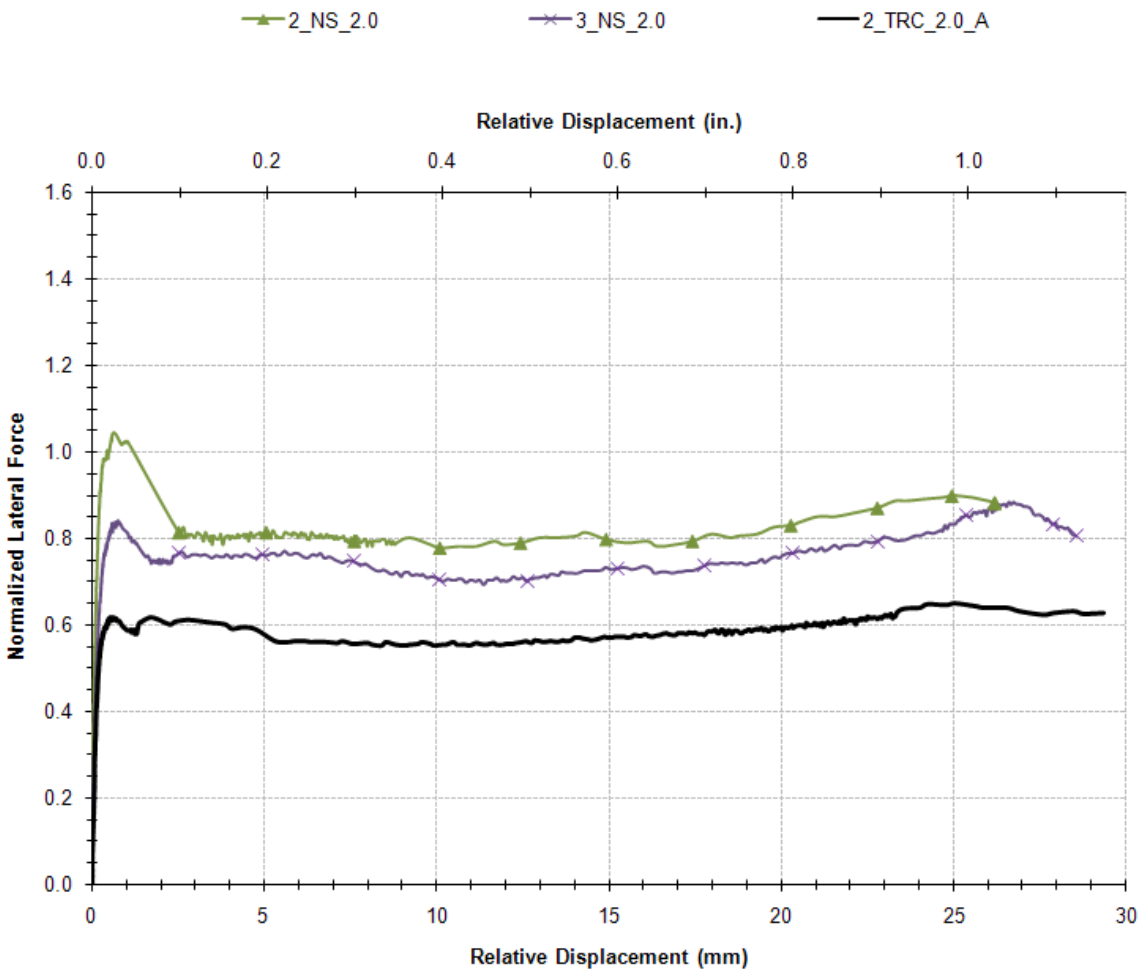

Fig. 33—Plot of normalized lateral force vs. relative displacement to show grouping effects between the NS specimens. The 2_TRC_2.0_A is also shown as a baseline for comparison.

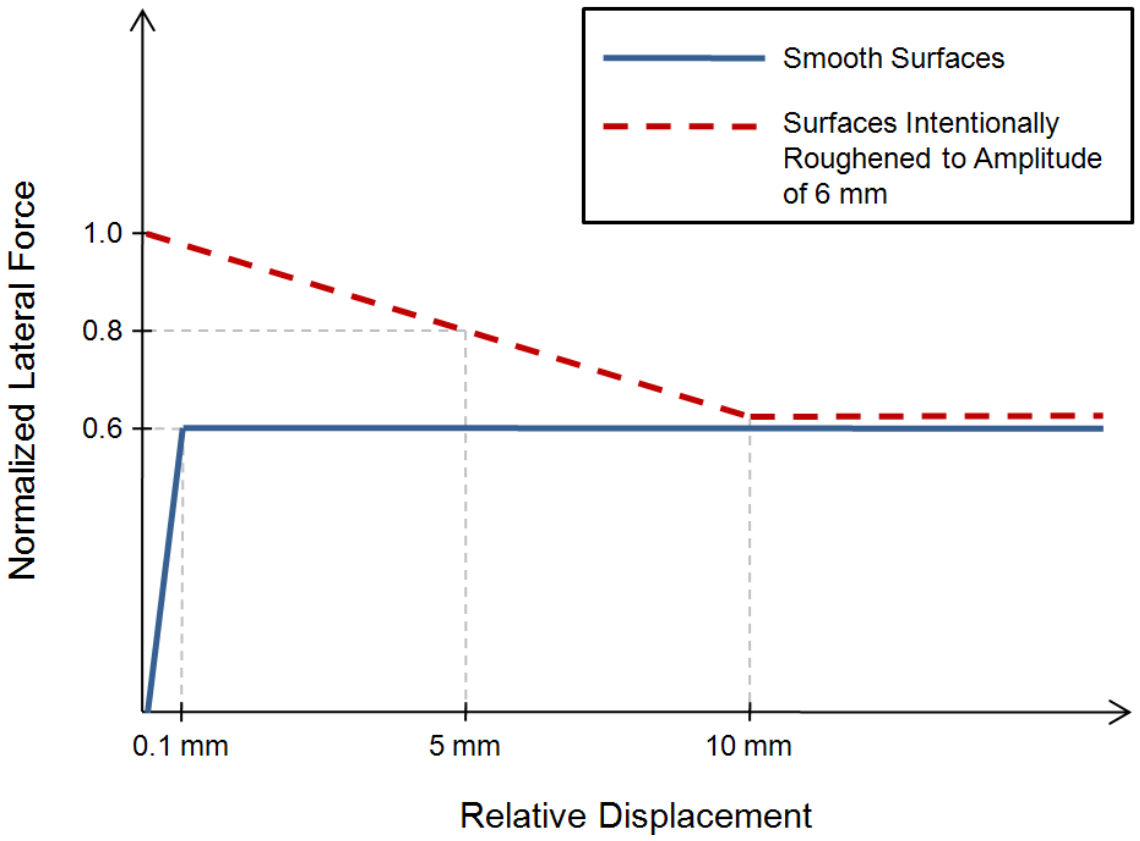

Fig. 34—Proposed design shear and friction capacity for full-depth precast concrete deck to concrete girder connections.

is the effective embedment depth of the anchor. Clearly there were insufficient hoops for this purpose in some of the tests, particularly for the 89-mm (3.5-in.) haunch specimens. Thus the beam shear reinforcement required for each connection should be detailed per Fig. 35 in order to prevent premature failure.

The required shear reinforcement should be determined such that the capacity of the hoops within $0.5h_{ef}$ of the fasteners should be no greater than the maximum fastener load. More formally,

$$nA_{sh}f_{yh} \geq n_f A_{sf} f_{yf} \tag{13}$$

where n is the number of hoopsets required within $\pm 0.5h_{ef}$, A_{sh} is the cross-sectional area of one hoopset, f_{yh} is the yield stress of the hoop steel, n_f is the number of fasteners within each pocket, A_{sf} is the net cross-sectional area of the shear connector, and f_{yf} is the yield stress of the shear connector (not greater than $0.8f_{uf}$, where f_{uf} is the tensile strength of the shear connector).

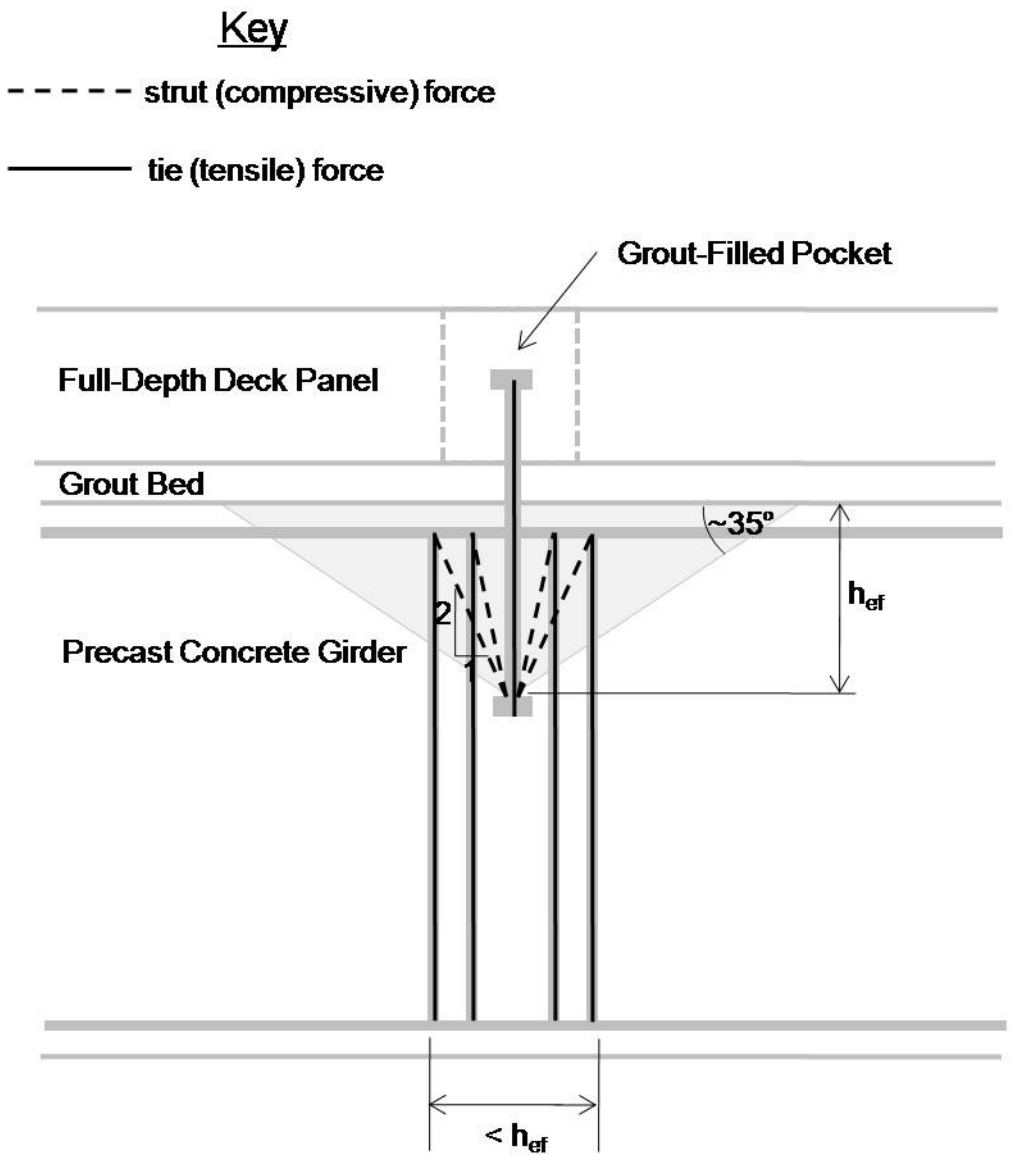

Fig. 35—Detailing of beam shear reinforcement required for each shear connection.

CHAPTER VI
DESIGN APPLICATIONS

6.1 Introduction

This chapter presents the steps of applying the results and analysis of the shear tests to the design of a structure. The design process is outlined first followed by a example problem.

6.2 Design process

The design of the shear connection of a bridge system with full-depth precast panels on prestressed concrete girders begins with calculating the design shear at each panel. The shear demand per unit length for each panel is then calculated assuming uncracked properties of the composite section to resist the design loading and multiplied by the length of the panel to determine the design shear force per panel, Q_p. Utilizing this value, the connector yield force, $A_s f_y$, and assuming a coefficient of friction, μ_f, allows the calculation of the number of pockets required, n, per Equation (14):

$$n = \frac{Q_p}{\mu_f A_s f_y} \tag{14}$$

Per the scope of this thesis and the practical limits of providing adequate shear reinforcement for each pocket, only one- or two-connector options are recommended at this time for 25-mm (1.0-in.) nominal diameter high-strength connectors. For the coefficient of friction, two values should be used that correlate to dependable design values from the inferred friction coefficient shown in the simplified force-displacement model in Fig. 34 – 0.8 for connections intentionally roughened to an amplitude of 6 mm and 0.6 for connections not intentionally roughened. Design numbers of pockets and fasteners are designated for each calculated value to ensure that the total number of fasteners is adequate. For practicality in the reinforcing of the prestressed girders, panels will only be considered with two or more pockets. The design can be established such that each panel is identical, both in roughening and in the number of pockets, or the

design can be optimized to find the most efficient combination of pockets and fasteners in each panel and whether roughening is required. Finally, the shear reinforcing of the girders must be clustered per the procedure specified in Section 5.6 to ensure sufficient shear capacity to anchor the shear connectors.

6.3 Design example

6.3.1 Problem statement

A bridge is to be constructed using prestressed concrete girders and a full-depth precast deck panel system using a TRC connection system. The bridge span is 36.6 m, and the length of each deck panel, l_p, is 2.44 m. The distance between the internal compressive and tensile resultants, jd, of the composite section is 1.5 m. The yield force per TRC connection, $A_s f_y$, is 554 kN. The design load case of AASHTO standard HL-93 produces design shear loads, Q, of 802 kN and 270 kN at the ends and midspan, respectively.

6.3.2 Solution

Assume symmetry of the bridge on either side of the midspan and a linear shear relationship from the end to the midspan. Calculate the shear per unit length, q, as

$$q = \frac{Q}{jd} \tag{15}$$

The shear values this example are tabulated in Table 7. The calculated and design number of fasteners and pockets per panel are presented in Table 8 based on the procedure outlined in Section 6.2, providing solutions for both matching and optimized panels with and without roughening.

In order to demonstrate the variety of the procedure, a selected design solution utilizing optimized panels with and without roughening is highlighted in gray in Table 8: only panels 1-3 need to be roughened, panels 1-6 have 2 connectors while panels 7-8 have 1 connector, and all panels require 3 pockets. An alternate design solution is also presented utilizing connectors of larger diameter, a solution not yet confirmed through experimental testing. Such a design is a practical solution if intentionally roughening the surfaces is not desired. Further discussion of this issue is found in Section 7.2.

Table 7—Shear values for example panels

Panel #	Q, kN (kips)	q, kN/m (kips/ft)	Q_p, kN (kips)
1	802 (180)	535 (37)	1283 (293)
2	726 (163)	484 (33)	1162 (266)
3	650 (146)	433 (30)	1040 (238)
4	574 (129)	383 (26)	919 (210)
5	498 (112)	332 (23)	797 (182)
6	422 (95)	281 (19)	675 (154)
7	346 (78)	231 (16)	554 (127)
8	270 (61)	180 (12)	432 (99)

Table 8—Numbers of pockets and fasteners required in each panel for example problem

Panel #	$\mu_f = 0.6$			$\mu_f = 0.8$			Selected Design Solution	Alternate Design Solution
	Calculated number of fasteners	Design # of pockets (fasteners)		Calculated number of fasteners	Design # of pockets (fasteners)			
		Matching panels	Optimized panels		Matching panels	Optimized panels		
1	7.5	4 (2)	4 (2)	5.6	3 (2)	3 (2)	3 (2)[+]	3 (2)[#]
2	6.8	4 (2)	4 (2)	5.1	3 (2)	3 (2)	3 (2)[+]	3 (2)[#]
3	6.1	4 (2)	3 (2)	4.6	3 (2)	3 (2)	3 (2)[+]	3 (2)[#]
4	5.4	4 (2)	3 (2)	4.0	3 (2)	2 (2)	3 (2)	3 (2)
5	4.7	4 (2)	3 (2)	3.5	3 (2)	2 (2)	3 (2)	3 (2)
6	4.0	4 (1)	3 (2)	3.0	3 (1)	2 (2)	3 (2)	3 (2)
7	3.2	4 (1)	3 (1)	2.4	3 (1)	2 (2)	3 (1)	3 (1)
8	2.5	4 (1)	3 (1)	1.9	3 (1)	2 (1)	3 (1)	3 (1)

Gray shading denotes selected design solution

[+] Surfaces intentionally roughened

[#] Larger diameter fasteners, 29 or 32 mm, to be used

For a connection with two TR fasteners per pocket and using 12-mm (#4) hoops, Equation (13) has the solution

$$n \geq \frac{2A_{sf}f_{yf}}{A_{sh}f_{yh}} = \frac{(2 \times 335\ mm^2)(0.8{\times}945\ MPa)}{(253\ mm^2)(434\ MPa)} = 4.61 \quad (16)$$

So three 12-mm (#4) hoopsets would need to be clustered within $0.5h_{ef}$ of either side of the fasteners to provide adequate capacity and maintain symmetrical loading. However, if 16-mm (#5) hoops are used, the solution becomes

$$n \geq \frac{2A_{sf}f_{yf}}{A_{sh}f_{yh}} = \frac{(2 \times 335\ mm^2)(0.8{\times}945\ MPa)}{(396\ mm^2)(434\ MPa)} = 2.95 \quad (17)$$

Therefore two 16-mm (#5) hoopsets need to be clustered within $0.5h_{ef}$ both sides of the fasteners in place of the three 12-mm hoopsets. This appears to be a more manageable solution and would be selected for this case. Only minimum shear reinforcement would be required in between the hoop clusters. A representative diagram of the required shear reinforcing and strut-and-tie model for an entire three-pocket panel is shown in Fig. 36. Note that the angle between the connector-hoop compression strut and the vertical, φ, is such that $\tan\varphi$ is approximately the effective coefficient of friction obtained from the experimental testing, between 0.6 and 0.8.

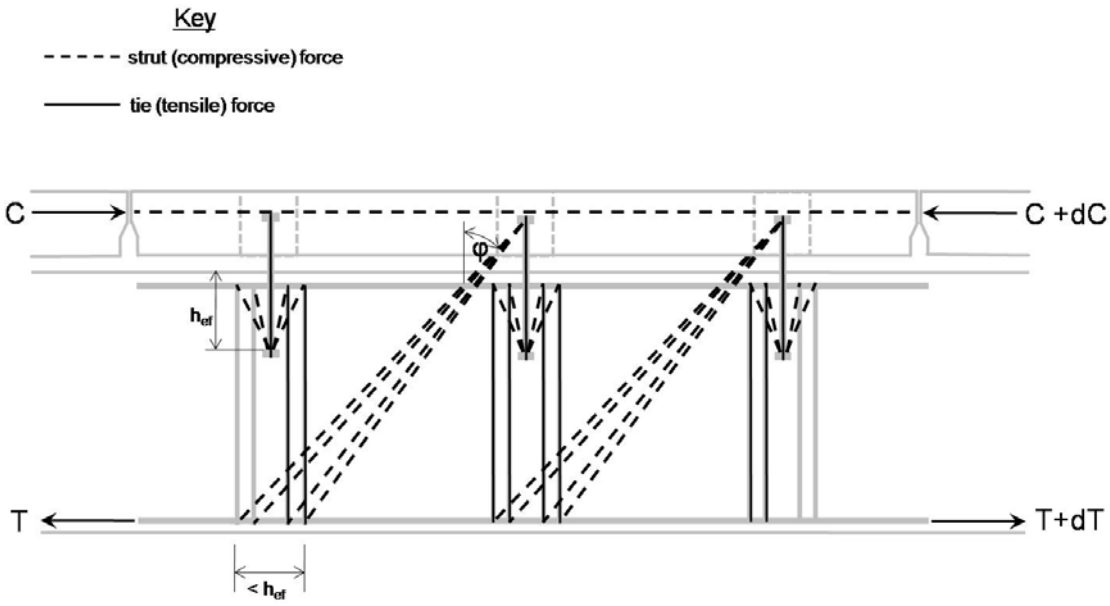

Fig. 36—Representative schematic of required shear reinforcement detailing and strut-and-tie model of a three-pocket panel.

CHAPTER VII
SUMMARY

7.1 Summary and conclusions

A total of 24 specimens were experimentally evaluated to determine their initial breakaway shear strength, post-breakaway resistance in terms of an implied coefficient of friction, and ultimate displacement limits of various connectors. Three failure mechanisms were observed from testing: 1) sliding shear, 2) beam failure, and 3) cone pullout failure. The sliding shear failure mechanism was the most common. The beam failure justified the importance of detailing, where hoopsets are needed to surround the connector to limit cone pullout and beam failure due to the shear stress concentration.

Conventional R-bars were tested as control specimens to compare the performance of both pre-installed (precast) and post-installed shear connectors. Several connectors and conditions were investigated to provide alternatives to optimize the performance of the deck-haunch-beam system. The interface shear capacity of the existing R-bar system used in present practice is sound. From the tests, the inferred coefficient of interface friction between cracked concrete-concrete interfaces that exist within the haunch of a prestressed concrete slab-on-girder bridge is at least 1.0. The best-performing shear connector (for these initial tests without intentionally roughened surfaces) was the threaded rod with the coupler, which yielded an implied coefficient of friction of 0.6. This specimen was used as the baseline model for comparing the performance of several other connection types and conditions explored. The TRC specimen provided a lower-bound peak load resistance of 311 kN (70 kips) and 285 kN (64 kips) for the 51-mm (2.0-in.) and 89-mm (3.5-in.) haunch heights, respectively, with adequate ductility.

Initial experimental test results revealed a coefficient of sliding friction in the cracked grout-bed that exists between the precast concrete slab and concrete girder of 0.4 to 0.6. The range of results was not expected, but revealed the importance and impact of surface roughening; the initial test specimens had relatively smooth shear

interface between the soffit of the precast panels and the grout in the haunch. Therefore, additional tests were conducted to investigate alternative connectors and to conduct parametric studies to explore the effects of haunch height, surface roughness, an alternative grout, and grouping effects of connectors. Several lessons were learned:

1. Due to inadequate beam detailing, the tests with a 89-mm (3.5-in.) haunch revealed brittle beam failure. This raised an important issue for the necessity of hoopsets that need to surround the connector.
2. The effect of surface roughness was a critical parameter that significantly affected the shear resistance.
3. An in-house grout was developed and yielded comparable results to the SikaGrout® 212 with a projected material cost that is much lower.
4. While not constructible for the system with prestressed concrete girders, Nelson studs provided adequate shear resistance and ductility compared to previous tests conducted (Scholz et al, 2007). BC connections serve as viable and efficient alternatives to TRC connections.
5. When the number of connectors increase, the connectors become less efficient in resisting lateral force due to grouping effects.
6. From the tests performed, it was shown that a reliable coefficient of friction was 0.8 in this roughened case compared to 0.6 without roughening the mating surface. Therefore, having more friction contributes to the resistance of the system, particularly the deck-haunch-beam system for this investigation, since the interface shear is dependent on both the coefficient of friction and tensile capacity of the connector.

A design procedure was provided for the determination of the number of pockets and TRC connectors needed to resist the shear flow in a design application. Adding a reasonable number of shear pockets can help distribute the shear load more evenly, though care should be taken to ensure that the pocket arrangement required can be included in the prestressing of the precast deck panels without undue effort and associated costs.

7.2 Recommendations for design and construction

Per the experimental results and analysis and the resulting conclusions outlined in Section 7.1, several recommendations are made for the engineering design and construction practices. The provisions in the applicable design codes are revisited and a simplified cost-benefit analysis is presented for the construction of various connection types.

7.2.1 Code change

Based on the results of the tests performed, the 2007 AASHTO LRFD Bridge Design Specification Eq. 5.8.4.1-3 should be modified for the deck-haunch-beam system such that the nominal resistance of the interface plane shall be taken as the yield force of the connector(s) multiplied by a friction coefficient, provided that the haunch grout provides satisfactory flow and compressive strength characteristics. Therefore, AASHTO LRFD Eq. 5.8.4.1-3 should be rewritten as

$$V_{ni} = \mu_f A_s f_y \tag{18}$$

In the application of Equation (18) to full-depth precast panel connections to prestressed concrete girders, μ_f should be taken as 0.8 for connections with mating surfaces intentionally roughened to an amplitude of 6 mm (0.25 in.) and 0.6 for grout-concrete connections not intentionally roughened. These friction factors are comparable to the concrete-concrete friction factors given in the 2007 AASHTO LRFD Bridge Design Specifications, 5.8.4.3 Cohesion and Friction Factor, where surface roughness of the shear plane is critical in affecting the interface shear transfer (LRFD 5.8.4, Interface Shear Transfer - Shear Friction) and an amplitude of 6 mm (0.25-in.) for surface roughening is cited.

Additionally, the shear reinforcing of the girders of a system that utilizes a full-depth precast panel must be clustered to withstand the concentrated shear loads from the pockets. Fig. 35 should be added to the AASHTO LRFD Specification, and any beams utilizing this connection should be designed accordingly.

7.2.2 Specifications for application

This thesis has demonstrated the efficacy of several shear connections for a full-depth precast panel to prestressed concrete girder structure, including the TR, TRC, and BC connections. In practice there are advantages and disadvantages of each.

The TRC connection served as the baseline for comparison of different pre- and post-installed connection systems because of its excellent performance in terms of both strength and ductility. The couplers increase the material cost of the connection and the labor cost at the prestressing contractor, but having a flat-topped girder will make transportation and panel placement easier. One major drawback of this system is the potential for problems during the installation process. The rods will have to be cut and filed to the correct length, either by a supplier or by the on-site contractor. Both a nut and a rod have to be installed for each connector, and a second nut has to be used during installation as a lock-nut to ensure that the rod is properly seated in the threads of the coupler. Also any damage to the threads in the coupler or on the rod could prevent the connection from being made without filing. Another drawback is that threaded rods once cut to specific length lack a standard marking system, so care must be taken to ensure that high-strength threaded rod is kept separate from any other similar threaded rod on the job site.

The BC system appears to perform very similarly to the TRC system, but further testing would add redundancy to the understanding of its strength and ductility. The coupler in the BC system provides the same advantages as the coupler for the TRC system during precasting, transportation, and panel placement. The main advantage would come in the installation phase of the connectors, as the bolt is a one-piece connector that could quickly be installed with an impact wrench. Also the standard markings on structural bolts reduce the chance of the installation of an incorrect connector. There is still a chance for installation delays due to damage to the threads of the connector or coupler, but they are somewhat lessened for the connector since the bolt threads are factory-finished.

The material cost of the TR connection system is less than the TRC and BC systems because no coupler is required. Labor costs for installation are also less because the connection is less complicated and requires less rod cutting. The drawbacks of this system are the complications in transportation and panel placement and the fact that it did not perform quite as well as the TRC baseline, though it generally exhibited satisfactory strength and ductility.

It should also be noted that, with the exception of the CIP control specimens and the NS specimens for comparison with Scholz et al. (2007), this research only investigated the shear capacity of connections made using one or two high-strength steel connectors with a nominal diameter of 25 mm (1 in.). In the case where a planned pocket shear capacity exceeds that of two such fasteners, more pockets should be used on the panel(s) in question. If the number of pockets is constrained by other design parameters, the use of three or more 25-mm (1-in.) fasteners is not recommended, both because such a connection is outside of the scope of this research and for a number of practical considerations. The first consideration is that prestressed concrete girders are generally cast with a web that is significantly narrower than the width of the top flange. This is especially true of so-called "Texas girders" and other girder designs developed to maximize component efficiency. Thus the web is generally the controlling dimension for the width of the connector arrangement, which must include not only the connector head diameter but also the required spacing and concrete cover. A second practical consideration is that the length of each panel pocket is limited by the interference of the pockets with the transverse prestressing strands in the precast panels. Thus the benefit of any increase in pocket length must be weighed against the cost of sacrificing the continuity of an additional panel prestressing strand.

A viable alternative to the use of three connectors in a pocket is to investigate the use of two connectors with a slightly larger diameter of 29 mm (1⅛ in.) or 32 mm (1¼ in.). The use of such connectors significantly increases the area of steel across the shear interface without proportionately increasing the space required in the panel pocket.

7.3 Recommendations for future research

Though this thesis provides several viable solutions to provide a satisfactory shear connection, there are several aspects of this complex problem that were not fully investigated. The aspects should be considered for further research in order to better understand the behavior of the variety of configurations of this structure.

1. The clustering of girder hoops as explained in Chapter V. This proposed method to provide adequate shear reinforcement for multiple connectors and the increased moment arm of a taller haunch, such as the 89-mm (3.5-in.) connection tested, are key to realizing the efficacy of a wider range of shear connections.
2. The use of larger-diameter shear connectors as explained in Section 7.2. In reviewing the results of this research, this sort of connector appears to be a viable solution to the problem created when the yield force of two connectors is insufficient and increasing the number of pockets is undesirable. However, testing of such connections is required to substantiate that theory.
3. Multiple pocket effects. It is unknown how multiple pockets would interact if tested simultaneous on a full-panel system shear test.
4. Fatigue testing. The fatigue of highway structures is often the controlling design factor, but this thesis examines only quasi-static loading to the point of failure. Shear fatigue testing of connections under cyclical service loads would provide valuable information for forecasting the long-term performance of the system in the field.

REFERENCES

AASHTO. (2007). *AASHTO LRFD bridge design specifications and commentary, AASHTO LRFD-07*, 4th Ed., Washington, D.C.

ACI Committee 318. (2008). *Building code requirements for structural concrete (ACI 318-08) and commentary (ACI 318R-08)*, Farmington Hills, Mich.

AISC. (2005). *AISC steel construction manual, AISC-13*, 13th Ed., Chicago, Ill.

Badie, S.S., Tadros, M.K., and Girgis, A.F. (2006). "Full-depth precast concrete bridge deck panel systems." *National Cooperative Highway Research Board Report 584*, Transportation Research Board, Washington, D.C.

Burnet, M.J. and Oehlers, D.J. (2001). "Fracture of mechanical shear connectors in composite beams." *Mech. Struct. Mach.*, 29(1), 1-41.

Fuchs, W., Eligehausen, R., and Breen, J.E. (1995). "Concrete capacity design (CCD) approach to fastening to concrete," *ACI Struct. J.*, 92(6), 787-802.

Gattesco, N., Giuriani, E., and Gubana, A. (1997). "Low-cycle fatigue test on stud shear connectors." *J. Struct. Eng.*, 123(2), 145-150.

Kwon, G., Hungerford, B., Kayir, H., Schaap, B., Ju, Y.K., Klingner, R., and Engelhardt, M. (2007). "Strengthening existing non-composite steel bridge girders using post-installed shear connectors." *Report No. 0-4124-1*, Center for Transportation Research, Austin, Tex.

Muratli, H., Klingner, R.E., and Graves, H.L. (2004). "Breakout capacity of anchors in concrete – part 2: shear." *ACI Struct. J.,* 101(6), 821-829.

Oehlers, D.J. (1990). "Deterioration in strength of stud connectors in composite bridge beams." *J. Struct. Eng.,* 116(12), 3417-3431.

Oehlers, D.J. (1995). "Design and assessment of shear connectors in composite bridge beams." *J. Struct. Eng.,* 121(2), 214-224.

Oehlers, D.J. and Sved, G. (1995). "Composite beams with limited slip capacity shear connectors." *J. Struct. Eng.,* 121(6), 932-938.

Oehlers, D.J., Seracino, R., and Yeo, M.F. (2000). "Effect of friction on shear connectors in composite bridge beams." *J. Bridge Eng.*, 5(2), 91-98.

Olgaard, J., Slutter, R., and Fisher, J. (1971). "Shear strength of stud connectors in lightweight and normal weight concrete." *Eng. J. AISC*, 8(2), 55-64.

Scholz, D.P., Wallenfelsz, J.A., Lijeron, C., and Roberts-Wollmann, C.L. (2007). "Recommendations for the connection between full-depth precast bridge deck panel systems and precast I-beams." *Report No. 07-CR17*, Virginia Transportation Research Council, Charlottesville, Vir.

Shirvani, M., Klingner, R.E., and Graves, H.L. (2004). "Breakout capacity of anchors in concrete – part 1: tension." *ACI Struct. J.,* 101(6), 812-820.

Slutter, R.G. and Driscoll, G.C. (1965). "Flexural strength of steel-concrete composite beams." *J. Struct. Eng.,* 91(2), 71-99.

Slutter, R.G. and Fisher, J.W. (1966). "Fatigue strength of shear connectors." *Highway Research Record No. 147*, Highway Research Board, Washington, D.C.

Trejo, D., Hite, M., Mander, J., Ley, T., Mander, T.J., Henley, M.D., Scott, R.S., and Patil, S. (2008). "Development of a precast overhang system for the Rock Creek bridge." *Technical Report 0-6100-2*, Texas Transportation Institute, College Station, Tex.

Xue, W., Ding, M., Wang, H., and Luo, Z. (2008). "Static behavior and theoretical model of stud shear connectors." *J. Bridge Eng.,* 13(6), 623-634.

APPENDIX A
SHEAR TEST SUMMARIES

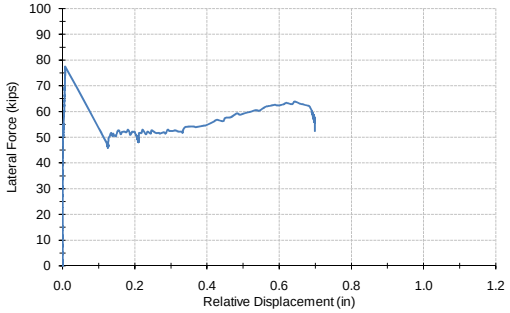

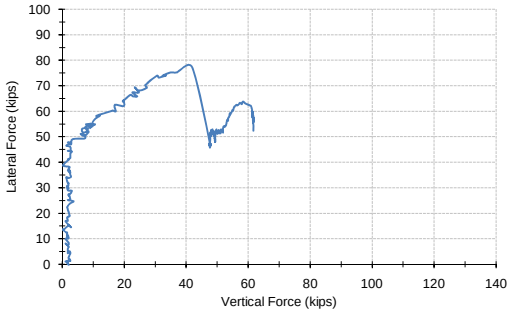

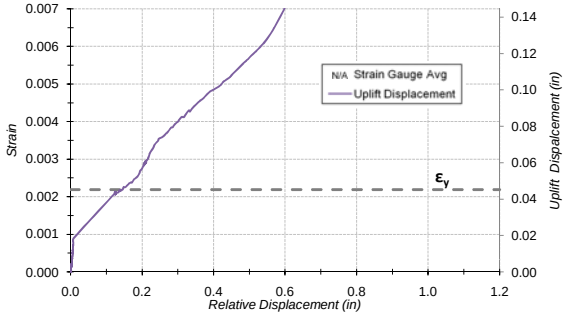

4_CIP_2.0_A - "Douglas"

- First test - no formal notes
- Loading was done with the hydraulic pump valves fully open using "bumps"

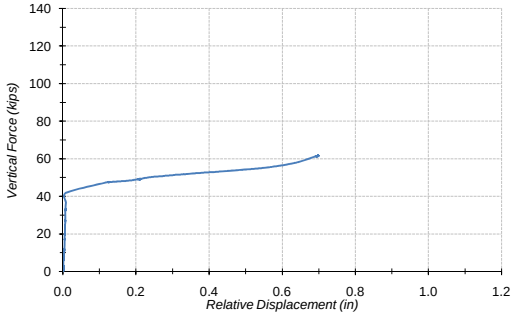

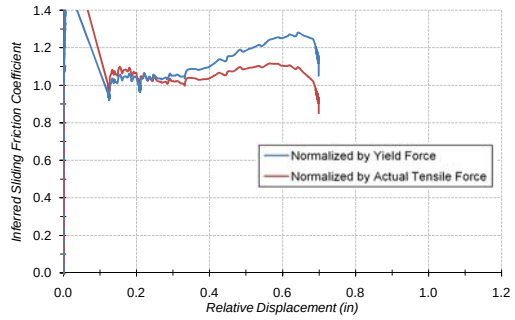

ETS Input		
Length between SPs	16.0	in
Width between LVs	16.5	in
Width between SPs	15.0	in
Distance from LV2 to LV4	4.5	in
Gauge Length	10.00	in
Length of SP25 cable	12.00	in
Length of SP26 cable	12.00	in
Length of SP27 cable	12.00	in
Length of SP28 cable	12.00	in
Effective area of connector	0.7854	in2
Connector Material Input		
εy =	0.0022	
εsu =	0.0885	
εsh =	0.0066	
fy =	63	ksi
fsu =	99	ksi
Es =	29000	ksi
Esh =	1175	ksi
P =	2.671	

Yield Tensile Force **49.8 kips**

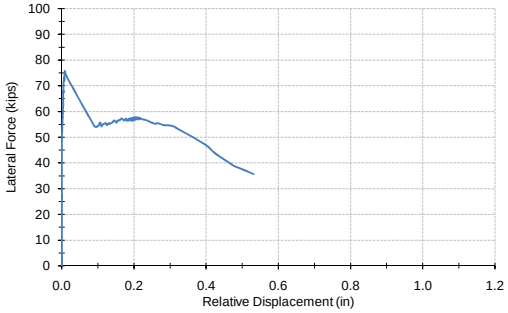

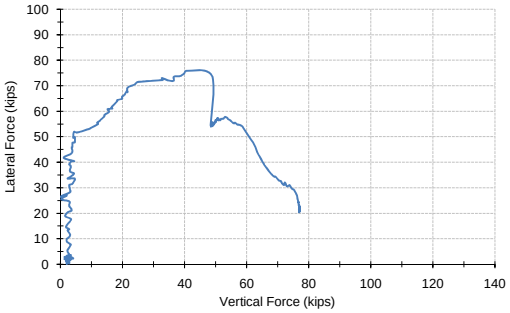

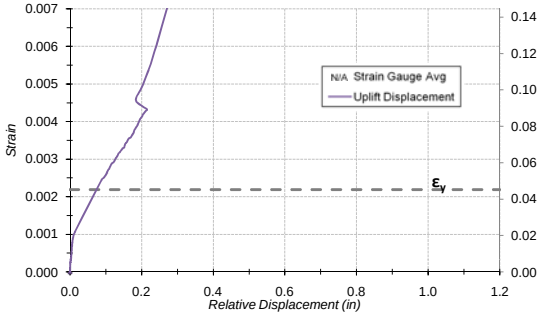

4_CIP_2.0_B - "Jennifer"

- Tightened to 10k, back to 0
- Prestressed dywi to 6000 psi (120 k)
- Used hyrdaulic pump valve barely open for constant loading (worked well)
- Smooth failure at ~75k w/significant bucking
- Video and pictures
- Lost LV1 somewhere around initial failure
- SPs may have been altered by LV blocks
- Added LV3 (nugget-column) and LV4 (donut-column; 10.5 in from N)

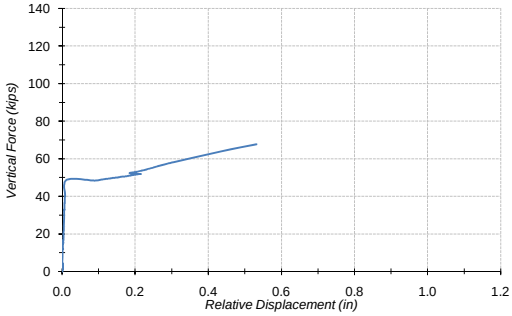

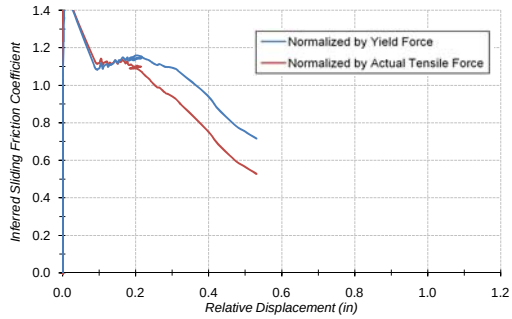

ETS Input		
Length between SPs	16.0	in
Width between LVs	16.5	in
Width between SPs	15.0	in
Distance from LV2 to LV4	4.5	in
Distance between nuts	10.00	in
Length of SP25 cable	12.00	in
Length of SP26 cable	12.00	in
Length of SP27 cable	12.00	in
Length of SP28 cable	12.00	in
Effective area of connector	0.7854	in2
Connector Material Input		
εy =	0.0022	
εsu =	0.0885	
εsh =	0.0066	
fy =	63	ksi
fsu =	99	ksi
Es =	29000	ksi
Esh =	1175	ksi
P =	2.671	

Yield Tensile Force **49.8** **kips**

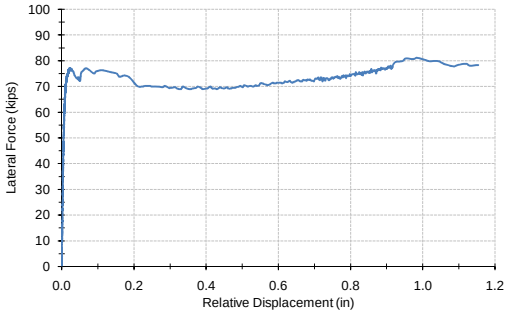

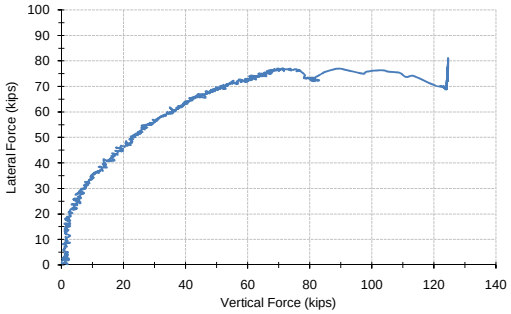

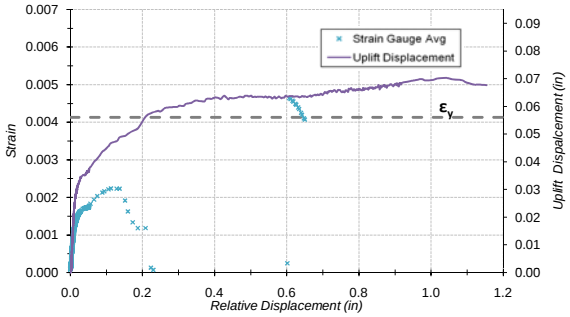

2_TRC_2.0_A - "Emily"

- Pretensioned to 6000 psi; problems tightening; used rope with coupler...standard for remained of tests.
- Nugget bucked up ~1/2" and failed
- Specimen cored at interior edge to allow for beam-floor prestressing

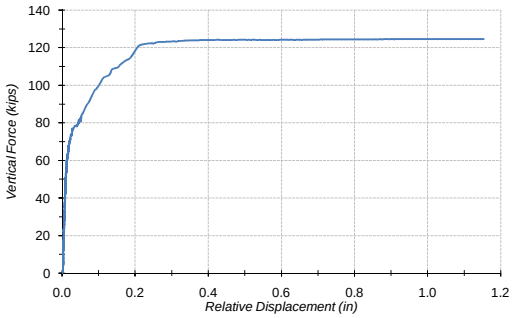

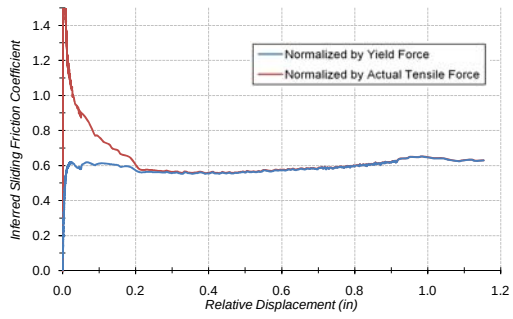

ETS Input		
Length between SPs	16.0	in
Width between LVs	16.5	in
Width between SPs	15.0	in
SP25 Height	12.5	in
SP26 Height	12.5	in
SP27 Height	12.5	in
SP28 Height	12.5	in
Distance from LV2 to LV4	4.5	in
Effective Gauge Length	13.57	in
Effective area of connector	1.0408	in2
Connector Material Input		
εy =	0.0041	
εsu =	0.0277	
εsh =	0.0060	
fy =	120	ksi
fsu =	137	ksi
Es =	29000	ksi
Esh =	1250	ksi
P =	1.572	

Yield Tensile Force **124.6 kips**

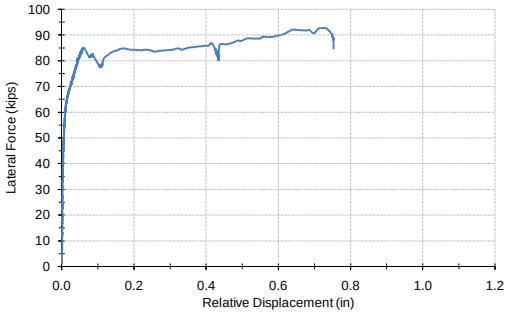

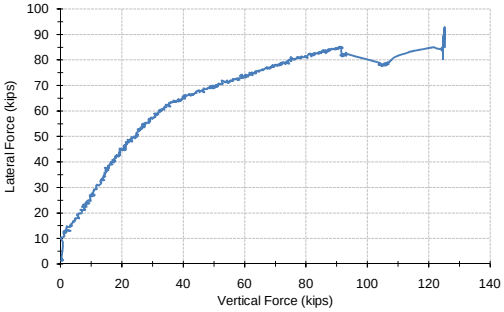

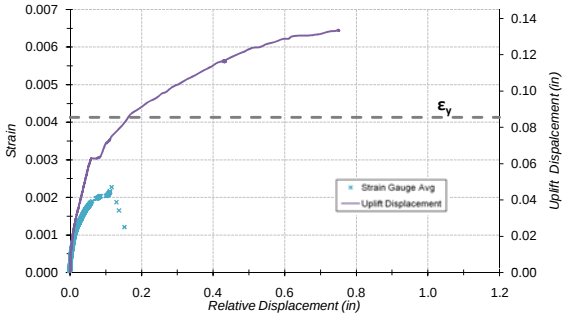

2_TRC_2.0_B - "Dopey"

- This was the one with bolts in the nugget and TRs in the donut.
- Good gradual fail
- First specimen tested in N-S setup.

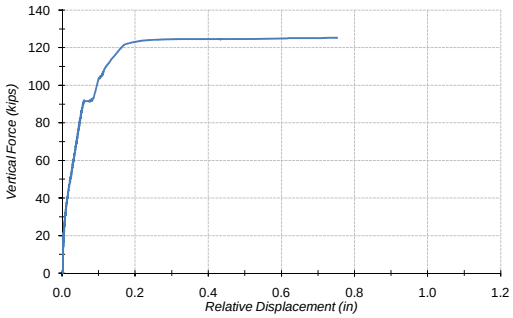

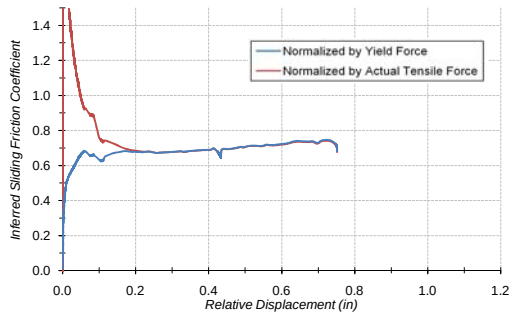

ETS Input		
Length between SPs	16.0	in
Width between LVs	16.5	in
Width between SPs	15.0	in
SP25 Height	12.5	in
SP26 Height	12.5	in
SP27 Height	12.5	in
SP28 Height	12.5	in
Distance from LV2 to LV4	4.5	in
Effective Gauge Length	20.71	in
Effective area of connector	1.0408	in2
Connector Material Input		
εy =	0.0041	
εsu =	0.0277	
εsh =	0.0060	
fy =	120	ksi
fsu =	137	ksi
Es =	29000	ksi
Esh =	1250	ksi
P =	1.572	

Yield Tensile Force **124.6 kips**

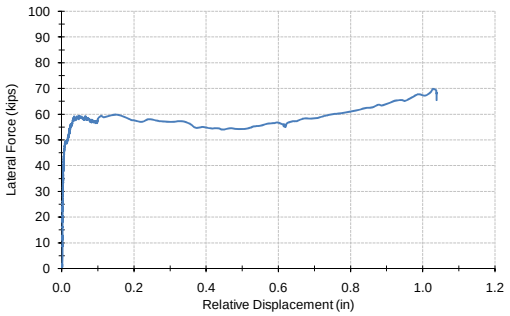

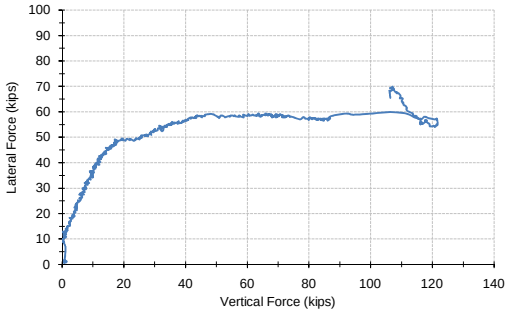

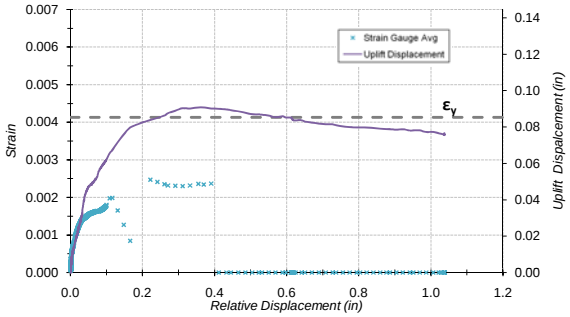

2TR_2.0_A - "Happy"

- Good, gradual fail.

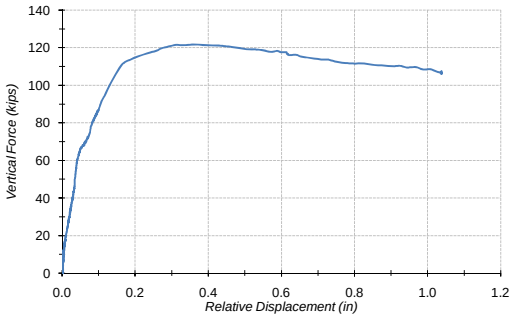

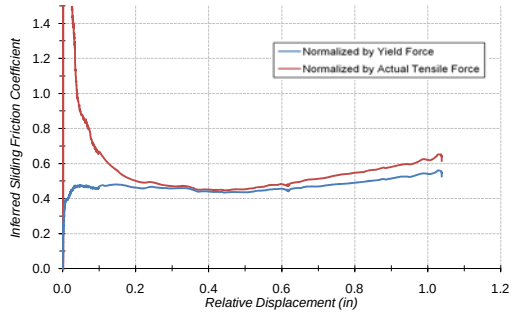

ETS Input		
Length between SPs	16.0	in
Width between LVs	16.5	in
Width between SPs	15.0	in
SP25 Height	12.5	in
SP26 Height	12.5	in
SP27 Height	12.5	in
SP28 Height	12.5	in
Distance from LV2 to LV4	4.5	in
Effective Gauge Length	21.43	in
Effective area of connector	1.0408	in2
Connector Material Input		
ey =	0.0041	
esu =	0.0277	
esh =	0.0060	
fy =	120	ksi
fsu =	137	ksi
Es =	29000	ksi
Esh =	1250	ksi
P =	1.572	

Yield Tensile Force **124.6 kips**

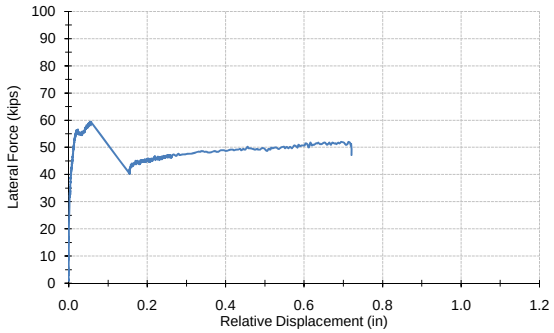

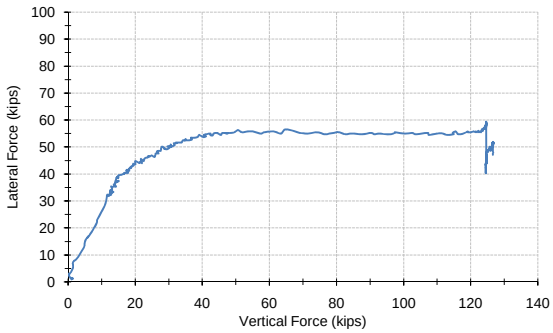

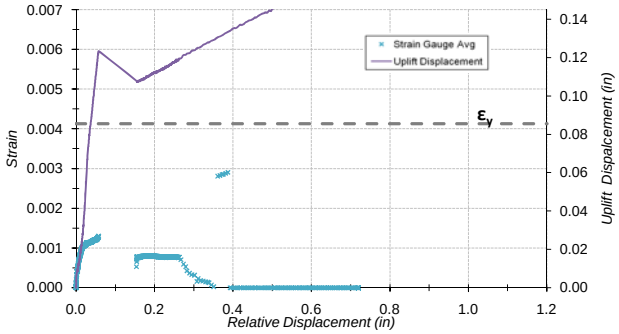

2TR_2.0_B - "Sneezy"

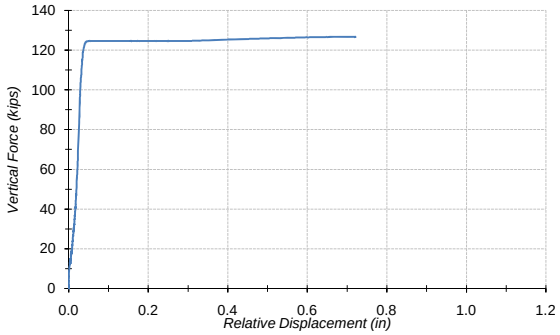

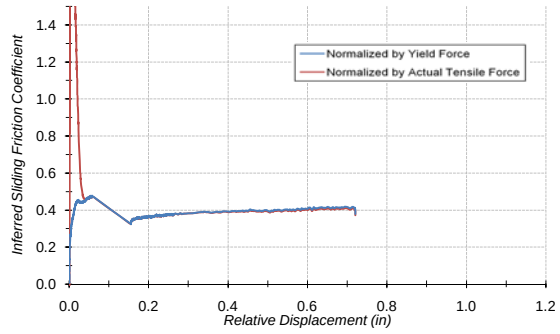

ETS Input		
Length between SPs	16.0	in
Width between LVs	16.5	in
Width between SPs	15.0	in
SP25 Height	12.5	in
SP26 Height	12.5	in
SP27 Height	12.5	in
SP28 Height	12.5	in
Distance from LV2 to LV4	4.5	in
Effective Gauge Length	20.71	in
Effective area of connector	1.0408	in2
Connector Material Input		
ey =	0.0041	
esu =	0.0277	
esh =	0.0060	
fy =	120	ksi
fsu =	137	ksi
Es =	29000	ksi
Esh =	1250	ksi
P =	1.572	

Yield Tensile Force **124.6 kips**

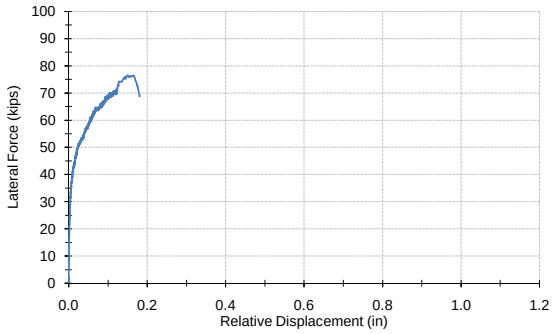

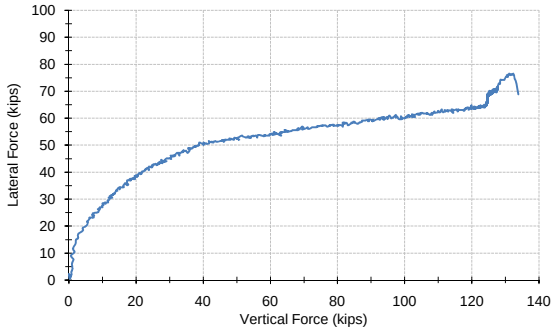

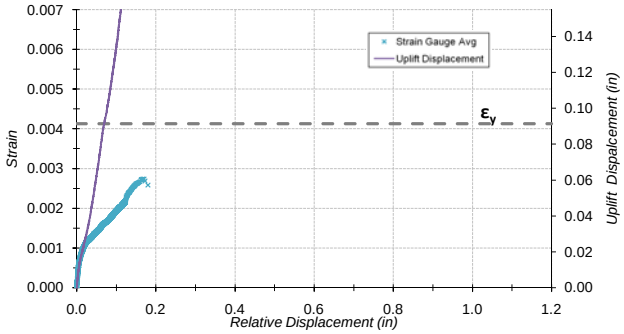

2_TRC_3.5_A - "Snow White"

- Initial cracking of grout at 53k
- Sudden composite failure of grout, pocket concrete, and donut unconfined concrete
- Lost LV2 (and maybe SP28) at fail

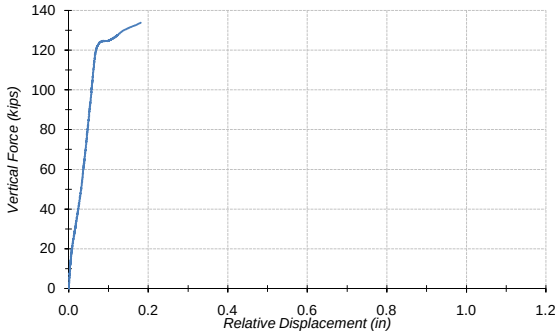

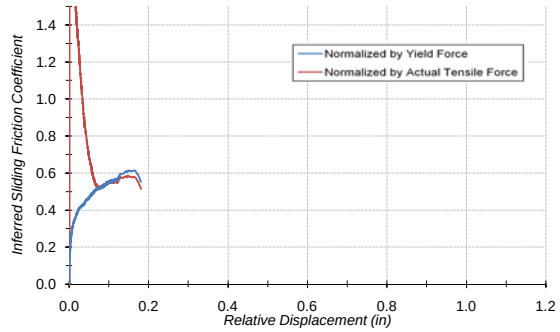

ETS Input		
Length between SPs	16.0	in
Width between LVs	16.5	in
Width between SPs	15.0	in
SP25 Height	12.5	in
SP26 Height	12.5	in
SP27 Height	12.5	in
SP28 Height	12.5	in
Distance from LV2 to LV4	4.5	in
Effective Gauge Length	22.14	in
Effective area of connector	1.0408	in2
Connector Material Input		
ey =	0.0041	
esu =	0.0277	
esh =	0.0060	
fy =	120	ksi
fsu =	137	ksi
Es =	29000	ksi
Esh =	1250	ksi
P =	1.572	

Yield Tensile Force **124.6 kips**

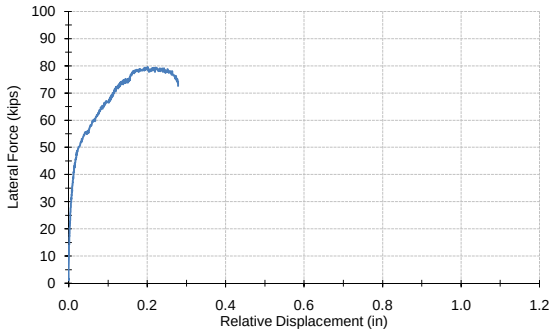

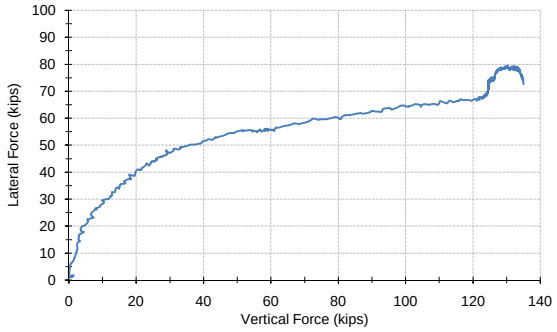

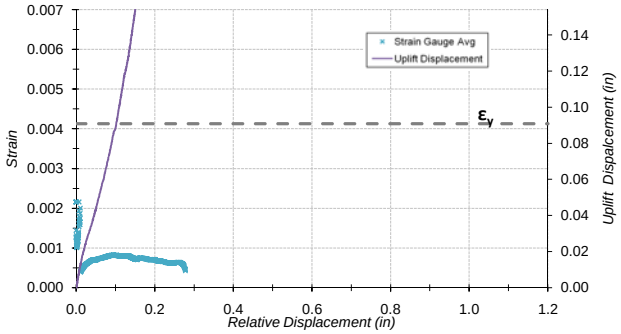

2_TRC_3.5_B - "Bashful"

- Strain gauge A looks faulty ~4000 mstrain after chiseling out Snow White for SP5 string...SG2 used for correlation.
- Load rate a little fast...slowed at 55k
- Initial grout cracking at <55k
- Somewhat sudden failure at ~80k

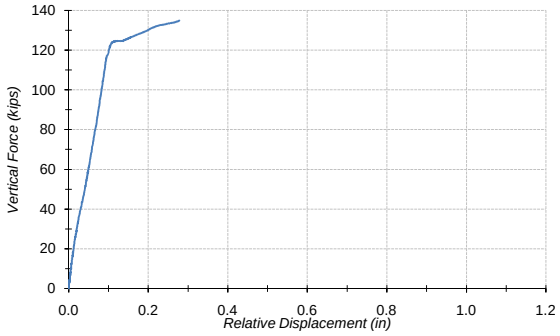

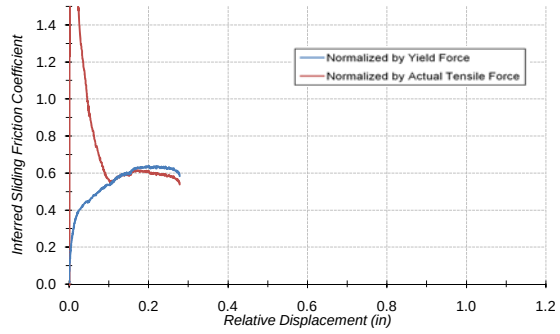

ETS Input		
Length between SPs	16.0	in
Width between LVs	16.5	in
Width between SPs	15.0	in
SP25 Height	12.5	in
SP26 Height	12.5	in
SP27 Height	12.5	in
SP28 Height	12.5	in
Distance from LV2 to LV4	4.5	in
Effective Gauge Length	22.00	in
Effective area of connector	1.0408	in2
Connector Material Input		
εy =	0.0041	
εsu =	0.0277	
εsh =	0.0060	
fy =	120	ksi
fsu =	137	ksi
Es =	29000	ksi
Esh =	1250	ksi
P =	1.572	

Yield Tensile Force **124.6 kips**

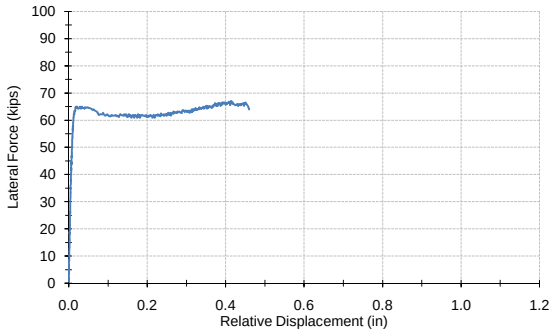

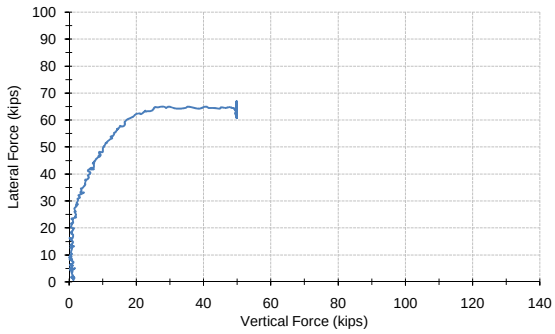

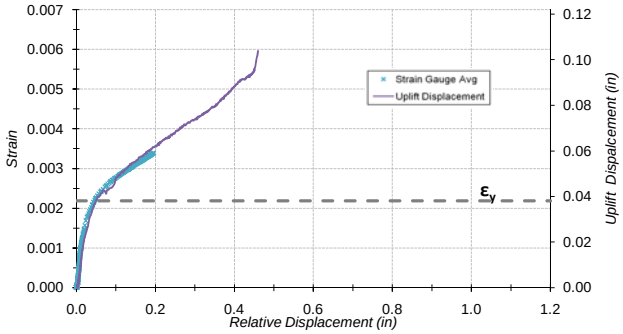

4_R_2.0-A - "Gavin"

- Took off Emily as 1 TR had sheared; Gavin had a sandy bottom; Used steel buildup as other bearing for prestressing dywidag
- No LV3
- Accidentally unplugged SP28 at ~60k

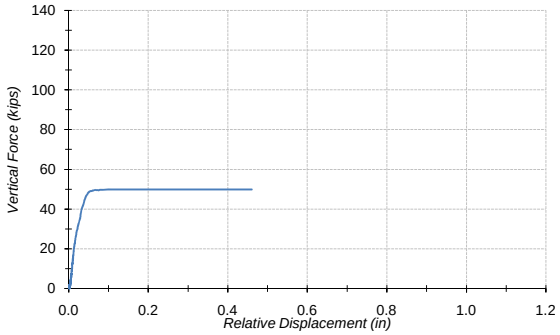

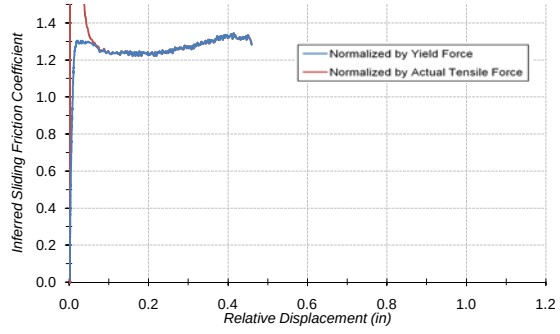

ETS Input		
Length between SPs	16.0	in
Width between LVs	16.5	in
Width between SPs	15.0	in
SP25 Height	12.5	in
SP26 Height	12.5	in
SP27 Height	12.5	in
SP28 Height	12.5	in
Distance from LV2 to LV4	4.5	in
Effective Gauge Length	17.43	in
Effective area of connector	0.7854	in2
Connector Material Input		
ey =	0.0022	
εsu =	0.0885	
εsh =	0.0066	
fy =	63	ksi
fsu =	99	ksi
Es =	29000	ksi
Esh =	1175	ksi
P =	2.671	

Yield Tensile Force **49.8 kips**

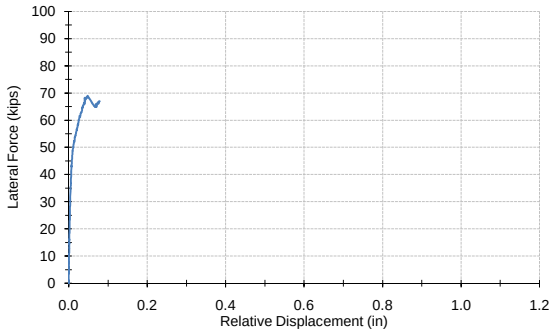

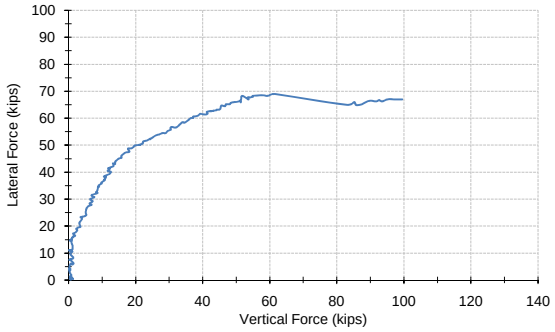

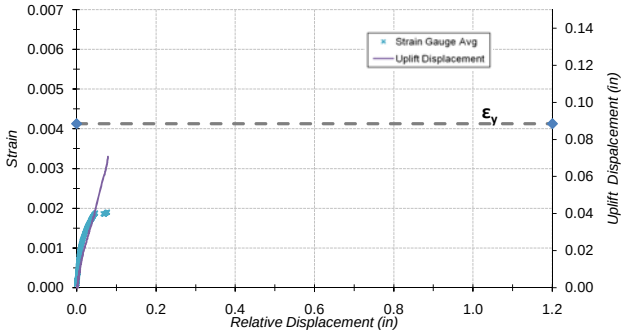

2_TR_3.5_A - "Grumpy"

- Data isn't very easy to work with due to the small displacements and brittle failure...Lg is low, perhaps because these longer TRs have sufficient development length
- First hairline crack at 40k; Beam fail at ~68k

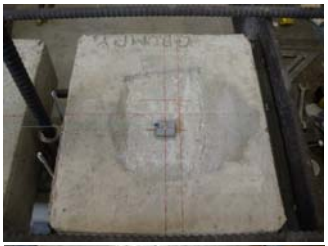

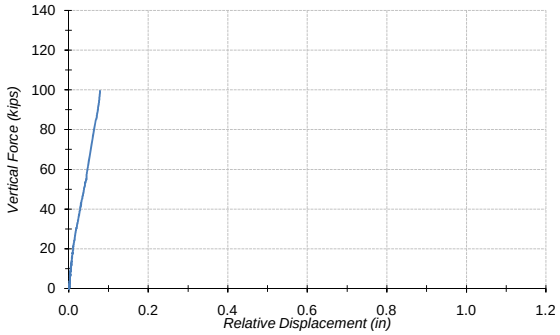

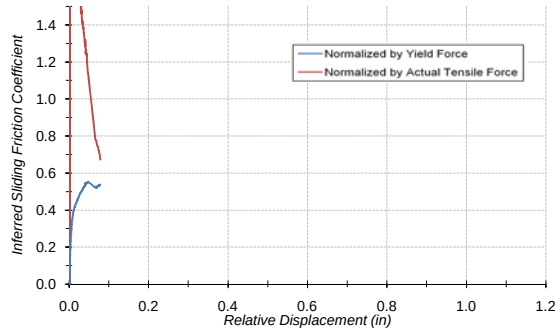

ETS Input		
Length between SPs	16.0	in
Width between LVs	16.5	in
Width between SPs	15.0	in
SP25 Height	12.5	in
SP26 Height	12.5	in
SP27 Height	12.5	in
SP28 Height	12.5	in
Distance from LV2 to LV4	4.5	in
Effective Gauge Length	21.43	in
Effective area of connector	1.0408	in2
Connector Material Input		
ey =	0.0041	
esu =	0.0277	
esh =	0.0060	
fy =	120	ksi
fsu =	137	ksi
Es =	29000	ksi
Esh =	1250	ksi
P =	1.572	

Yield Tensile Force **124.6 kips**

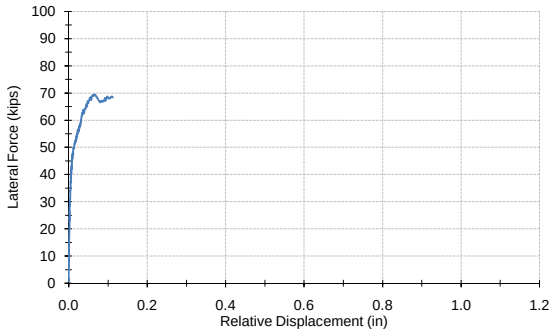

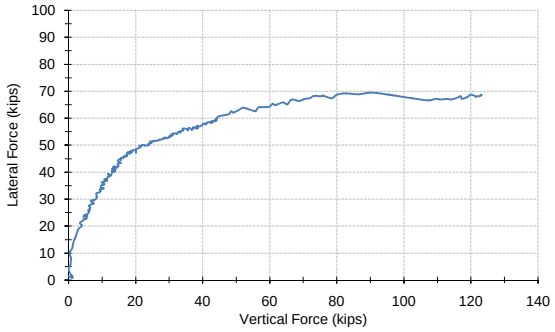

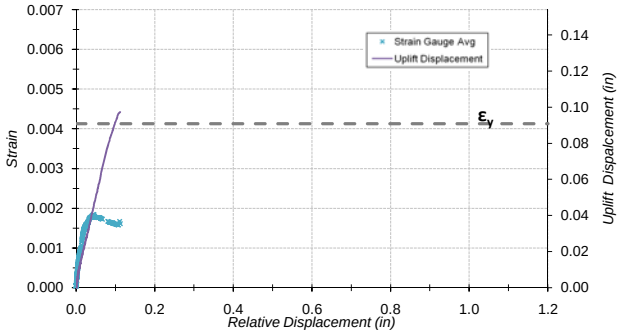

2_TR_3.5_B - "Doc"

- Not a lot of data here due to the short ride
- Damage to concrete under SP28 during shifting
- First crack at 45-50k; Beam fail at ~68k

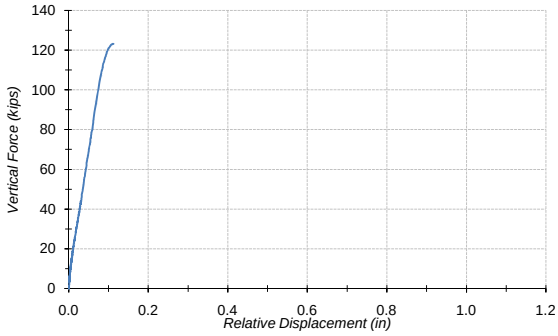

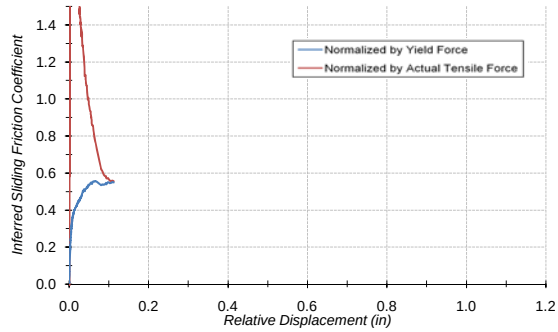

ETS Input		
Length between SPs	16.0	in
Width between LVs	16.5	in
Width between SPs	15.0	in
SP25 Height	12.5	in
SP26 Height	12.5	in
SP27 Height	12.5	in
SP28 Height	12.5	in
Distance from LV2 to LV4	4.5	in
Effective Gauge Length	22.00	in
Effective area of connector	1.0408	in2
Connector Material Input		
ey =	0.0041	
εsu =	0.0277	
εsh =	0.0060	
fy =	120	ksi
fsu =	137	ksi
Es =	29000	ksi
Esh =	1250	ksi
P =	1.572	

Yield Tensile Force **124.6 kips**

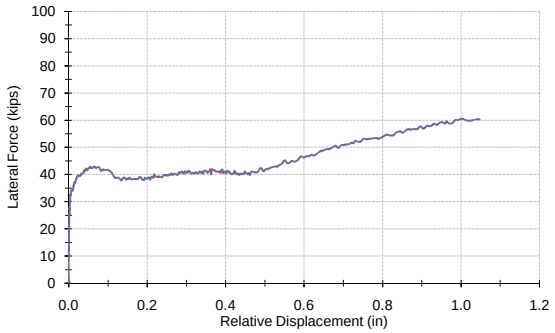

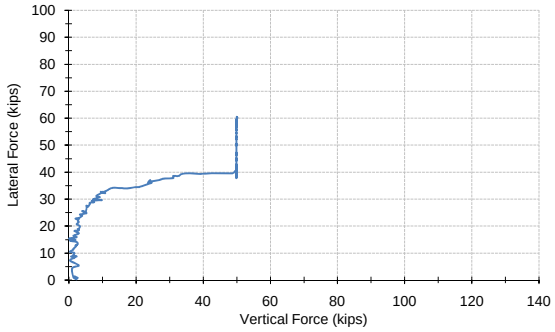

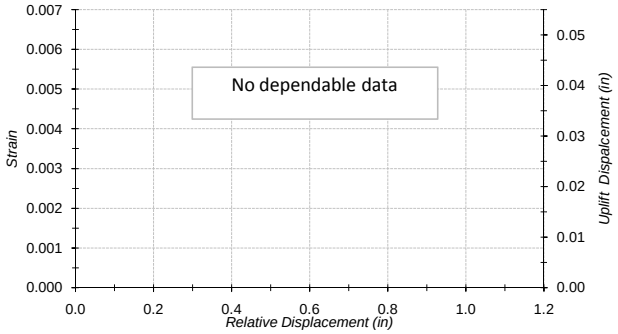

4_CIP_3.5_A - "Meredith"

- Beamed cracked under SP28 during placement - moved up 3", so 9.5" instead of 12.5" from top of SP to bottom of hook
- First haunch crack at 40k
- No dependable data for strain and uplift.

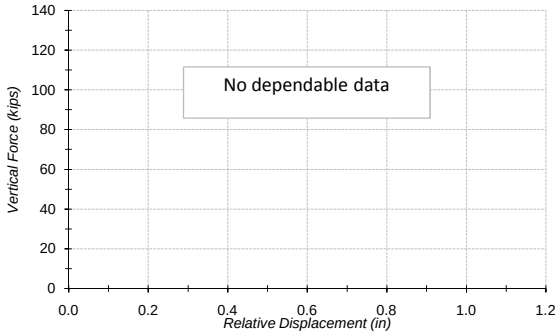

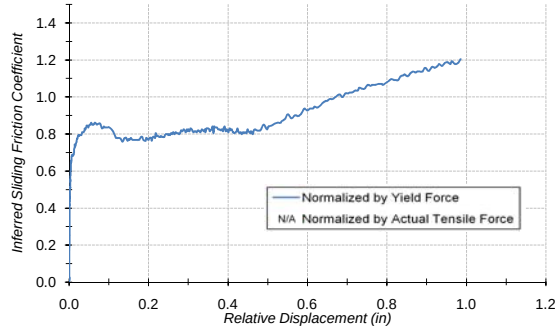

ETS Input		
Length between SPs	16.0	in
Width between LVs	16.5	in
Width between SPs	15.0	in
SP25 Height	12.5	in
SP26 Height	12.5	in
SP27 Height	12.5	in
SP28 Height	9.5	in
Distance from LV2 to LV4	4.5	in
Effective Gauge Length	7.86	in
Effective area of connector	0.7854	in2
Connector Material Input		
εy =	0.0022	
εsu =	0.0885	
εsh =	0.0066	
fy =	63	ksi
fsu =	99	ksi
Es =	29000	ksi
Esh =	1175	ksi
P =	2.671	

Yield Tensile Force **49.8 kips**

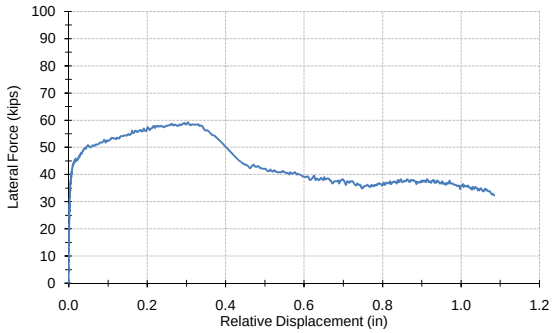

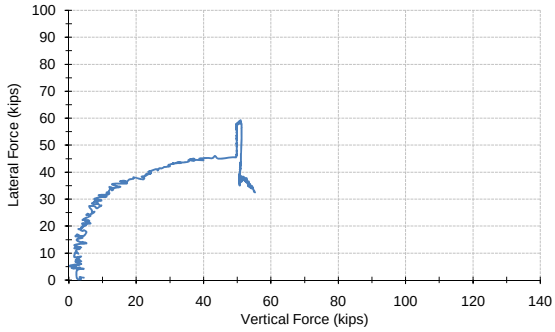

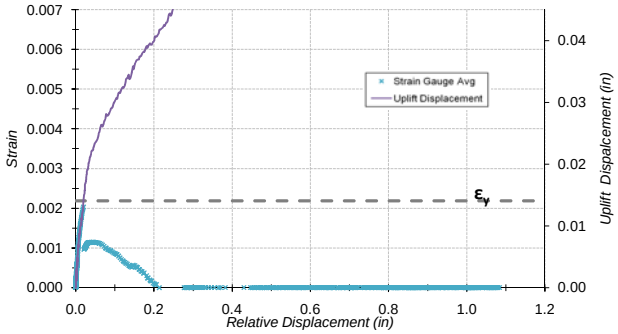

4_CIP_3.5_B - "Luis"

- Epoxy of LV3 and SP5 issue close to testing, but appear fine
- Initial crack at 47k
- Lots of displacement
- Small failure jump

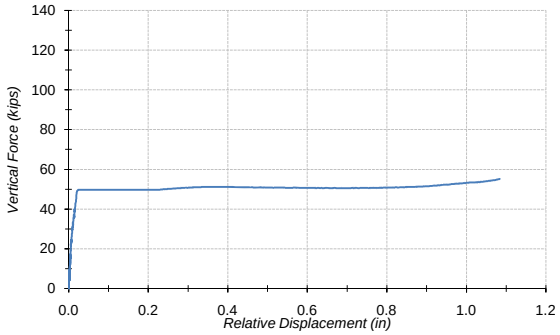

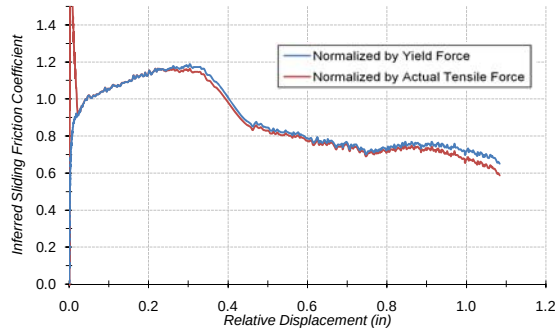

ETS Input		
Length between SPs	16.0	in
Width between LVs	16.5	in
Width between SPs	15.0	in
SP25 Height	12.5	in
SP26 Height	12.5	in
SP27 Height	12.5	in
SP28 Height	12.5	in
Distance from LV2 to LV4	4.5	in
Effective Gauge Length	6.43	in
Effective area of connector	0.7854	in2
Connector Material Input		
ey =	0.0022	
esu =	0.0885	
esh =	0.0066	
fy =	63	ksi
fsu =	99	ksi
Es =	29000	ksi
Esh =	1175	ksi
P =	2.671	

Yield Tensile Force **49.8 kips**

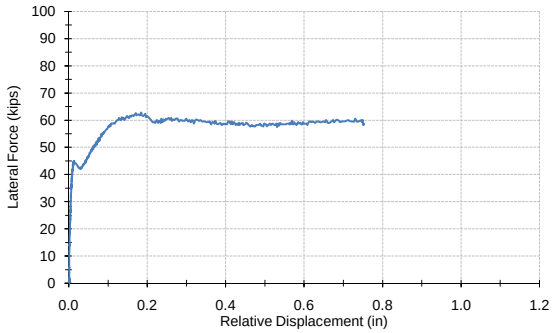

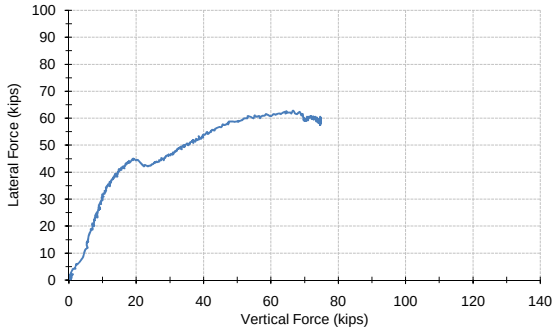

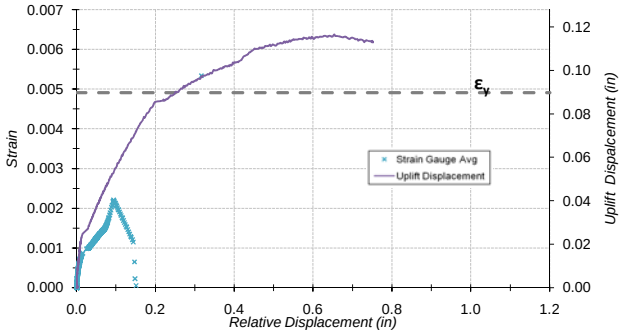

1_BC_2.0_A - "Sleepy"

- Large Lg at 18.29 in, but solid results
- Performance seems very good - strong, ductile, good μ
- Initial grout crack at ~44k
- Smooth initial failure at ~60k; Smooth travel out to 0.7 in at ~60k

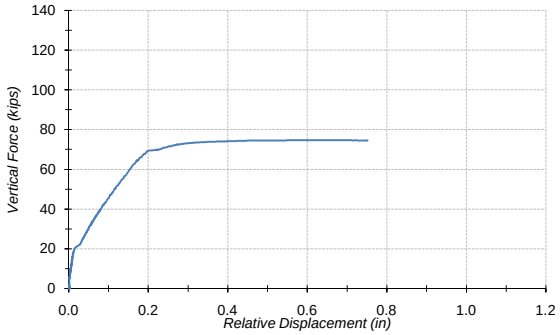

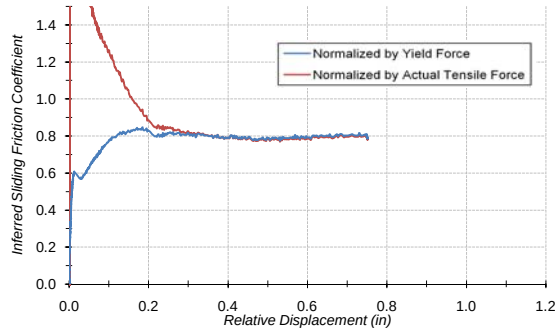

ETS Input		
Length between SPs	16.0	in
Width between LVs	16.5	in
Width between SPs	15.0	in
SP25 Height	12.5	in
SP26 Height	12.5	in
SP27 Height	12.5	in
SP28 Height	12.5	in
Distance from LV2 to LV4	4.5	in
Effective Gauge Length	18.29	in
Effective area of connector	0.5204	in2
Connector Material Input		
ey =	0.0049	
εsu =	0.0180	
εsh =	0.0050	
fy =	142	ksi
fsu =	171	ksi
Es =	29000	ksi
Esh =	911	ksi
P =	0.411	

Yield Tensile Force **74.1 kips**

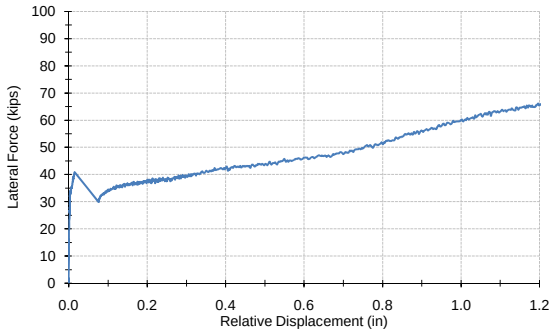

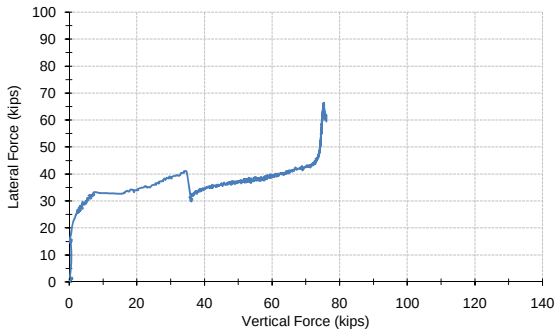

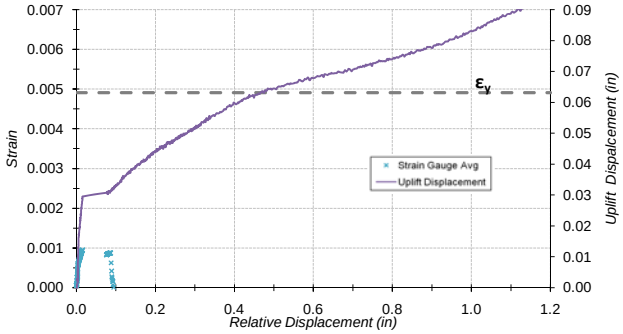

1_BC_2.0_B - "Hannah"

- Nothing out of LV2 - LV1 gives a solid plot
- Strength gain with displacement is interesting
- Initial grout crack at ~35-40k
- Bit of a jump at ~40-45k

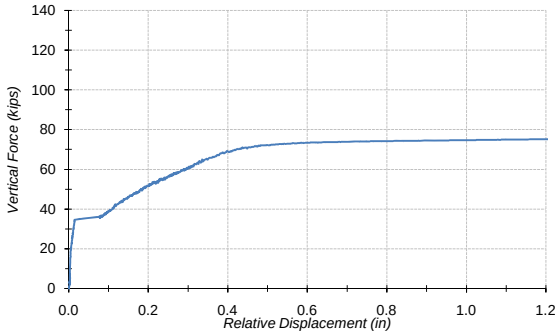

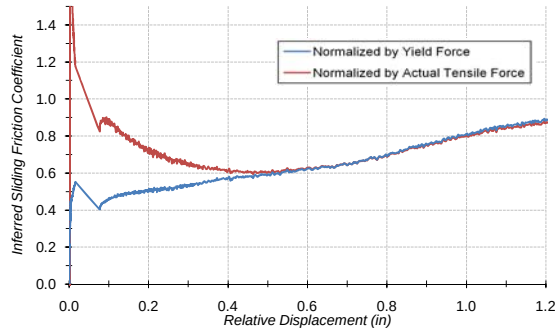

ETS Input		
Length between SPs	16.0	in
Width between LVs	16.5	in
Width between SPs	15.0	in
SP25 Height	12.5	in
SP26 Height	12.5	in
SP27 Height	12.5	in
SP28 Height	12.5	in
Distance from LV2 to LV4	4.5	in
Effective Gauge Length	12.86	in
Effective area of connector	0.5204	in2
Connector Material Input		
ey =	0.0049	
esu =	0.0180	
esh =	0.0050	
fy =	142	ksi
fsu =	171	ksi
Es =	29000	ksi
Esh =	911	ksi
P =	0.411	

Yield Tensile Force **74.1** **kips**

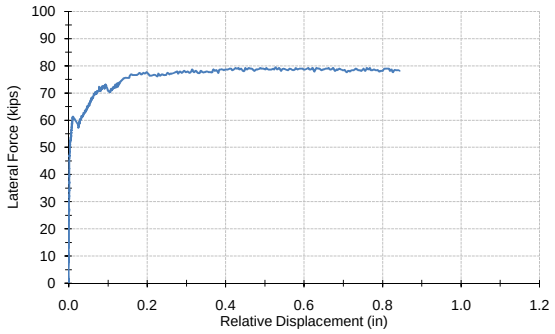

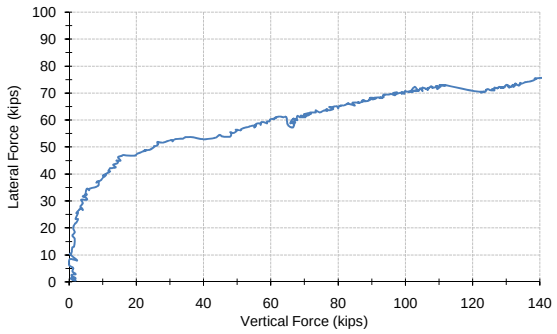

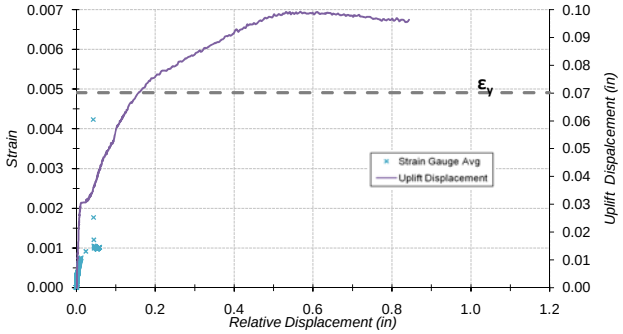

2_BC_2.0 - "Thomas"

- No LV2
- Again, the bolts seem to perform well, better than the TRs.
- Initial grout crack at ~50k
- Ductile failure of beam at ~1.2" (78->71k)
- Cone pullout

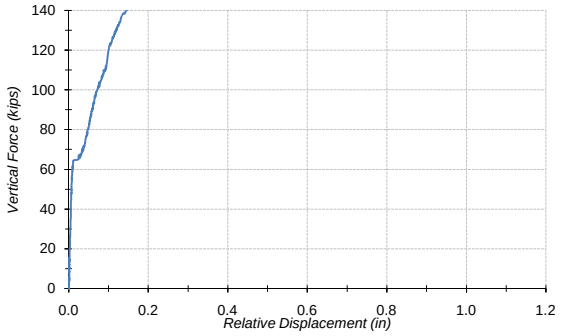

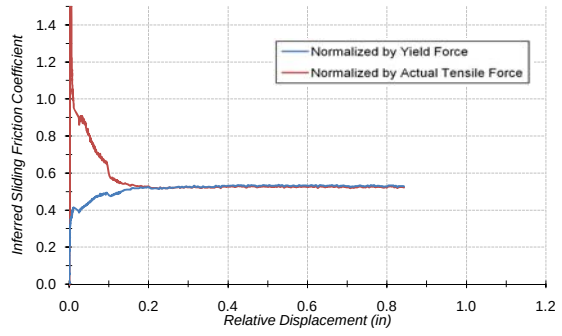

ETS Input		
Length between SPs	16.0	in
Width between LVs	16.5	in
Width between SPs	15.0	in
SP25 Height	12.5	in
SP26 Height	12.5	in
SP27 Height	12.5	in
SP28 Height	12.5	in
Distance from LV2 to LV4	4.5	in
Effective Gauge Length	14.29	in
Effective area of connector	1.0408	in2
Connector Material Input		
ey =	0.0049	
esu =	0.0180	
esh =	0.0050	
fy =	142	ksi
fsu =	171	ksi
Es =	29000	ksi
Esh =	911	ksi
P =	0.411	

Yield Tensile Force **148.2** **kips**

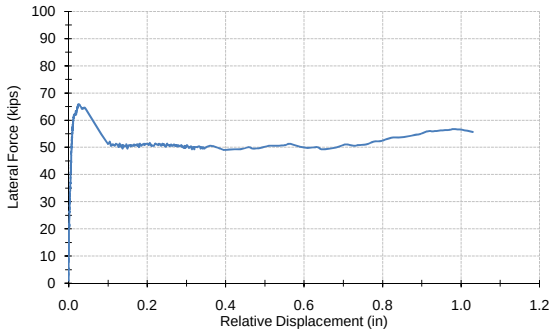

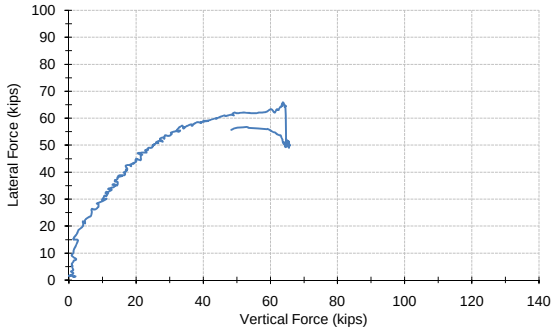

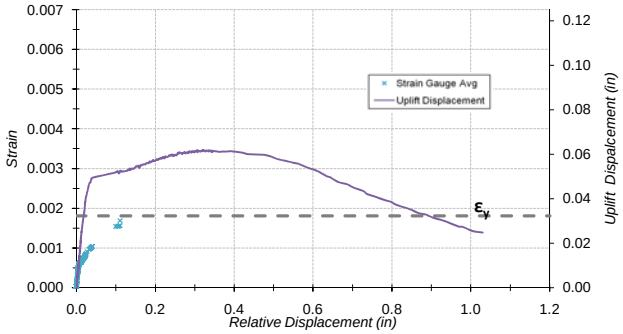

2_NS_2.0 - "Jonathan"

- Appears that the steel yielded, vever fractured or even strain-hardened.
- Rising branch is interesting...perhaps the second stud is engaging
- Power issue at ~55k; Initial crack at ~60k; Opened at ~65k
- Sudden fail at ~60k, around 1.0"

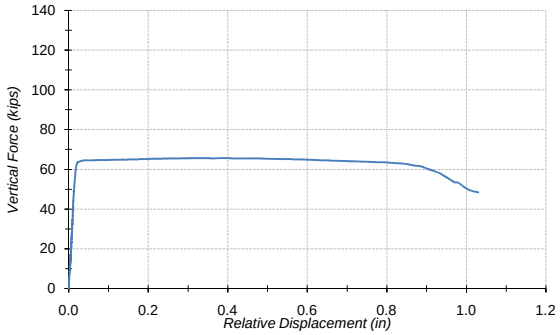

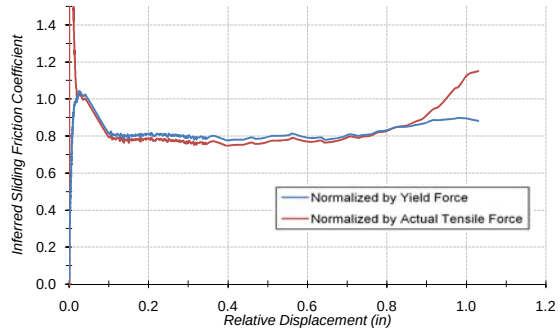

ETS Input		
Length between SPs	16.0	in
Width between LVs	16.5	in
Width between SPs	15.0	in
SP25 Height	12.5	in
SP26 Height	12.5	in
SP27 Height	12.5	in
SP28 Height	12.5	in
Distance from LV2 to LV4	4.5	in
Effective Gauge Length	17.85	in
Effective area of connector	1.2026	in2
Connector Material Input		
ey =	0.0018	
esu =	0.0194	
esh =	0.0019	
fy =	53	ksi
fsu =	78	ksi
Es =	29000	ksi
Esh =	1309	ksi
P =	0.885	

Yield Tensile Force **63.2** **kips**

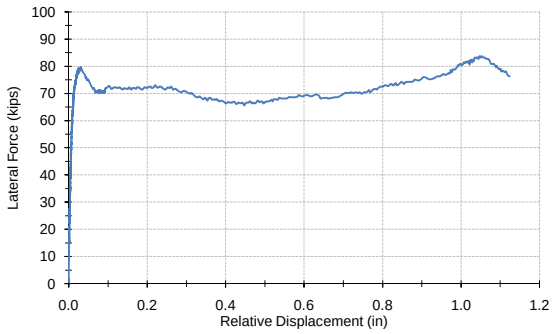

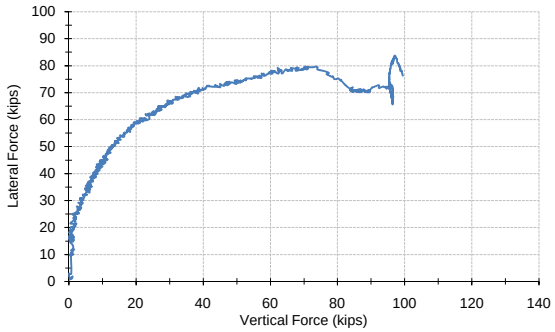

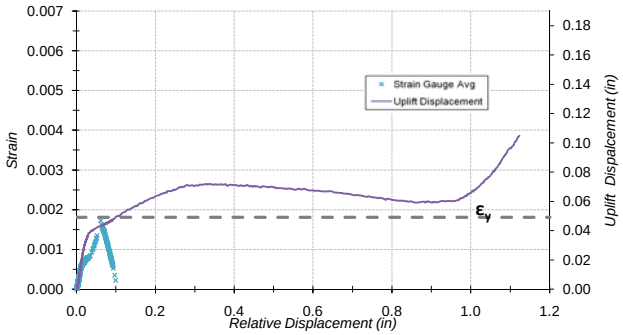

3_NS_2.0 - "John"

- The steel yields, but doesn't fracture or SH
- Again, there is a rising branch at the end (like in the other NS).
- Initial crack at ~59k; Very ductile failure at ~73k out to ~1.2 in
- Slight jump at failure

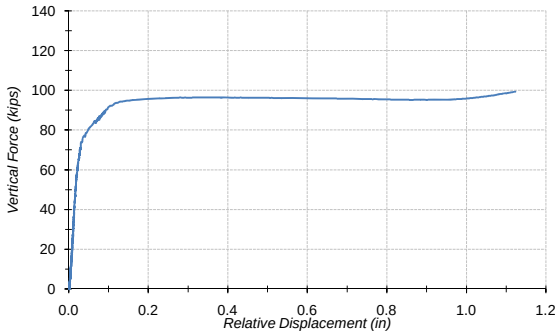

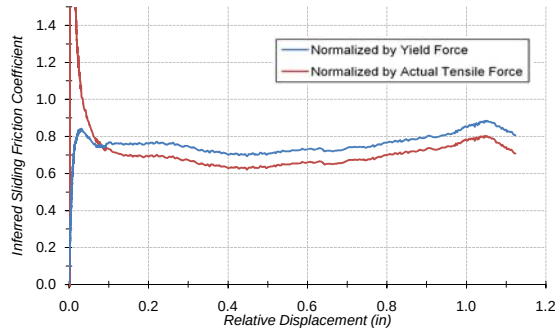

ETS Input		
Length between SPs	16.0	in
Width between LVs	16.5	in
Width between SPs	15.0	in
SP25 Height	12.5	in
SP26 Height	12.5	in
SP27 Height	12.5	in
SP28 Height	12.5	in
Distance from LV2 to LV4	4.5	in
Effective Gauge Length	27.14	in
Effective area of connector	1.8040	in2
Connector Material Input		
ey =	0.0018	
esu =	0.0194	
esh =	0.0019	
fy =	53	ksi
fsu =	78	ksi
Es =	29000	ksi
Esh =	1309	ksi
P =	0.885	

Yield Tensile Force **94.7** **kips**

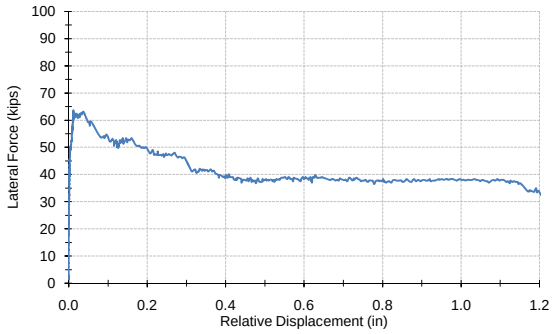

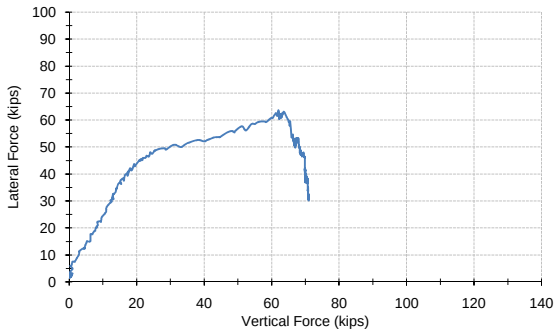

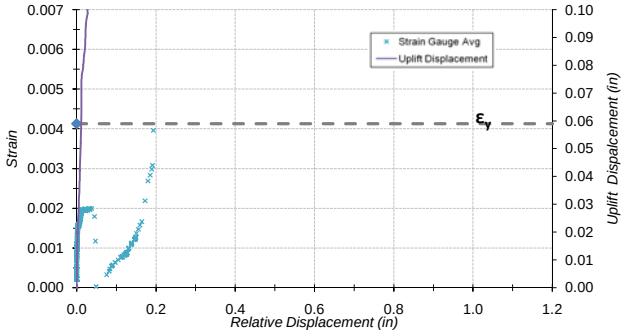

1_TRS_2.0_Rough - "David"

- LV1/LV2 displacement no good, so SP5-LV3 used instead.
- Not too sure about how any slip of the anchoring Sika would show up, but it seems reasonable, though somewhat poor.
- Tightening load accidentally went to 25 kips

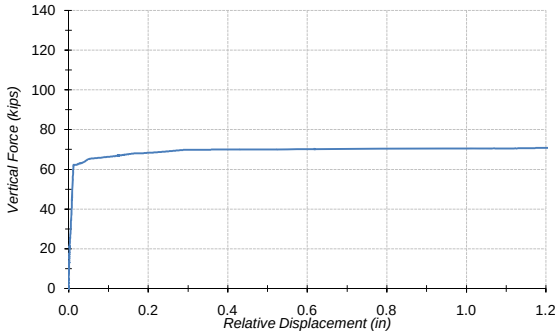

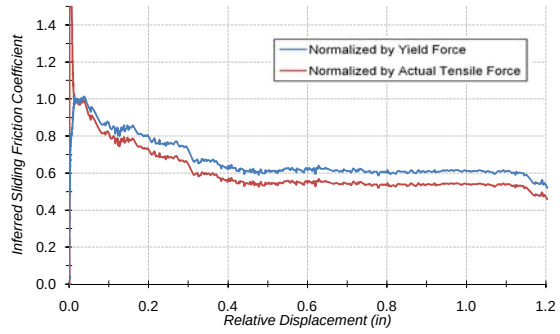

ETS Input		
Length between SPs	18.0	in
Width between LVs	16.5	in
Width between SPs	15.0	in
SP25 Height	12.3	in
SP26 Height	12.3	in
SP27 Height	12.3	in
SP28 Height	12.3	in
Distance from LV2 to LV4	4.5	in
Effective Gauge Length	14.28	in
Effective area of connector	0.5204	in2
Connector Material Input		
ey =	0.0041	
esu =	0.0277	
esh =	0.0060	
fy =	120	ksi
fsu =	137	ksi
Es =	29000	ksi
Esh =	1250	ksi
P =	1.572	

Yield Tensile Force **62.3 kips**

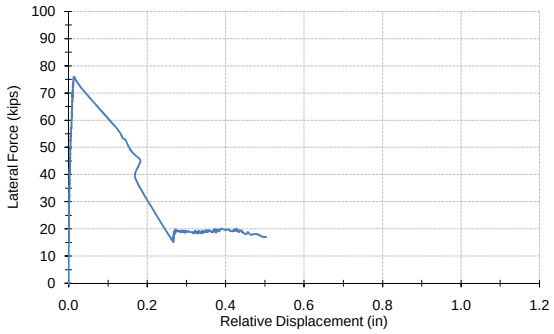

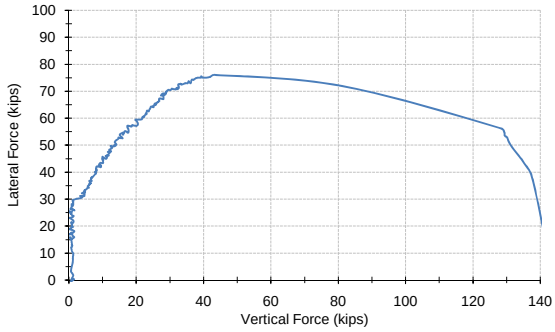

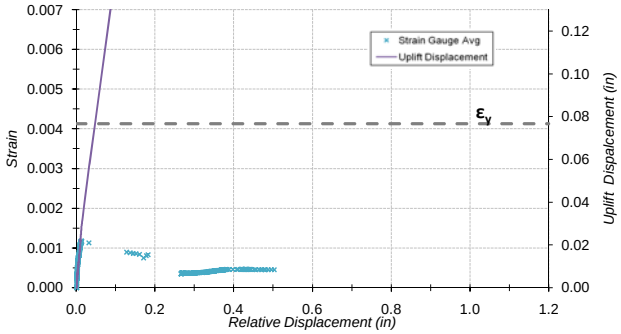

2_TRS_2.0_Rough - "Monique"

- This was a beam failure and no SG1, so the data is not as good.
- Initial crack at 71 k
- Beam fail in top 1/3 around 75 k

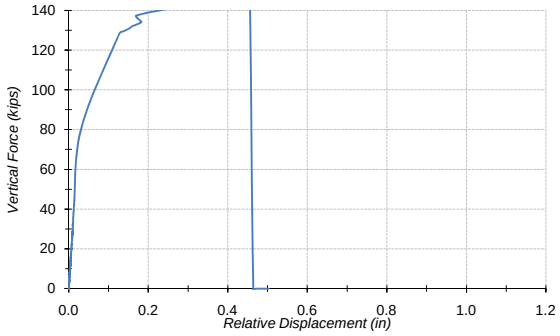

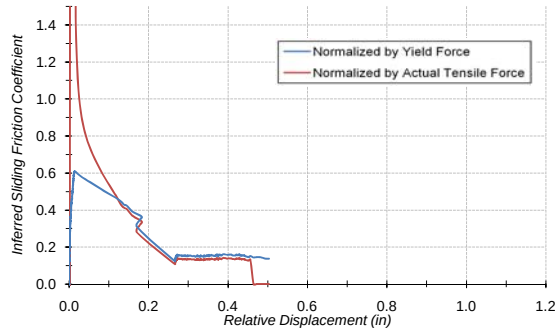

ETS Input		
Length between SPs	18.0	in
Width between LVs	16.5	in
Width between SPs	15.0	in
SP25 Height	12.3	in
SP26 Height	12.3	in
SP27 Height	12.3	in
SP28 Height	12.3	in
Distance from LV2 to LV4	4.5	in
Effective Gauge Length	20.67	in
Effective area of connector	1.0408	in2
Connector Material Input		
ey =	0.0041	
esu =	0.0277	
esh =	0.0060	
fy =	120	ksi
fsu =	137	ksi
Es =	29000	ksi
Esh =	1250	ksi
P =	1.572	

Yield Tensile Force **124.6 kips**

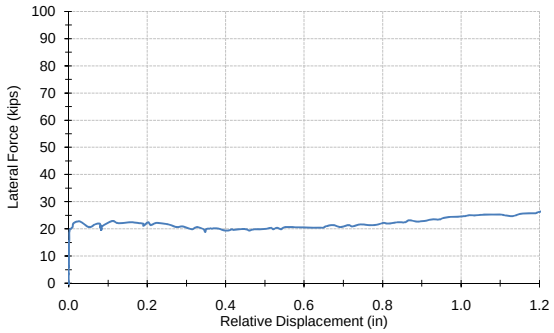

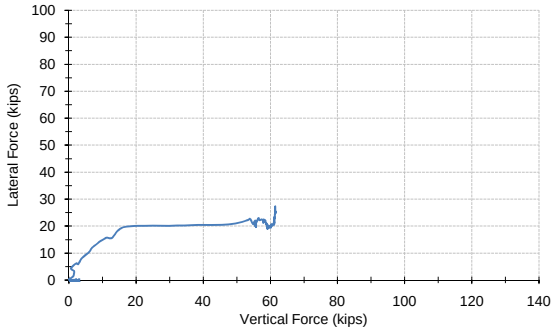

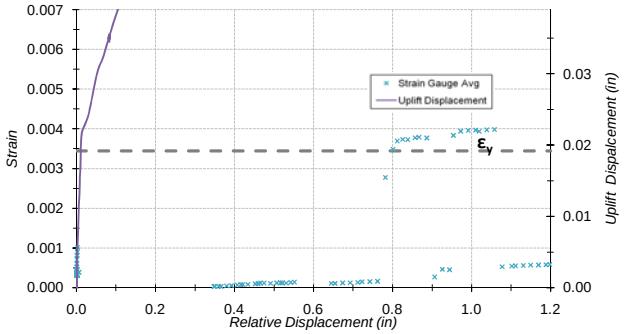

1_KB_2.0 - "William"

- Lg is small, but there was only 6 1/4" above the nugget surfarce.
- Initial crack at < 20k
- Slid at ~ 20 k -- not too good
- Might have hit coupler at the end

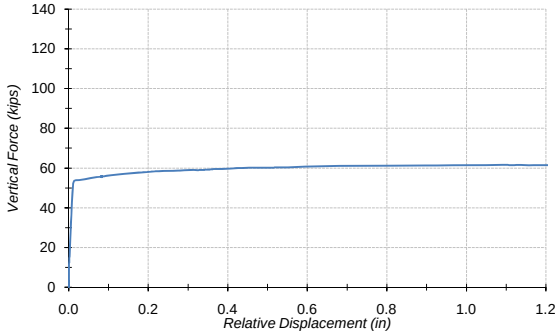

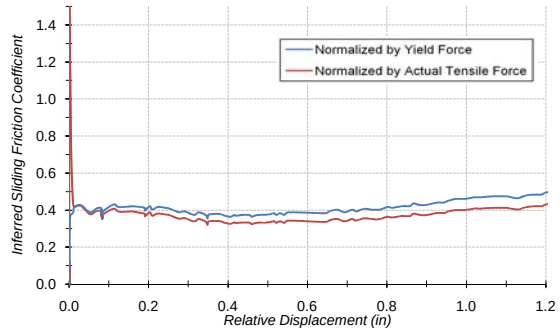

ETS Input		
Length between SPs	18.0	in
Width between LVs	16.5	in
Width between SPs	15.0	in
SP25 Height	12.3	in
SP26 Height	12.3	in
SP27 Height	12.3	in
SP28 Height	12.3	in
Distance from LV2 to LV4	4.5	in
Effective Gauge Length	5.57	in
Effective area of connector	0.5333	in2
Connector Material Input		
ey =	0.0034	
esu =	0.0203	
esh =	0.0037	
fy =	100	ksi
fsu =	123	ksi
Es =	29000	ksi
Esh =	1690	ksi
P =	1.205	

Yield Tensile Force **53.3 kips**

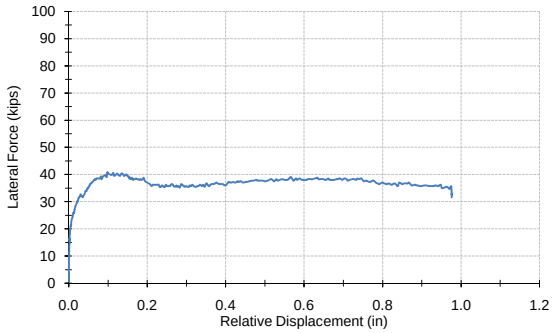

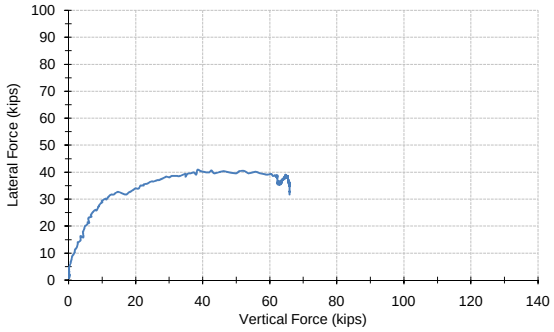

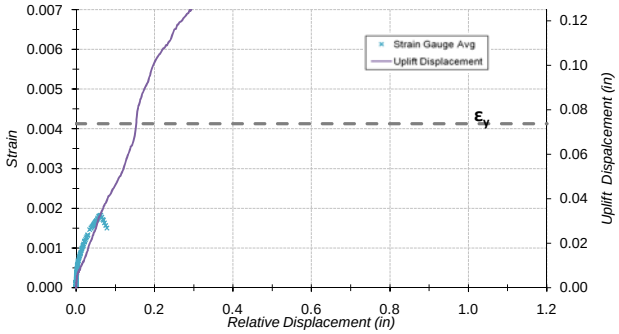

1_TRE_2.0 - "Jackson"

- No data from LV2
- Initial crack at 30 k
- Back 1/3 of grout fractured off
- Sliding at 40 k

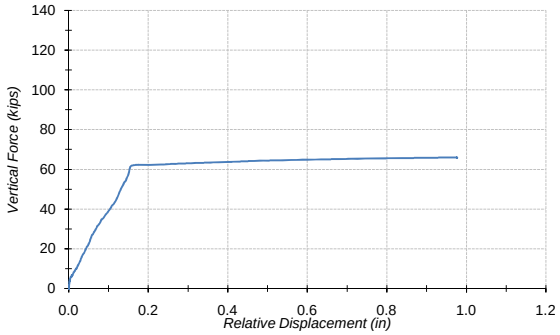

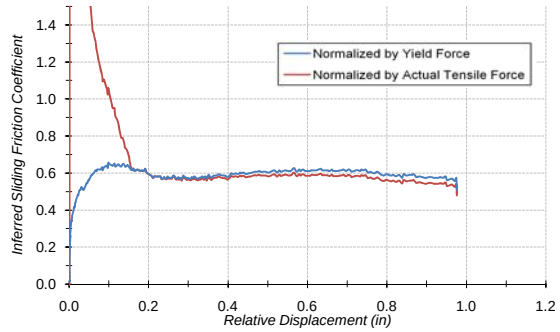

ETS Input		
Length between SPs	18.0	in
Width between LVs	16.5	in
Width between SPs	15.0	in
SP25 Height	12.3	in
SP26 Height	12.3	in
SP27 Height	12.3	in
SP28 Height	12.3	in
Distance from LV2 to LV4	4.5	in
Effective Gauge Length	17.86	in
Effective area of connector	0.5204	in2
Connector Material Input		
ey =	0.0041	
esu =	0.0277	
esh =	0.0060	
fy =	120	ksi
fsu =	137	ksi
Es =	29000	ksi
Esh =	1250	ksi
P =	1.572	

Yield Tensile Force **62.3 kips**

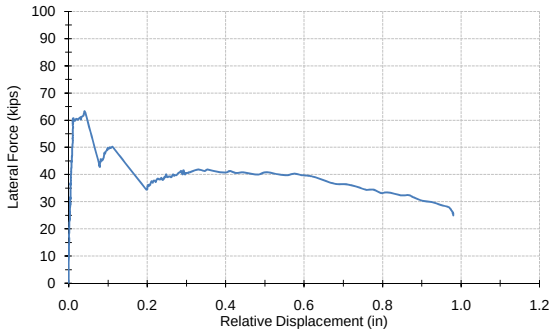

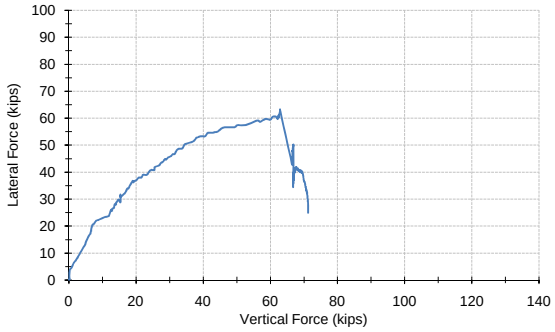

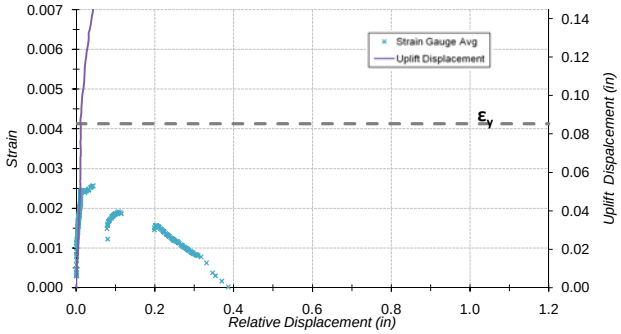

1_TRS/AG_2.0_Rough - "Reece"

- No data from LV2
- Initial crack at 25 k
- Lost LV2
- Beam fail in top 1/4 at jump

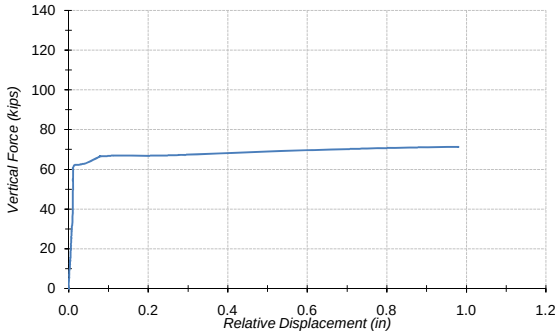

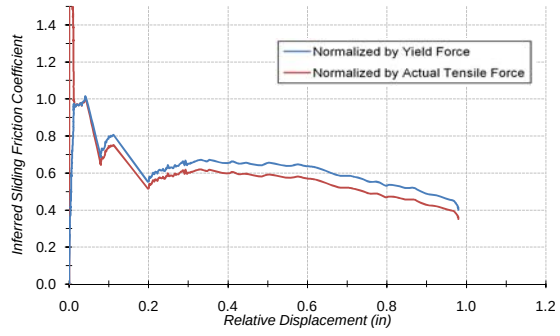

ETS Input		
Length between SPs	16.0	in
Width between LVs	16.5	in
Width between SPs	15.0	in
SP25 Height	12.5	in
SP26 Height	12.5	in
SP27 Height	12.5	in
SP28 Height	12.5	in
Distance from LV2 to LV4	4.5	in
Effective Gauge Length	20.67	in
Effective area of connector	0.5204	in2
Connector Material Input		
ey =	0.0041	
esu =	0.0277	
esh =	0.0060	
fy =	120	ksi
fsu =	137	ksi
Es =	29000	ksi
Esh =	1250	ksi
P =	1.572	

Yield Tensile Force **62.3 kips**

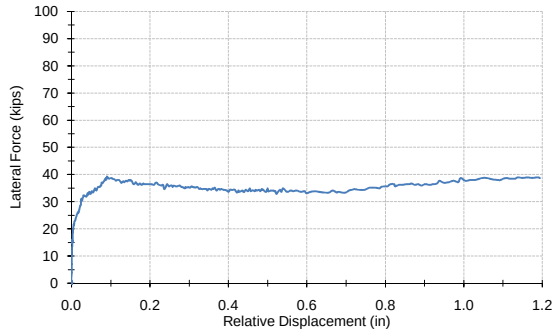

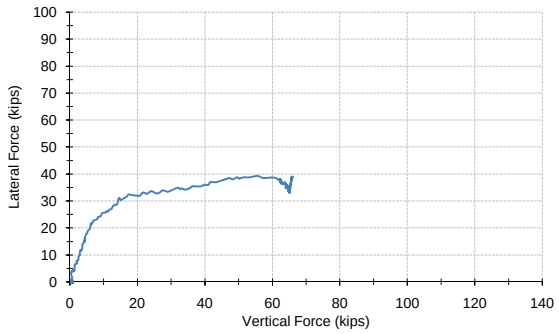

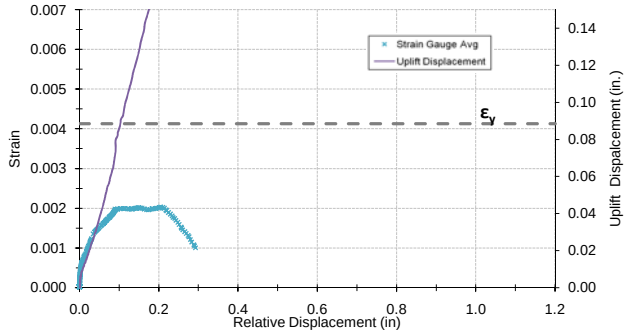

1_TRS_2.0 - "Matt"

- NoLV2; aside from that, the data looks pretty solid and consistent.
- Lg = 21.43" is a bit large
- Initial crack at 25 k
- Separation at the top of grout/donut bottom
- Cracking of donut and sliding at 36 k

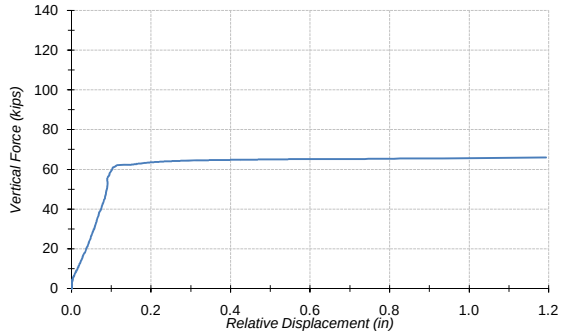

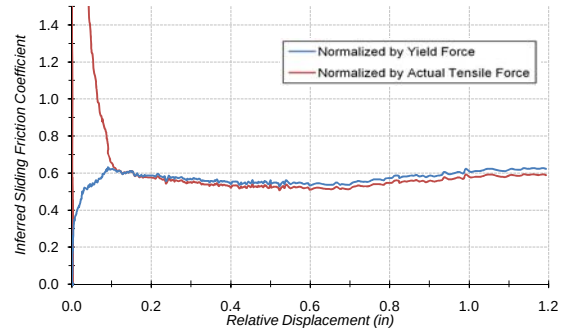

ETS Input		
Length between SPs	16.0	in
Width between LVs	16.5	in
Width between SPs	15.0	in
SP25 Height	12.5	in
SP26 Height	12.5	in
SP27 Height	12.5	in
SP28 Height	12.5	in
Distance from LV2 to LV4	4.5	in
Effective Gauge Length	21.43	in
Effective area of connector	0.5204	in2
Connector Material Input		
ey =	0.0041	
esu =	0.0277	
esh =	0.0060	
fy =	120	ksi
fsu =	137	ksi
Es =	29000	ksi
Esh =	1250	ksi
P =	1.572	

Yield Tensile Force **62.3 kips**

APPENDIX B

ADDITIONAL MATERIAL TESTING INFORMATION

Test Matrix

				Nugget					Donut			Connection								Test Day				
Test #	Tested	Name	Haunch	Type	#	Cast	Test Age	Set	Cast	Test Age	Set	#	Size	Type	Rough	Haunch	Pocket	Assembled	Test Age	Nugget	PI	Donut	Haunch	Pocket
1	30-May	Douglas	2"	CIP	A	18-Feb	102	1	28-Mar	63	CIP	2	#4	Rebar stirrups	-	Concrete	Concrete	28-Mar	63	7340	-	9091	9091	9091
2	5-Jun	Jennifer	2"	CIP	A	18-Feb	108	1	28-Mar	69	CIP	2	#4	Rebar stirrups	-	Concrete	Concrete	28-Mar	69	7340	-	9091	9091	9091
3	6-Jun	Emily	2"	T.R. w/coupler	C	7-Mar	91	2	28-Mar	70	1	2	1"	T.R. w/nut	-	Sika	Sika	1-May	36	5938	-	9091	7023	8314
4	17-Jun	Dopey	2"	Bolt w/coupler	I	7-Mar	102	2	14-Apr	64	2	2	1"	T.R. w/nut	-	Sika	Concrete	3-Jun	14	6236	-	7980	6059	5354
5	17-Jun	Happy	2"	T.R.	E	23-May	25	3	14-Apr	64	2	2	1"	Nut on T.R.	-	Sika	Concrete	3-Jun	14	6129	-	7980	6059	5354
6	17-Jun	Sneezy	2"	T.R.	E	23-May	25	3	14-Apr	64	2	2	1"	Nut on T.R.	-	Sika	Concrete	3-Jun	14	6129	-	7980	6059	5354
7	18-Jun	Snow White	3.5"	T.R. w/coupler	F	23-May	26	3	14-Apr	65	2	2	1"	T.R. w/nut	-	Sika	Concrete	3-Jun	15	6129	-	7980	6132	5354
8	18-Jun	Bashful	3.5"	T.R. w/coupler	F	23-May	26	3	14-Apr	65	2	2	1"	T.R. w/nut	-	Sika	Concrete	3-Jun	15	6129	-	7980	6132	5354
9	18-Jun	Gavin	2"	R-bars	C	7-Mar	103	2	28-Mar	82	1	2	#4	Rebar stirrups	-	Sika	Sika	1-May	48	6236	-	9091	7377	8314
10	19-Jun	Grumpy	3.5"	T.R.	G	23-May	27	3	14-Apr	66	2	2	1"	Nut on T.R.	-	Sika	Concrete	3-Jun	16	6129	-	7980	6200	5354
11	19-Jun	Doc	3.5"	T.R.	G	23-May	27	3	14-Apr	66	2	2	1"	Nut on T.R.	-	Sika	Concrete	3-Jun	16	6129	-	7980	6200	5354
12	19-Jun	Meredith	3.5"	CIP	H	23-May	27	3	3-Jun	16	CIP	2	#4	Rebar stirrups	-	Concrete	Concrete	3-Jun	16	6129	-	5706	5706	5706
13	19-Jun	Luis	3.5"	CIP	H	23-May	27	3	3-Jun	16	CIP	2	#4	Rebar stirrups	-	Concrete	Concrete	3-Jun	16	6129	-	5706	5706	5706
14	30-Jun	Sleepy	2"	Bolt w/coupler	I	7-Mar	115	2	14-Apr	77	2	1	1"	Bolt	-	Sika	Concrete	3-Jun	27	6236	-	6379	6594	6525
15	30-Jun	Hannah	2"	Bolt w/coupler	B	7-Mar	115	2	28-Mar	94	1	1	1"	Bolt	-	Sika	Sika	1-May	60	6236	-	9091	6517	8314
16	30-Jun	Thomas	2"	Bolt w/coupler	B	7-Mar	115	2	28-Mar	94	1	2	1"	Bolt	-	Sika	Sika	1-May	60	6236	-	9091	6517	8314
17	1-Jul	Jonathan	2"	RC w/steel plate	D	7-Mar	116	2	28-Mar	95	1	2	7/8"	Nelson Stud	-	Sika	Sika	1-May	61	6236	-	9091	6517	8314
18	1-Jul	John	2"	RC w/steel plate	D	7-Mar	116	2	28-Mar	95	1	3	7/8"	Nelson Stud	-	Sika	Sika	1-May	61	6236	-	9091	6517	8314
19	26-Aug	David	2"	Post-Installed	L	18-Feb	190	1	23-May	95	3	1	1"	TR w/Sika	Roughened	Sika	Sika	4-Aug	22	7340	6193	6702	5833	7916
20	27-Aug	Monique	2"	Post-Installed	L	18-Feb	191	1	23-May	96	3	2	1"	TR w/Sika	Roughened	Sika	Sika	4-Aug	23	7340	6193	6702	5833	7970
21	27-Aug	William	2"	Post-Installed	J	18-Feb	191	1	28-Mar	152	1	1	1"	Kwik-Bolt 3	-	Sika	Sika	4-Aug	23	7340	-	9480	5833	7970
22	27-Aug	Jackson	2"	Post-Installed	J	18-Feb	191	1	28-Mar	152	1	1	1"	TR w/HY150	-	Sika	Sika	4-Aug	23	7340	-	9480	5833	7970
23	28-Aug	Reece	2"	Post-Installed	K	18-Feb	192	1	23-May	97	3	1	1"	TR w/Sika	Roughened	RM	RM	11-Aug	17	7340	6193	6702	6114	6114
24	28-Aug	Matt	2"	Post-Installed	K	18-Feb	192	1	23-May	97	3	1	1"	TR w/Sika	-	Sika	Sika	4-Aug	24	7340	6193	6702	5833	8021

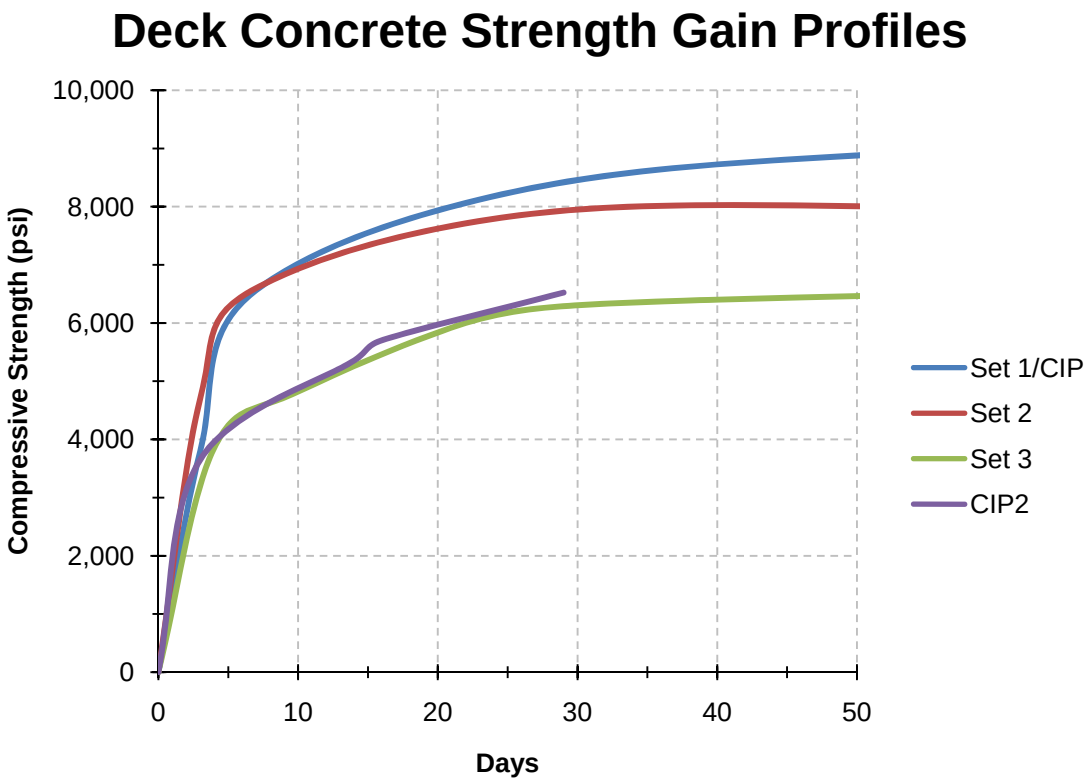
Deck Concrete Strength Gain Profiles
Compressive Strength (psi)
10,000
8,000
6,000
4,000
2,000
0
0
10
20
30
40
50
Days
Set 1/CIP
Set 2
Set 3
CIP2

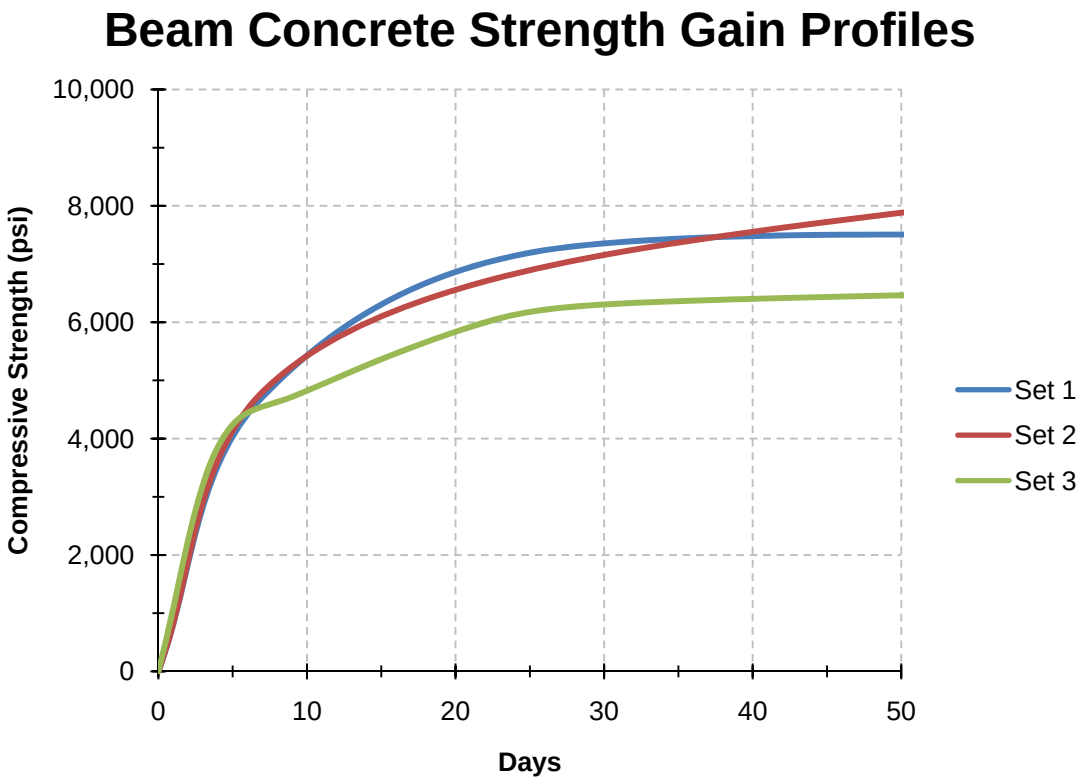
Beam Concrete Strength Gain Profiles
Compressive Strength (psi)
10,000
8,000
6,000
4,000
2,000
0
0
10
20
30
40
50
Days
Set 1
Set 2
Set 3

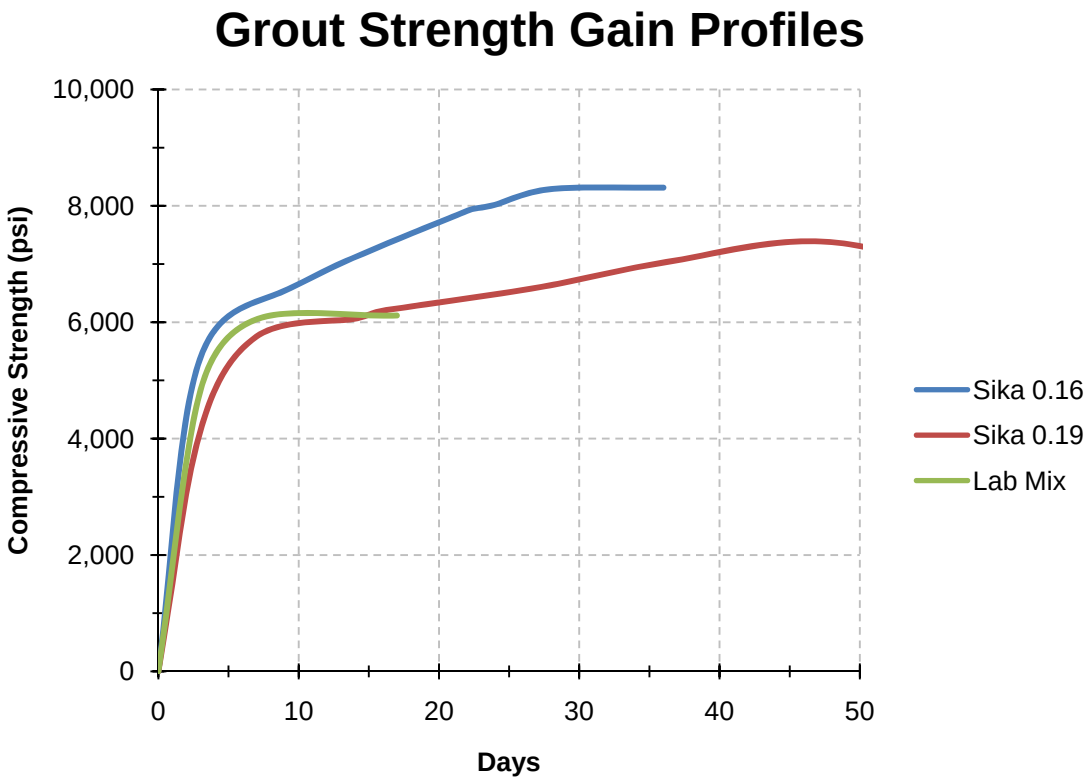
Grout Strength Gain Profiles
Compressive Strength (psi)
10,000
8,000
6,000
4,000
2,000
0
0
10
20
30
40
50
Days
Sika 0.16
Sika 0.19
Lab Mix

Construction

Product Data Sheet
Edition 6.2003
Identification no. 525-501
SikaGrout 212

SikaGrout® 212

High performance, cementitious grout

Description	SikaGrout 212 is a non-shrink, cementitious grout with a unique 2-stage shrinkage compensating mechanism. It is non-metallic and contains no chloride. With a special blend of shrinkage-reducing and plasticizing/water-reducing agents, SikaGrout 212 compensates for shrinkage in both the plastic and hardened states. A structural grout, SikaGrout 212 provides the advantage of multiple fluidity with a single component. SikaGrout 212 meets Corps of Engineers' Specification CRD C-621 and ASTM C-1107 (Grade C).
Where to Use	▪ Use for structural grouting of column base plates, machine base plates, anchor rods, bearing plates, etc. ▪ Use on grade, above and below grade, indoors and out. ▪ Multiple fluidity allows ease of placement: ram in place as a dry pack, trowel-apply as a medium flow, pour or pump as high flow.
Advantages	▪ Easy to use...just add water. ▪ Multiple fluidity with one material. ▪ Non-metallic, will not stain or rust. ▪ Low bleed. ▪ Low heat build-up. ▪ Excellent for pumping: Does not segregate...even at high flow. No build-up on equipment hopper. ▪ Non-corrosive, does not contain chlorides. ▪ Superior freeze/thaw resistance. ▪ Resistant to oil and water. ▪ Meets CRD C-621. ▪ Meets ASTM C-1107 (Grade C). ▪ Shows positive expansion when tested in accordance with ASTM C-827. ▪ SikaGrout 212 is USDA-approved.
Coverage	Approximately 0.44 cu. ft./bag at high flow.
Packaging	6 lb. pail, 6/case, 36/pallet; 50-lb. multi-wall bags; 36 bags/pallet.

Typical Data *(Material and curing conditions @ 73°F (23°C) and 50% R.H.)*

Shelf Life	One year in original, unopened bags.			
Storage Conditions	Store dry at 40°-95°F (4°-35°C). **Condition material to 65°-75°F before using.**			
Color	Concrete gray			
Flow Conditions		**Plastic[1]**	**Flowable[1]**	**Fluid[2]**
Typical Water Requirements:		6 pt.+	6.5 pt.	8.5 pt.
Set Time (ASTM C-266):	**Initial**	3.5-4.5 hr.	4.0-5.0 hr.	4.5-6.5 hr.
	Final	4.5-5.5 hr.	5.5-6.5 hr.	6.0-8.0 hr.
Tensile Splitting Strength, psi (ASTM C-496)				
28 day		600 (4.1 MPa)	575 (3.9 MPa)	500 (3.4 MPa)
Flexural Strength, psi (ASTM C-293)				
28 day		1,400 (9.6 MPa)	1,200 (8.2 MPa)	1,000 (6.8 MPa)
Bond Strength, psi (ASTM C-882 modified): Hardened concrete to plastic grout				
28 day		2,000 (13.7 MPa)	1,900(13.1 MPa)	1,900 (13.1 MPa)
Expansion % (CRD C-621)	**28 day**	+0.021%	+0.056%	+0.027%
Compressive Strength, psi (CRD C-621)				
1 day		4,500 (31.0 MPa)	3,500 (24.1 MPa)	2,700 (18.6 MPa)
7 day		6,100 (42.0 MPa)	5,700 (39.3 MPa)	5,500 (37.9 MPa)
28 day		7,500 (51.7 MPa)	6,200 (42.7 MPa)	5,800 (40.0 MPa)

[1]CRD C-227: 100-124% (plastic), 124-145% (flowable)
[2]CRD C-611: 10-30 sec efflux time.

Construction

How to Use

Surface Preparation	Remove all dirt, oil, grease, and other bond-inhibiting materials by mechanical means. Anchor bolts to be grouted must be de-greased with suitable solvent. Concrete must be sound and roughened to promote mechanical adhesion. Prior to pouring, surface should be brought to a saturated surface-dry condition.
Forming	For pourable grout, construct forms to retain grout without leakage. Forms should be lined or coated with bond-breaker for easy removal. Forms should be sufficiently high to accommodate head of grout. Where grout-tight form is difficult to achieve, use SikaGrout 212 in dry pack consistency.
Mixing	Mix manually or mechanically. Mechanically mix with low-speed drill (400-600 rpm) and Sika mixing paddle or in appropriately sized mortar mixer. **Product Extension:** For deeper applications, SikaGrout 212 (plastic and flowable consistencies only) may be extended with 25 lbs. of 3/8" pea gravel. The aggregate must be non-reactive, clean, well-graded, saturated surface dry, have low absorption and high density, and comply with ASTM C33 size number 8 per Table 2. Add the pea gravel after the water and SikaGrout 212.
Mixing Procedure	Make sure all forming, mixing, placing, and clean-up materials are on hand. Add appropriate quantity of clean water to achieve desired flow. Add bag of powder to mixing vessel. Mix to a uniform consistency, minimum of 2 minutes. Ambient and material temperature should be as close as possible to 70 °F If higher, use cold water; if colder, use warm water.
Application	Within 15 minutes after mixing, place grout into forms in normal manner to avoid air entrapment. Vibrate, pump, or ram grout as necessary to achieve flow or compaction. SikaGrout 212 must be confined in either the horizontal or vertical direction leaving minimum exposed surface. After grout has achieved final set, remove forms, trim or shape exposed grout shoulders to designed profile. SikaGrout 212 is an excellent grout for pumping, even at high flow. For pump recommendations, contact Technical Service. Wet cure for a minimum of 3 days or apply a curing compound which complies with ASTM C-309 on exposed surfaces.
Limitations	▪ Minimum ambient and substrate temperature 45°F and rising at time of application. ▪ Minimum application thickness: 1/2 in. ▪ Maximum application thickness (neat): 2 in. Deeper applications are possible, please contact Sika's technical services department. ▪ Do not use as a patching or overlay mortar or in unconfined areas. ▪ Material must be placed within 15 minutes of mixing. ▪ As with all cement based materials, avoid contact with aluminum to prevent adverse chemical reaction and possible product failure. Insulate potential areas of contact by coating aluminum bars, rails, posts etc. with an appropriate epoxy such as Sikadur Hi-Mod 32.

Caution

Irritant	Suspect carcinogen - contains portland cement and crystalline silica. Skin and eye irritant. Avoid breathing dust. Use only with adequate ventilation. May cause delayed lung injury (silicosis). IARC lists crystalline silica as having sufficient evidence of carcinogenicity in laboratory animals and limited evidence of carcinogenicity in humans. NTP also lists crystalline silica as a suspect carcinogen. Use of safety goggles and chemical resistant gloves is recommended. In case of high dust concentrations or exceedance of PELs, use an appropriate NIOSH approved respirator. Remove contaminated clothing.
First Aid	In case of skin contact, wash thoroughly with soap and water. For eye contact, flush immediately with plenty of water for at least 15 minutes; contact physician immediately. Wash clothing before re-use.
Clean Up	In case of spillage, ventilate area of spill, confine spill, vacuum or scoop into appropriate container. Dispose of in accordance with current applicable local, state and federal regulations. Uncured material can be removed with water. Cured material can only be removed mechanically.

KEEP CONTAINER TIGHTLY CLOSED
NOT FOR INTERNAL CONSUMPTION

KEEP OUT OF REACH OF CHILDREN
FOR INDUSTRIAL USE ONLY

CONSULT MATERIAL SAFETY DATA SHEET FOR MORE INFORMATION

Sika warrants this product for one year from date of installation to be free from manufacturing defects and to meet the technical properties on the current technical data sheet if used as directed within shelf life. User determines suitability of product for intended use and assumes all risks. Buyer's sole remedy shall be limited to the purchase price or replacement of product exclusive of labor or cost of labor.

NO OTHER WARRANTIES EXPRESS OR IMPLIED SHALL APPLY INCLUDING ANY WARRANTY OF MERCHANTABILITY OR FITNESS FOR A PARTICULAR PURPOSE. SIKA SHALL NOT BE LIABLE UNDER ANY LEGAL THEORY FOR SPECIAL OR CONSEQUENTIAL DAMAGES.

Visit our website at www.sikausa.com **1-800-933-SIKA NATIONWIDE**

Regional Information and Sales Centers. For the location of your nearest Sika sales office, contact your regional center.

Sika Corporation
201 Polito Avenue
Lyndhurst, NJ 07071
Phone: 800-933-7452
Fax: 201-933-6225

Sika Canada Inc.
601 Delmar Avenue
Pointe Claire
Quebec H9R 4A9
Phone: 514-697-2610
Fax: 514-694-2792

Sika Mexicana S.A. de C.V.
Carretera Libre Celaya Km. 8.5
Corregidora, Queretaro
C.P. 76920 A.P. 136
Phone: 52 42 25 0122
Fax: 52 42 25 0537

QUALITY ISO 9001 9002 ACHIEVEMENT

VITA

Matthew Dale Henley, Capt, USAF, received his Bachelor of Science degree in civil engineering from Texas A&M University in December 2003 and was commissioned into the United States Air Force. He served over three years of traditional active duty as a civil engineer in the 47th Civil Engineer Squadron, Laughlin Air Force Base, Texas, before being assigned to pursue a graduate degree. He entered the Structures program at Texas A&M University in August 2007 and received his Master of Science degree in May 2009. His research interests include structural evaluation of expedited construction methods, particularly those with potential military and reconstruction applications. He will be serving a follow-on tour as an instructor at the Civil Engineer and Services School of the Air Force Institute of Technology at Wright-Patterson Air Force Base, Ohio.

Capt Henley may be reached at AFIT/CESS, 2950 Hobson Way, WPAFB, OH 45433-7765. His email is matthenley03@aggienetwork.com.